# Arctic Oil Spills: A Risk Assessment of Transport in Sea Ice and Ocean Surface Waters from Current Exploration Sites

Hauke Blanken

Master of Engineering

Department of Civil Engineering and Applied Mechanics

McGill University

Montreal,Quebec

2014

A thesis submitted to McGill University in partial fulfilment of the requirements for the degree of Master of Engineering

## ACKNOWLEDGEMENTS

I am thankful to my family and friends. Without their support this project would not have been possible. I'd also like to thank my advisors, Prof. Bruno Tremblay and Prof. Susan Gaskin for their guidance and inspiration, as well as Dr. Alexander Slavin for his patient tutorials in the use of MITgcm, and Mr. David Huard for the use of his pickup files. My thanks also go to Quebec Ocean for supporting this project.

**ABSTRACT**

In recent years the level of oil and gas activity in the Arctic Ocean Basin has increased significantly. Permitting and reasonably safe execution of these activities in ice-infested waters require risk assessments that stretch the limits of currently available oil spill trajectory models. Research has suggested that using a coupled atmosphere-ice-ocean model to simulate oil spill trajectories in ice-infested waters could provide higher accuracy than traditionally parameterized models. This study is a first step towards the development of such a model within the framework of the MIT general circulation model. Oil spills are simulated by continuous release of passive tracers at ten locations in the Arctic Ocean Basin, and tracked in the ocean and sea ice for one year starting at the end of the drilling season, using classical parameterizations to model oil-ice interaction. Trajectories in sea ice are compared to historical sea ice drift data and found to agree reasonably well. 31 simulations with differing sets of historical environmental forcing are carried out to quantify inter-annual variability. Sensitivity to the key parameter, fraction of ice coverage, is found to be low. In general it is concluded that, depending on location, oil spills may be advected up to ~1,700km over a winter season and ~3,500km over one year. The furthest advection of spilled oil is observed in the Beaufort and Chukchi Seas, Baffin Bay, and East Greenland. Oil spills originating in the Beaufort, Chukchi, and Barents Seas are confirmed to cross international boundaries, and all spills are found to have potentially severe impact on coastlines. Where mobile drift ice is present, transport with sea ice is more extensive than transport with ocean currents.

# ABRÉGÉ

Les activités liées à l'exploitation de gaz et de pétrole dans le bassin de l'océan Arctique se sont fortement intensifiées ces dernières annés. La conduite raisonnablement sûre d'activités dans des eaux couvertes de glace, mais aussi l'autorisation de telles activités, nêcessitent d'êvaluer les risques au-delà des limites des modèles actuels prédisant les trajectoires de déversements accidentels d'hydrocarbures en mer. Des études ont suggéré une meilleure précision gràce à l'utilisation d'un modèle couplant atmosphère, glace, et océan pour simuler les trajectoires de déversements accidentels d'hydrocarbures dans des eaux couvertes de glace par rapport à les modelles usuelles. Cette étude est une première étape dans le développement d'un tel modèle au sein du modèle général de circulation des flux atmosphériques, océaniques et climatiques développé par le MIT. Des déversements accidentels d'hydrocarbures sont simulès par le rejet en continu de traceurs passifs en dix endroits situés dans le bassin de l'océan Arctique. Ces rejets débutent en fin de période de forage et leur déplacement est suivi dans l'océan et la glace pendant un an. Les trajectoires d'hydrocarbures dans les eaux gelées sont comparées à des données historiques issues d'un modèle Lagrangien de vitesses de déplacement de blocs de glace et ils correspondent raisonnablement bien. 31 simulations avec différents jeux de données environnementales ont permis de quantifier la variabilité interannuelle. L'interaction entre pétrole et blocs de glace marins a été modélisée par des paramétrisations usuelles. La sensibilité au paramétre-clé, la fraction de surface recouverte de glace, est jugée relativement négligeable. De manière gènèrale, dèpendamment de leur position, les

rejets d'hydrocarbures peuvent se déplacer par advection jusqu' environ 1,700 km en hiver et 3,500 km sur une anne. Les déplacements d'hydrocarbures les plus longs sont observés en mers de Beaufort et Chukchi, en baie de Baffin et dans le Groenland de l'Est. Les déversements en mers de Beaufort, Chukchi, et Barents, traversent les limites internationale, et l'ensemble de ces rejets ont de potentiellement graves conséquences sur les côtes. Le transport d'hydrocarbures avec les blocs de glace à la dérive, le cas échéant, est plus facile qu'avec les courants océaniques.

TABLE OF CONTENTS

LIST OF TABLES

LIST OF FIGURES

# CHAPTER 1
# Introduction

## 1.1 Renewed Interest

The U.S. Geological Survey released a study in 2008 which estimated that 16% of the world's remaining recoverable hydrocarbon resources are located in the Arctic Circle offshore (Gautier et al., 2008). In the context of the Canadian Arctic offshore, this was confirmed by discoveries made through exploratory drilling done between 1969 and 1990. However, given the logistical difficulties associated with working in the remoteness of the Arctic and the limited working season due to forbiddingly harsh environmental conditions in the winter, these discoveries were deemed uneconomical for commercial exploitation (Callow, 2012).

The sea ice cover, which previously posed unprecedented challenges to offshore drilling for oil and gas, has been receding in recent years due to the Earth's warming climate. Because of this, and the pressure to meet the world's growing energy demand, exploration and production activities in the Arctic have increased significantly in recent years. According to the Northern Oil and Gas Reports, which are published annually by the Department of Aboriginal Affairs and Northern Development Canada (AANDC), the amount of land leased for oil and gas activities in the Canadian Arctic offshore has doubled from $2.4x10^6$ ha in 1997 to a high of $5.0x10^6$ ha in 2012 (AANDC, 2013).

As will be described in more detail in Chapter 2, this renewed interest in exploitation of Arctic resources is not confined to Canadian territory. Active exploration and/or production of oil and gas is occurring in the offshore regions of all five Arctic nations.

## 1.2 Arctic Spill Response

A major spill of oil and gas, such as the Deepwater Horizon disaster in the Gulf of Mexico in 2010, would be unprecedented in Arctic waters and procedures for response to such a spill are uncertain. Also, given the remoteness and low population density of the region, there are less resources available for spill response than at more temperate latitudes.

For response to oil spills at the ocean surface, containment and recovery methods consisting of booms and skimmers deployed from barges have been the preferred primary response mechanism for large scale spills. However, field testing has found these systems to be difficult to operate in ice-covered waters and recovery efficiency is highly dependent on fractional ice coverage and the size distribution of ice floes (Sørstrom et al., 2010). This leaves in-situ burning and dispersant use as potential response measures.

In-situ burning can remove large fractions of an oil slick on water or ice, provided the water content in the oil is less than $\sim$25% and the slick is at least 1-2mm thick. Slick thickness is increased in cold temperatures and aided by herding between ice floes, however booms may be required to obtain necessary slick thicknesses in areas of low ice coverage. Burning does not remove all of the oil and adverse environmental impacts are to be expected from the residue, as well as the smoke emitted from the burn (SL Ross, 2010).

Dispersant application has been shown to work reasonably well for breaking up oil slicks in ice-covered waters, provided adequate mixing energy is available. This may present an issue in dense ice conditions, since the ice damps wave action which has traditionally provided this mixing energy. Additional energy may need to be added, for example using ship props (Sørstrom et al., 2010). However dispersant application results in large volumes of oil drifting at depth (Drozdowski et al., 2011). Natural degradation processes are slowed in the cold Arctic environment and this oil at depth may resurface.

Response to a well blowout at the seabed is even more uncertain. In the Canadian context, the National Energy Board (NEB) requires all operators to demonstrate the capability to stop flow from an out-of-control well within the same drilling season. Operators preparing for exploratory drilling in the Canadian Beaufort Sea have petitioned the National Energy Board to allow departure from this policy for the Arctic offshore operations due to the limited seasonal window for operations in Arctic environmental conditions. A ruling from the NEB on this petition is still pending at the time of writing (NEB, 2014).

### 1.3 Long-Term Accuracy of Predictions

As was described in the previous two sections, the frequency of oil spills in the Arctic environment is likely to increase with increasing oil and gas activity and efficient and timely response to such a spill is difficult within the limited window of opportunity for response to an oil spill in the Arctic environment. Spilled oil that is not remediated by the beginning of the winter will likely persist in the environment until cleanup becomes feasible again in the following spring. Therefore a trajectory model that is able to predict the movement of spilled oil in the Arctic Ocean and sea ice is crucial for risk assessments required as part of the permitting process of new developments and reasonably safe operations of existing wells.

During the field experiment of Reed & Aamo (1994), which is described in Section 4.2.1, it was found that traditional oil spill trajectory models can provide accurate forecasts of spill movement while ice and other environmental conditions are relatively constant. However the model results begin to deviate from reality once conditions change, which occurs frequently in the Arctic environment where storms and strong wind events are common. This is because traditionally oil spill models use user input environmental conditions taken from various sources to compute trajectories. The components of the atmosphere-ice-ocean system are treated separately and coupling is parameterized. These parameterizations are particularly problematic for the atmosphere-ocean coupling, since winds are usually the primary determining factor of oil trajectories (Reed & Aamo, 1994). Predictions over longer timescales would require continuous monitoring of environmental conditions in the affected area throughout the study period, and adjustment of the coupling parameters based on interpretation of these conditions. These traditional approaches are described in more detail in Chapter 4.

## 1.4 Motivation for Fully Coupled Oil Spill Trajectory Modelling

The reviews of Khelifa (2010) and Drozdowski et al. (2011) identify the use of a fully coupled atmosphere-ice-ocean numerical model for trajectory prediction as a potential solution to the issue identified above, since the coupling is accounted for in the equations of motion of the model and adapts to changing environmental conditions. This study is intended to be a first step towards the development of such a model within the framework of the Massachusetts Institute of Technology General Circulation Model (MITgcm).

Use of a fully coupled model also has other advantages, the primary being the ease with which model resolution is adjusted compared to the traditional approach. As is described in Sections 3.4 and 4.1, the processes by which oil in the ocean environment interacts with sea ice occur on a spatial scale that is small compared to the currently available resolution of most environmental data sets and general circulation models. Hence parameterizations which introduce further uncertainty are required to model this interaction. As increased computational power becomes available the spatial resolution of a model such as the one described in this study can be increased uniformly, until the oil-ice interaction can be resolved and modelled based on the fundamental principles of physics. This increase in resolution would be more difficult in traditionally formulated spill trajectory models where the accuracy of the model is limited by the resolution of the available input data.

The fully coupled approach offers another advantage from an operational perspective, since the model can be run in real-time to provide forecasts of environmental data such as ice conditions at the site and spills could easily be initialized for tracking within these real-time runs without extensive setup times. Observational data could be incorporated in such real-time modelling through periodic restarts whenever new data is available.

## 1.5 Synopsis of Thesis

This thesis is spilt into two main sections, beginning with a literature review. This review first describes potential and known locations of exploratory and production drilling for oil in the Arctic Ocean Basin in Chapter 2. Chapter 3 first describes the circulation patterns in the Arctic Ocean, before moving on to a description of the mathematical representation of the dynamics of the ocean, atmosphere, and sea ice. The chapter concludes by describing the general theory of the interaction of oil with these media. The literature review concludes in Chapter 4 with descriptions of oil spill trajectory model development, field testing for the verification of such models, and two recent modelling studies in the Arctic Ocean.

The second part of this thesis concerns the risk assessment performed in this study using the MITgcm. Chapter 5 describes the setup of the model and its offline components as well as the historical data set of sea ice drift used for verification of the model results. Results are divided into general observations and conclusions given in Chapter 6, and results specific to the locations identified in Chapter 2, given in Chapter 7. The thesis concludes with a summary of the findings and recommendations for the further development of this modelling approach, in Chapter 8.

# CHAPTER 2
## Locations

The choice of tracer initialization locations, i.e. locations of potential oil spills, was motivated by several factors, all pertaining to the likelihood of drilling occurring in these regions in the near future. Broad regions were selected based on the previously mentioned study by the U.S. Geological Survey, which divided the area north of the Arctic Circle (>66.56°N latitude) into geologic provinces and evaluated the resource potential of each of these provinces by probabilistic analysis of the likelihood of the local geology to contain significant undiscovered hydrocarbon resources (Gautier et al., 2008). Provinces that were found to have a high resource potential and contain existing leases for oil and gas activity at the time of writing were then selected for further consideration. Consideration was also given to the likelihood of accidental releases from these provinces to impact Canadian territory.

With reference to Gautier et al. (2008), the selected provinces are: Amerasia Basin/Franklinian Shelf, Arctic Alaska, West Greenland - East Canada (Baffin Bay), Sverdrup Basin, East Greenland Rift Basin, Barents Plateau/East Barents Basin, and West Siberian Basin.

For each province, local government-issued maps of oil and gas exploration leases were examined and release locations determined based on the leases identified herein. Where government-issued maps were not available, scientific reports on oil findings as well as news releases were used. Due to the appreciable computational expense of processing tracer fields, not every existing lease could be included as a potential spill location. Locations were chosen based on lease ownership, with preference given to leases held by owners with more resources to exploit hydrocarbon resources and/or owners who are currently or have previously been engaged in exploration in Arctic environments. The selected locations are shown in Figure 2–1, and coordinates, water depths (Smith & Sandwell, 1997; GEBCO, 2014), times of significant ice coverage, defined as average modelled ice concentration greater than 30%, and likelihood of landfast ice presence for these sites are listed in Table 2–1.

In the following sections the reasons for selections are detailed, categorized by the five countries bordering the Arctic Ocean.

## 2.1 Canada

Four locations in three of the above-mentioned provinces are included in Canadian territory. As of December 31, 2013 the Department of Aboriginal Affairs and Northern Development of the Canadian government had issued rights in offshore areas in the form of 15 active Exploration Licenses (EL) and 59 Significant Discovery Licenses (SDL) awarded for discoveries from drilling done between 1969 and 1990 and one well drilled in 2005 - 2006. As of this date no offshore Production Licenses had been awarded (AANDC, 2013). From these 74 licenses, four areas were chosen for inclusion in this study.

### 2.1.1 Beaufort Sea Continental Slope

The area delineated by EL476 & 477 has been identified by an Imperial Oil information package dated December 2012 as a target for exploration by a joint venture between ExxonMobil, British Petroleum (BP), ESSO, and Imperial Oil, the


Figure 2–1: Locations of simulated oil spills

official leaseholder. This area is located in the Amerasia Basin, very close to the border with the Franklinian Shelf. Gautier et al. (2008) ranked this area as having the $6^{th}$ largest reserve of recoverable hydrocarbons in the study area and the $2^{nd}$ largest reserve of recoverable oil. The joint venture has completed 3D seismic surveys of the lease, as well as other auxiliary studies regarding development of the project. According to one scenario given in the information package provided by the joint venture, it anticipates to be able to commence drilling of an exploratory well in EL477

Table 2–1: Co-ordinates, water depths, ice coverage, and landfast ice presence for potential spill locations.

| **Location** | **Co-ordinates** | **Depth** | **Ice Coverage** | **Landfast Ice** |
|---|---|---|---|---|
| Beaufort Sea Continental Slope | 70°54'59"N, 135°41'02"W 71°15'10"N, 135°20'52"W | 677m 1109m | Oct. - Aug. | Unlikely |
| Mackenzie Delta | 70°07'01"N, 137°18'21"W | 51m | Oct. - Aug. | Possible |
| Sverdrup Islands | 77°49'16"N, 104°18'59"W | 384m | Year-Round | Likely |
| Baffin Bay | 73°53'20"N, 76°26'18"W | 891m | Oct. - Jul. | Possible |
| US Beaufort Sea | 70°54'31"N, 148°26'07"W | 40m | Oct. - Aug. | Unlikely |
| US Chukchi Sea | 71°11'29"N, 162°35'09"W | 44m | Nov. - Aug. | Unlikely |
| East Greenland | 77°29'19"N, 11°01'31"W | 279m | Year-Round | Unlikely |
| Barents Sea | 71°40'11"N, 20°58'11"E | 306m | Rare | None |
| Pechora Sea | 69°09'05"N, 57°22'16"E | 20m | Dec. - Jun. | Likely |
| Kara Sea | 73°59'06"N, 66°23'39"E | 78m | Nov. - Jul. | Possible |

by the summer of 2020 and to complete drilling over a period of three or more 120-day summer seasons, should it decide to proceed with the operation (Imperial, 2012). However, a report by the Beaufort Regional Environmental Assessment (BREA) indicates that drilling in these areas may commence as early as 2016 (Callow, 2012). The provided information package indicates that drilling would take place in water depths of 400 - 700m and therefore a spill location in a water depth of 677m has been chosen (AANDC, 2013a; Smith & Sandwell, 1997; GEBCO, 2014). However water depths within the license area range from 58 - 1330m (Smith & Sandwell, 1997; GEBCO, 2014), making this one of the deepest areas actively under consideration for exploratory drilling in the Arctic Ocean. To date, the deepest water depth in the Beaufort Sea that a well has been successfully drilled in is 68m (Callow, 2012). For this reason the model setup used for this study has been configured with a second spill location near the deepest point of the lease area, in a water depth of 1109m (Smith & Sandwell, 1997; GEBCO, 2014) and is included along with the aforementioned location to study the effect of slight changes in location in an area of high current variability.

### 2.1.2 Mackenzie Delta

The second area, defined by EL480, is much shallower, with water depths ranging from 48-162m (Smith & Sandwell, 1997; GEBCO, 2014). The license area is located entirely on the continental shelf, near the Mackenzie Delta (AANDC, 2013a). The modeled release location is in a water depth of 51m (Smith & Sandwell, 1997; GEBCO, 2014). This area is also in the Amerasia Basin and near the border with the Arctic Alaska region, which, according to Gautier et al. (2008), holds the largest reserve of recoverable oil in the study area. The current exploration license is held by Chevron, however the area also contains Significant Discovery Licenses (SDL 89, 113, 114) from previous drilling done by BP (AANDC, 2013a). Callow (2012) indicates that Chevron is currently in the process of processing data from seismic surveys in the area and exploratory drilling could commence in this area by 2016. This location was chosen to include the effects of shallow water, and to improve geographic coverage on the Canadian continental shelf.

### 2.1.3 Sverdrup Islands

The third location in Canadian territory is in the Sverdrup Islands. This area was ranked relatively low in terms of resource potential in Gautier et al. (2008) (16th of 25 quantitatively assessed provinces), however estimates by the Geological Survey of Canada are approximately five times higher, which would place the region near the top five in the context of the USGS rankings. Panarctic Oils (now part of Suncor Energy) completed a significant number of exploration wells in the Arctic Islands between 1969 and 1986 and as a result holds a number of Significant Discovery Licenses in the region, though the exploration program was discontinued due to logistical difficulties (Hogg & Enachescu, 2013). Due to the relatively high density of islands and exposure to shoreline in the area, a spill in this region would likely have a high environmental impact. The location corresponding to SDL076, between Ellel Ringnes Island and Lougheed Island, was chosen for inclusion in the study due to the relatively deep water at this location as well as larger distance from the nearby islands, which is thought to correspond to higher potential for movement of oil spilled at this location due to a lesser likelihood of landfast ice in the area (AANDC, 2013b).

### 2.1.4 Baffin Bay

The final location to be considered in Canadian territory is near the northwestern corner of Baffin Bay, at the mouth of Lancaster Sound. With respect to Gautier et al. (2008) it is located in the West Greenland - East Canada province, which is ranked 7th in terms of total recoverable hydrocarbon resources and 5th in terms of recoverable crude oil. Due to its significant environmental importance as habitat and migration routes for polar bears, migratory birds, narwhal, and beluga whales, among others, the area has been the subject of a feasibility study for the creation of a National Marine Conservation Area since 2009. The borders of the proposed conservation area are not yet clearly established, however the conservation area will either encompass part of, or be immediately adjacent to lands leased to Shell Canada for oil and gas exploration, exploration leases A6326 to A408 (AANDC, 2013c; Parks Canada, 2012; Murphy, 2013). These leases were issued under the old Canada Oil and Gas Land Regulations and are no longer shown in The Northern Oil and Gas Annual Report from 2013 (AANDC, 2013), however no mention is made of their termination.

## 2.2 USA

Two locations in the US Arctic offshore will be included for consideration in this study.

### 2.2.1 Beaufort Sea

The first is in the Beaufort Sea, near Prudhoe Bay on the North Slope of Alaska. With respect to the assessment of Gautier et al. (2008) the area is in the Arctic Alaska province, which is ranked 2nd in terms of recoverable hydrocarbon resources and 1st in terms of recoverable crude oil. Exploration for oil and gas in this area began in the 1960s with the Prudhoe Bay Field being discovered in 1968 and opened for production by BP in 1977 with the completion of the Alaska Pipeline (BP, 2006). The area considered in this study is further offshore than the production wells in the Prudhoe Bay field and is leased to Shell (BOEM, 2013). Shell began exploratory drilling in this area in 2012, however was faced with severe operational difficulties and discontinued exploration (USDOI, 2013). Operations could resume in 2015 upon the completion of a court-ordered revision of the Environmental Impact Study prepared by the US Bureau of Ocean Energy Management (BOEM) for the 2008 offshore exploration lease sale in the neighbouring Chukchi Sea (Brehmer, 2014).

### 2.2.2 Chukchi Sea

The second location under consideration is the 'Burger' field in the US Chukchi Sea, also leased by Shell (BOEM, 2013). This field is also located in the Arctic Alaska province and was also subject to drilling of partial exploration wells in 2012. These exploration activities are expected to resume upon acceptance of the revised Environmental Impact Study by BOEM mentioned above, unless further legal challenges are received (Bradner, 2014). Information made public by Shell in November 2013 indicates that the company plans to drill six exploration wells in the lease area, including the one begun in 2012, once operations recommence (Shell, 2013).

## 2.3 Greenland

Exploration for oil and gas resources is occurring on both the west coast and, more recently, the east coast of Greenland. Exploration off the west coast of the country has not been promising to date with 14 exploration wells drilled since the 1970s and no resulting commercial discoveries (Cairn, 2014). Given this, coupled with the fact that the parts of the exploration area north of the Arctic Circle are geographically quite close to the simulation location in Canadian territory at the mouth of Lancaster Sound, these locations will not be included here.

On December 20, 2013 the government of Greenland awarded four exploration licenses on the east coast of the country (GBMP, 2014) and 15 more leases in this area are under consideration for 2014 (Casey, 2014). In terms of Gautier et al. (2008)

assessment these leases are located in the East Greenland Rift Basins province, which ranks 4th in terms of recoverable hydrocarbon resources and 3rd in terms of recoverable crude oil. Between 1990 and 1996 a consortium of firms composed of Exxon-Mobil, Statoil, BP, Japan National Oil Company, Texaco, Shell and NUNAOIL, conducted extensive seismic surveys in the area in the so-called Kanumas project, which aimed to make exploitation of Greenland's hydrocarbon resources more attractive. As a result of this, the companies listed above were granted, and exercised, preferential bidding rights on exploration licenses. It should be noted that these seismic surveys were only possible due to a number of years with unusually low sea ice concentration in these areas in the early 1990s. Between 2001 and 2010 the Danish Meteorological Institute reported zero ice-free days in the northern and western sections of the lease area. In 2013 some partially ice-free days were recorded in the months of July and August in 2013. In the eastern section of the area the number of ice-free days in the summer months has been increasing since 2000. These high ice concentrations are due to the leases' geographic location in the Fram Strait (Casey, 2014), which also implies that oil accidentally released in these locations could impact Canadian territory if the spill is not remediated.

### 2.4 Norway

Norway's offshore regions in the North Sea contain vast hydrocarbon reserves and production from these fields is ongoing with new discoveries being made regularly. However these fields are mainly below the Arctic Circle and will therefore not be considered in this study. While they are technically just within the MITgcm model domain, tracers are artificially removed near the boundary to avoid complications with tracers being reintroduced by the periodic boundary conditions, as described in Section 5.2.1. Because of this only one location in Norway's Barents Sea will be considered.

The assessment of Gautier et al. (2008) places the Norwegian portion of the Barents Sea in the East Barents Basin province, which is ranked 3rd in terms of total recoverable hydrocarbon resources and 4th in terms of recoverable crude oil. Oil was first discovered in the here in 2000 in the Goliat field. Due to a moratorium on exploration in this area being in place from 2001 until 2005 production from this field is not expected to commence until Fall 2014. In 2011 an additional commercial field, named Johan Castberg, was discovered. Production is expected to begin here in 2018 (USEIA, 2014). Exploration and production in these areas is significantly simplified by the rarity of sea ice, even in the winter months. This low ice cover is explained by the warming influence of the North Atlantic inflow (Sorteberg & Kvingedal, 2006). The location considered in this study corresponds to two leases held by Lundin, Bayerngas, Dong, and Repsol, which are approximately longitudinally centered in Norway's Barents Sea leasing area, 85 nautical miles offshore from the port of Hammerfest (NMPE, 2013).

## 2.5 Russia

Government issued maps outlining active areas of petroleum exploration and production are not publicly available for the Russian Arctic Ocean territory.

### 2.5.1 Pechora Sea

One certain location of a production well was determined from news releases following the attempted boarding of the drilling rig by environmental activists in

2013. This is the Prirazlomnaya rig in the Pechora Sea, located between the island of Novaya Zemlya and mainland Russia (Guardian, 2014). With respect to Gautier et al. (2008) assessment this location is in the Timan-Pechora Basin province, which ranks 13th in terms of total recoverable hydrocarbons and 12th in terms of recoverable crude oil. This location is quite sheltered, both due to its location between two landmasses with relatively close proximity to both shores, as well as the shallow water depth.

### 2.5.2 Kara Sea

A more exposed location in Russian territory will also be considered in this study. The East-Prinovozemelsky field is located in the Kara Sea, east of Novaya Zemlya. No development is known to be occurring here yet, however in 2010 licenses for exploitation were awarded to Rosneft, who have announced a partnership with ExxonMobil for the exploitation of this field (Rosneft, 2013). In the terms of Gautier et al. (2008) assessment the field is located in the West Siberian Basin province, which ranks first in terms of total recoverable hydrocarbons and 7th in terms of recoverable crude oil. A centered location in the Kara Sea was chosen to represent the area given by Rosneft (2013).

# CHAPTER 3
# Theoretical Background

This chapter will outline the basic theoretical knowledge required to perform oil spill trajectory modelling in an Arctic environment. The dynamics of the Arctic Ocean and sea-ice are discussed in Sections 3.1 and 3.2, with reference to implementation by the MITgcm model. Sections 3.3 and 3.4 introduce the processes governing the fate and behaviour of crude oils in this environment, and the aspects of these processes that must be included in an accurate, complete spill trajectory forecast.

## 3.1 General Arctic Oceanography

In this section the general oceanographic principles which could influence oil spill trajectories in the Arctic Ocean will be introduced. The predominant large-scale circulation patterns give an indication of the drift direction of oil accidentally released into the water and covering sea ice, as well as predict areas of vertical movement of oil that is trapped below the water surface. After the main circulation patterns are introduced, the equations of motion used by MITgcm to model ocean dynamics, including these currents, will be discussed. It should be noted that Arctic Ocean circulation is changing due to the earth's warming climate, however a review of what these changes might look like and the factors involved is beyond the scope of this study (Morrison et al., 2000).

### 3.1.1 Large-scale Circulation

The predominant, relevant horizontal circulation in the interior of the Arctic Ocean basin is divided into the Beaufort Gyre and the Transpolar Drift. The Beaufort Gyre is an anticyclonically recirculating system over the Canadian Basin, which is bordered by the continental shelves of the Canadian Archipelago, Alaska, the Lomonosov Ridge, and the East Siberian and Chukchi Seas. This current intensifies near the Alaskan shelf, however an undercurrent in the reverse direction (eastward) exists on the continental slope in this area as well.

The Transpolar Drift runs from the East Siberian and Laptev Seas across the North Pole and eventually into the North Atlantic. It returns water that has entered the Arctic Ocean basin from both the North Atlantic and the Pacific.

The in- and outflows of the Arctic Ocean basin can be grouped into three areas, the Fram and Bering Straits, and the Canadian Archipelago. Water from the Pacific Ocean enters through the shallow Bering Strait. Once this water has reached the Chukchi Sea the flow splits into two arms, one broad, weak current that flows westward towards the East Siberian Sea and a narrower, stronger current that flows eastward along the Alaska shelf towards the Canadian Archipelago. Most of this flow exits the Arctic Ocean through the archipelago and is returned to the Atlantic (Jones, 2001). The majority of the exchange of waters between the North Atlantic and Arctic Oceans occurs between the landmasses of Greenland and Norway. Warm, relatively salty Atlantic water enters through the Barents Sea, as well as on the west coast of Svalbard. This water generally flows eastward into the Kara and Laptev Seas. The majority of the outflow from the Arctic Ocean occurs through the Fram

Strait on the east coast of Greenland. This current also exports significant quantities of sea ice. Zonal deviations of these flows contribute to significant large-scale recirculation in this area (Carmack, 1990). These circulation patterns are summarized in Figure 3–1.

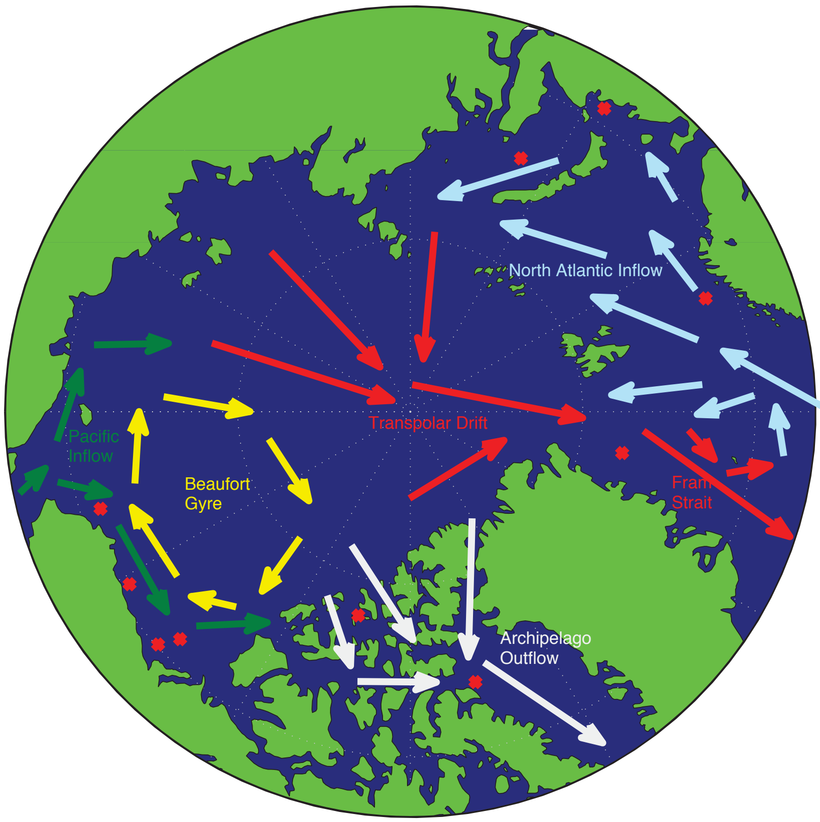


Figure 3–1: Generalized pattern of large scale Arctic Ocean Circulation. Arrows are not to scale and indicate direction only.

### 3.1.2 Equations of Motion

The 3D dynamics of the ocean and atmosphere are ideally represented by the full, compressible Navier-Stokes equations. However, the yet-unsolved turbulence closure problem involved in a full analytical solution requires numerical approximation. Given current computational limitations, a full numerical solution of these equations is generally not reasonably achievable for a coupled atmosphere-ice-ocean general circulation model. Hence approximations are made to simplify the governing equations. In this section the approximations to these equations made in the MITgcm model are discussed and the governing equations of motion used by the model are presented.

The model employs the Boussinesq approximation. This means that variations in the density of the working fluid are considered small and can therefore be neglected, except in the calculation of gravitational acceleration and the equation of state, which is the relationship between density, temperature, pressure, and salinity (moisture) for the ocean (atmosphere). To achieve this, density is split into a constant reference density $\rho_0$ and a small variation $\rho = \rho(\theta, S, p)$ where $\theta$ is temperature, S is salinity (humidity) in the ocean (atmosphere) and p is pressure. $\rho$ is only considered in the aforementioned two calculations and density is approximated as $\rho_0$ everywhere else (McWilliams, 2006). MITgcm uses the same set of equations for both the atmosphere and ocean, written in terms of a general vertical coordinate 'r'. In the ocean 'r' is interpreted as depth, z, and in the atmosphere as pressure, p. However, since historical wind data was used to force the model in this study and therefore the atmospheric solution was not calculated by MITgcm other than the stress generated on the ocean surface by the historical wind, only the oceanic equations will be considered here. Only the principal equations will be presented; the reader is referred to Marshall et al. (1997a,b) for the complete formulation. In their most general vector form the oceanic governing equations can be written as follows.

$$
\begin{aligned}
\frac{D\vec{v_h}}{Dt} + (2\vec{\Omega} \times \vec{v})_h + \nabla_h \phi = F_{\vec{v_h}} \\
\frac{Dw}{Dt} + \hat{k} \cdot (2\vec{\Omega} \times \vec{v}) + \frac{\delta\phi}{\delta z} + \frac{g(\rho - \rho_0)}{\rho_0} = F_w \\
\nabla \cdot \vec{v} = 0
\end{aligned}
\tag{3.1}
$$

Here $\vec{v_h}$ are the horizontal components of velocity u and v, w is vertical velocity, $\vec{\Omega}$ is the Earth's rotation, $F_{\vec{v_h}}$ and $F_w$ are atmospheric forcing and non-conservative dissipation in the horizontal and vertical, such as viscous dissipation of energy, and $\phi$ is the geopotential, defined as $\frac{p}{\rho_0}$. All other symbols retain their traditional definitions. The first two equations describe the conservation of momentum in the horizontal and vertical, and the third equation describes the conservation of mass in a fluid that is considered incompressible. In the momentum equations, the first term on the left-hand side describes advection, the second term the force due to the Earth's rotation, or Coriolis force, and the third term describes pressure gradients in the working fluid. The last term on the left-hand side of the vertical momentum equation describes vertical accelerations due to buoyancy induced by density fluctuations.

MITgcm permits several further approximations to the pressure field that will be briefly introduced here. First, the geopotential is split into surface, hydrostatic, and non-hydrostatic parts.

$$
\begin{aligned}
\phi(x, y, r) = \phi_s(x, y) + \phi_{hyd}(x, y, z) + \phi_{nh}(x, y, z) \\
\frac{\delta\phi_{hyd}}{\delta z} = -\frac{g(\rho - \rho_0)}{\rho_0}
\end{aligned}
\tag{3.2}
$$

Using this, the momentum equations can be re-written in spherical coordinates as follows.

$$
\begin{aligned}
&\frac{\delta u}{\delta t} + \frac{\delta \phi_s}{\delta x} + \frac{\delta \phi_{hyd}}{\delta x} + \epsilon_{nh}\frac{\delta \phi_{nh}}{\delta x} \\
&\qquad = -\vec{v} \cdot \nabla u - (\frac{uw}{r} - \frac{uv \tan\varphi}{r}) - (-2\Omega v \sin\varphi + 2\Omega w \cos\varphi) + F_u \\
&\frac{\delta v}{\delta t} + \frac{\delta \phi_s}{\delta y} + \frac{\delta \phi_{hyd}}{\delta y} + \epsilon_{nh}\frac{\delta \phi_{nh}}{\delta y} = -\vec{v} \cdot \nabla v - (\frac{vw}{r} - \frac{u^2 \tan\varphi}{r}) - 2\Omega u \sin\varphi + F_v \\
&\epsilon_{nh}\frac{\delta w}{\delta t} + \frac{\delta \phi_{nh}}{\delta z} = -\vec{v} \cdot \nabla w + \frac{u^2 + v^2}{z} + 2\Omega u \cos\varphi + F_w
\end{aligned}
\tag{3.3}
$$

New terms introduced here are the distance from the centre of the Earth, r, and latitude, $\varphi$, along with $\epsilon_{nh}$, a non-hydrostatic parameter defined in Marshall et al. (1997b). Equation 3.3 is simplified for the hydrostatic and quasi-hydrostatic formulations of MITgcm. In the quasi-hydrostatic version, the advection and forcing terms, the first and and fourth term on the right-hand side, are dropped from the vertical momentum equation. To obtain the hydrostatic approximation, all terms on the right-hand side of the vertical momentum equation are dropped, along with the first metric term arising from conversion to spherical coordinates, second term on right-hand side, in both horizontal momentum equations. Finally, the vertical component of Coriolis force in the zonal momentum equation, $2\Omega w \cos\varphi$, is eliminated. While implementation of all formulations is possible in MITgcm, the hydrostatic solution was used in this study. Therefore the final equations used to calculate the motion of the ocean in this study are as shown below.

$$
\begin{aligned}
\frac{\delta u}{\delta t} + \frac{\delta \phi_s}{\delta x} + \frac{\delta \phi_{hyd}}{\delta x} + \epsilon_{nh}\frac{\delta \phi_{nh}}{\delta x} &= -\vec{v}\cdot\nabla u + \frac{uv\tan\varphi}{r} + 2\Omega v\sin\varphi + F_u \\
\frac{\delta v}{\delta t} + \frac{\delta \phi_s}{\delta y} + \frac{\delta \phi_{hyd}}{\delta y} + \epsilon_{nh}\frac{\delta \phi_{nh}}{\delta y} &= -\vec{v}\cdot\nabla v + \frac{u^2\tan\varphi}{r} - 2\Omega u\sin\varphi + F_v \\
\epsilon_{nh}\frac{\delta w}{\delta t} + \frac{\delta \phi_{nh}}{\delta z} &= 0
\end{aligned}
\tag{3.4}
$$

Since the effect of temperature and salinity on the density of water is considered here, additional equations must be considered to form a closed set. The equations governing the advection and diffusion of temperature and salinity are.

$$
\begin{aligned}
\frac{\delta \theta}{\delta t} &= -\nabla\cdot(\vec{v}\theta) + F_\theta \\
\frac{\delta S}{\delta t} &= -\nabla\cdot(\vec{v}S) + F_S
\end{aligned}
\tag{3.5}
$$

The terms $F_\theta$ and $F_S$ represent sources and sinks of temperature and salinity (Marshall et al., 1997a,b).The equation of state relates these two variables to pressure to determine density variations. Due to it's complexity, it is approximated by a higher order polynomial, as given in Jackett & McDougall (1995), and will not be repeated here. The equation of state, together with Equations 3.2 and 3.4 forms a closed set that is solved for the dynamics of the ocean.

For completeness, it should be stated that the advection and diffusion of tracers, such as oil, is calculated by the standard advection-diffusion equation.

$$
\frac{\delta \tau}{\delta t} + \nabla(\vec{v}\tau) = \nabla\cdot(\vec{K}\nabla\tau) \tag{3.6}
$$

The vector $\vec{K}$ specifies the horizontal and vertical diffusivities of the tracer, $\tau$ (Adcroft et al., 2014). More information on the implementation of these equations specific to this study is given in Section 5.2.

### 3.2 Sea Ice Theory

The Arctic Ocean basin is partially covered by sea ice at all times, and during the winter months this coverage extends over the vast majority of the basin. Therefore the interaction of spilled oil with sea ice will have a significant influence on oil spill trajectories in this area. In this section the physical principles governing the presence and movement of sea ice will be introduced. Since an extensive review of sea ice behaviour modelling is beyond the scope of this study, only the algorithms used in the MITgcm will be described. First the sea ice dynamics, i.e. the motion of the ice under the influence of external forcing, will be introduced, followed by an overview of the mathematical description of the ice's rheology, its response to stress. The response to thermodynamic forcing, growth and melting of the ice cover, will be considered next. Since the most severe adverse affects from an oil spill occur at coastlines, this section will conclude with a discussion of landfast ice, which is ice that is frozen to landmasses near the coast.

#### 3.2.1 Dynamics

The movement of sea-ice occurs under the influence of several parameters. This is easily illustrated by examination of the momentum equation of the sea-ice model within MITgcm. This equation is based on the work of Zhang et al. (1998) and Campin et al. (2008).

$$m\frac{D\vec{v_h}}{Dt} = -mf\hat{k} \times \vec{v_h} + \vec{\tau}_{air} + \vec{\tau}_{ocean} - m\nabla\phi(0) + \vec{F} \qquad (3.7)$$

The term on the left-hand side gives the momentum of the sea-ice, with m being the combined mass of ice and snow and $\vec{v_h}$ the horizontal components of velocity. The first term on the right-hand side is the influence of the horizontal components of the Coriolis force, with f being the Coriolis frequency $2\Omega \sin \varphi$. The second and third terms are the air-ice and ocean-ice stress. The fourth term on the right-hand side is the contribution of the gradient of sea surface height, i.e. the local tilt of the ocean surface. $\phi(0)$ is the sea surface height potential, which is defined as follows.

$$\phi(0) = g\eta + \frac{p_a}{\rho_0} + \frac{mg}{\rho_0} \tag{3.8}$$

$\eta$ is the variation in water level due to hydrodynamics alone, $p_a$ is atmospheric pressure, and g is the acceleration due to gravity. In full, this quantity can be interpreted as a pressure term, a unit energy acting on the ocean surface due to oceanic dynamics ($g\eta$), atmospheric pressure loading ($\frac{p_a}{\rho_0}$), and ice and snow loading ($\frac{mg}{\rho_0}$) (Campin et al., 2008). Finally, the fifth term $\vec{F}$ represents the divergence of the internal ice stress, which is discussed further in the next section. But before proceeding to a discussion of sea-ice rheology, an observation that is useful with respect to this study can be made. This is that the term $\vec{\tau}_{ocean}$ causes a reciprocal stress in the ocean surface layer, but in the opposite direction. By this, as well as the inhibition of direct momentum transfer from the atmosphere to the ocean, the presence of sea ice slows the currents in the ocean surface layer and hence the transport of a surface oil slick moving with the ocean currents (Zhang et al., 1998).

### 3.2.2 Rheology

The sea-ice rheology algorithm employed by MITgcm is based on the original work of Hibler (1979, 1980) with refinement by Zhang & Hibler (1997) and Zhang et al. (1998), as well as improvements on the numerical schemes made by the authors of MITgcm (Adcroft et al., 2014). According to the review by Drozdowski et al. (2011), a significant number of ice-ocean models in use today are based on this body of work. Other models exist, but for brevity they will not be discussed here.

In addition to the dynamical component, this model computes the internal ice stress, the mean thickness of the sea-ice cover and the fraction of ocean covered by ice. This model assumes isotropy in the sea ice, which is appropriate for the interior of the ocean but not ideal near coasts where interaction with coastlines and landfast ice causes fractures in the sea-ice to have a preferred direction parallel to the coastline. This is a major criticism of the formulation, especially with respect to oil spill trajectory modelling, which is mostly done in areas relatively close to land. However, to date no sea-ice models that adequately represent this behaviour have been implemented in an operational ice-ocean model (Drozdowski et al., 2011). Using this assumption of isotropy, the ice stress tensor, as used in the calculation of $\vec{F}$ in the momentum equation, can be related to the ice strain rate/deformation and ice strength through a viscous-plastic response assumption and the specification of bulk and shear viscosities of the ice. This formulation ensures little strength under diverging stress, and high strength under converging stress. For the complete formulation of the rheological model the reader is referred to the original literature and Adcroft et al. (2014).

The ice strain rate, which is computed from the velocity shears, is also used in the calculation of the mean ice thickness and area covered by sea-ice. To accomplish this the sea-ice is split into two categories, thin and thick ice. Thin ice is assumed to be responsible for the formation and closing of leads, i.e. areas of open water, under diverging/converging strain conditions. In this model thin ice does not contribute to the mean ice thickness. Mean ice thickness, h, and area covered, A, are calculated by the following continuity equations.

$$\begin{aligned} \frac{\delta h}{\delta t} &= -\frac{\delta uh}{\delta x} - \frac{\delta vh}{\delta y} + \Gamma_h + D_h \\ \frac{\delta A}{\delta t} &= -\frac{\delta uA}{\delta x} - \frac{\delta vA}{\delta y} + \Gamma_A + D_A \end{aligned} \tag{3.9}$$

The $\Gamma$ terms are thermodynamic source/sink terms which are responsible for ice formation and melt due to ambient temperature. They are discussed in more detail in the next section. $D_h$ and $D_A$ are added diffusion terms which ensure numerical stability of the algorithm, as described in Hibler (1979).

### 3.2.3 Ice Growth and Decay

Many mathematical descriptions of the formation and melting of sea-ice exist, and several are implemented within MITgcm, however for this study the relatively basic model described in Hibler (1980) is used. It will be the only model discussed here, as a detailed review of sea-ice modelling is beyond the scope of this study.

The basics of this model can be summarized as follows. The main considerations are the temperature difference at the air-sea interface and lateral mixing of heat in the oceanic surface boundary layer. Vertical mixing of heat from lower layers of the ocean is considered by a constant flux. Based on the temperature difference at the air-sea interface, a growth/decay rate for ice of zero thickness is formulated by attempting to balance the heat budget between the two media. If ice is already present, a linear temperature profile through the ice sheet is assumed. The potential presence of snow is accounted for by modifying the surface albedo of the ice cover, following Zhang et al. (1998). This 'zero thickness' rate represents ice growth if the rate is positive and the temperature of the surface layer of the ocean has reached the freezing temperature of seawater, and no change if the rate is negative. If the conditions for growth are met, ice forms if none was present, and thickness is added to existing ice sheets. If the rate is negative, the absorbed heat from the atmosphere is allowed to mix laterally and may cause melting if it reaches locations where ice is present. The 'zero thickness' growth rate is then used in conjunction with the thickness of the local ice cover, if present, to determine growth rates for all possible thicknesses of ice at the location under consideration and these rates are used to calculate the $\Gamma$ terms in Equation 3.9. Once again, the reader is referred to Hibler (1980) for the complete mathematical formulation of the algorithm.

### 3.2.4 Landfast Ice

Currently all active and anticipated oil and gas wells in the Arctic Ocean basin are relatively close to coastlines, on continental shelves and slopes. Due to this, and the fact that the most severe adverse effects of oil spills occur when the spill reaches a coastline, landfast ice is an important, and unique, feature when assessing oil spill trajectories in the Arctic Ocean. Unfortunately MITgcm currently does not include landfast ice, however it is discussed here for completeness and to facilitate consideration in future work. Landfast ice is an immobile ice cover that forms near coastlines due to a combination of accumulation of mobile pack-ice and in-situ freezing. This generally occurs in water depths of 10-180m. Drozdowski et al. (2011) reports that in the Canadian Beaufort Sea the edge of landfast ice generally coincides with the 20m isobath which occurs approximately 5-50km from the coast. However, in Siberia landfast ice has been reported to extend hundreds of kilometres into the ocean, due to the large extent of the continental shelf in this area. Landfast ice is generally a seasonal phenomenon which forms slowly during the onset of winter, and may be unstable for some time before reaching a stable configuration. Once temperatures start to warm above freezing, landfast ice usually retreats rapidly, though multiyear landfast ice has been observed at some locations in the Canadian Archipelago and the Siberian Taymyr Peninsula (Mahoney et al., 2007). A feature of landfast ice that may have considerable impact on oil spill trajectories are Stamukhi. These are areas of significant deformation within the ice that form at the interface of landfast and mobile drift ice. The deformations extend down into the water column, forming an inverted dam that may serve as a barrier to the spread of an oil slick from either side (Drozdowski et al., 2011).

### 3.3 Characteristics of Oil in Water

Now that the dynamics of the Arctic Ocean environment have been introduced, the ways in which spilled oil interacts with these dynamics, and the Arctic environment in general, must be considered. First, the influence of the type of oil and how the properties of these oils evolve in the environment will be discussed. Horizontal movement through spreading on the water surface and advection by the ambient currents will be introduced next, followed by a discussion of factors to be considered when modelling oil spill trajectories in the unique Arctic environment. This leads into Section 3.4, which explains the ways that spilled crude oil can interact with sea ice. The following two sections are not intended to be exhaustive reviews of the physical and chemical interaction and fate of crude oils with the Arctic environment, but rather to highlight the considerations for spill trajectory modelling that arise from these interactions. Due to the complexity of integrating these processes into a coupled atmosphere-ice-ocean model, the majority of them were not considered in the modelling done for this study. They are given here for illustrative purposes only, and to facilitate inclusion in future modelling efforts.

### 3.3.1 Oil Types

The properties of crude oil vary based on the location in which they are found. Since knowing the exact properties of the crude oil in an area is not possible until the well has been drilled, and analysis of oils for spill-related properties was not common during the initial stages of Arctic oil exploration (SL Ross, 2010), only Alaska North Slope (ANS) crude oil will be presented here for illustrative purposes. This oil has been produced in Alaska since the 1960's and an extensive analysis of it's properties is available in Wang et al. (2003). Gearon et al. (2014) also used this oil as the representative oil in their spill trajectory modelling study, which is discussed in Section 4.3.2. The main characteristics of concern for spill trajectory modelling are density, weathering behaviour, and kinematic viscosity. The effect of these properties will be described later in this section, though these effects were not considered explicitly in this study. However, before proceeding it should be stressed that while only one type of oil is presented here, and the effect of it's properties has not been included in this study, the exact properties of the oil must be known in order to provide accurate operational trajectory forecasts.

### 3.3.2 Advection

Advection is the main mechanism by which spilled oil moves in space and time (ASCE, 1996). For open-ocean surface slicks, oil is generally accepted to be advected by ocean surface currents that are unaffected by the presence of an oil slick, provided that the slick is thin (Tsahalis, 1979). Whether this assumption holds for very cold environments, where slick thicknesses are known to increase significantly, remains to be determined. Ocean surface currents contain a significant contribution from surface wind, but also from other components, such as background currents from interior circulation patterns like those introduced in Section 3.1, density gradients, and Stokes' drift, which is a mean current induced by differences in water surface levels due to wave action. In numerical modelling studies, advection by currents generally includes components due to wind stress, mean velocity due to pressure and density gradients, tidal currents, Stokes' drift, as well as a parameterized component due to turbulent diffusion. The contribution of wind stress is included in the output of a coupled atmosphere-ice-ocean model, such as MITgcm. For many earlier modelling efforts, currents were derived from circulation models which did not consider the surface layer of the ocean. In these models the contribution of wind was parameterized by addition of a vector representing a fraction of the wind speed acting at an angle to the ocean current (ASCE, 1996). This is an empirical representation of the Ekman layer, the mathematical description of which is given in Chapter 6.1 of

McWilliams (2006). Experiments deriving these values are documented in papers such as Tsahalis (1979).

### 3.3.3 Spreading

Spreading is the term used to describe the tendency of oil on water to form a thin, continuous slick. It does so under gravitational, inertial, viscous, and surface tension forces (SL Ross, 2010). Many mathematical formulations exist to describe this, however an extensive review of these theories is beyond the scope of this study, since the focus here is on advection. For a more thorough treatment the reader may start with the reviews of Yapa & Dasanayaka (2006) and Reed et al. (1999).

Most current oil spill models operate using a spreading model based on the work by Fay (1969, 1971). Hence this will be the only work discussed in detail here, but only for illustrative purposes. It has been recognized that this model is inadequate to fully represent the spreading process, since it does not account for oil viscosity, external influences such as waves, and the formation of the thin mono layer at the outer events of the slick, as described by DiPietro & Cox (1979) (Reed et al., 1999).

Fay (1969) describes the axi-symmetric spread of an oil slick on perfectly still water to be the result of a balance between the driving forces gravity and surface tension, and retarding forces due to inertia and viscosity. Since these forces do not all govern simultaneously, the spreading process is divided into three phases, each governed by a different force balance. In the initial phase of the spill, gravity and inertial forces dominate. An order of magnitude estimate of this force balance is given by,

$$A \sim (\Delta g V t^2)^{\frac{1}{2}} \tag{3.10}$$

Here A is the area of the slick, $\Delta$ is the fractional buoyancy of oil, $\frac{\rho_{water}-\rho_{oil}}{\rho_{water}}$, g is the acceleration due to gravity, V is the volume of oil spilled, and t is the elapsed time. This phase persists until the thickness of the slick, $h \sim \frac{V}{l^2}$ is equal to the thickness of the viscous ocean surface boundary layer induced by the motion of the oil, $\delta$. At this point the viscous forces become greater than the inertial forces, resulting in the following balance.

$$A \sim (\frac{\Delta g V^2 t^{\frac{3}{2}}}{\nu^{\frac{1}{2}}})^{\frac{1}{3}} \tag{3.11}$$

Here $\nu$ is the kinematic viscosity of water. Transition from this stage to the final stage of spreading, where surface tension balances viscous forces, occurs when the slick reaches a critical thickness, $h_c \sim (\frac{\sigma}{\Delta\rho_{water}g})^{\frac{1}{2}}$, and this thickness is equal to the ocean boundary layer $\delta$. $\sigma$ is the net surface tension per unit volume of oil. Fay (1969) notes that this is unlikely to occur in a natural setting since the viscous retarding force will stop the spread before surface tension becomes significant. However, the resulting balance will be mentioned here for completeness.

$$A \sim (\frac{\sigma^2 t^3}{\rho_{water}^2 \nu})^{\frac{1}{2}} \tag{3.12}$$

The above relationships can be fitted to experimental data using proportionality constants.

For example, SL Ross & DF Dickins (1987) proposed the that the right-hand sides of Equations 3.10 - 3.12 be multiplied by proportionality constants 4.1, 6.6, and 16.6 to fit the equations to their observed field data. However, these coefficients are likely to vary with local ice conditions. Fingas & Hollebone (2003) recommends making the following adjustment to account for the viscosity of oil and the fraction of ice cover.

$$A_{\mu I} = [\frac{\mu_{oil}}{\mu_{water}}]^{-0.15}(1 - f_I)^A \tag{3.13}$$

In this correction, $A_{\mu I}$ is the corrected area, $\mu$ is the absolute viscosity, $\rho\nu$, and $f_I$ is the ice concentration.

Spreading depends on many external factors and a large-scale spill such as the ones described in this study may encounter a variety of environmental conditions. Therefore a single spreading model may not be appropriate for all areas of the spill at all times. Buist et al. (2009) recommends a combination of empirical spreading models for various aspects of the slick, based on the results a four-year laboratory testing program.

Several researchers have also formulated spreading theories based on oil as a viscous fluid that conserves mass and momentum. Yapa & Chowdhury (1990) describe a model for spreading under ice based on the Navier-Stokes equations and Gjosteen (2004) describes a model for spreading in cold water.

### 3.3.4 Weathering Effects and Vertical Movement

The vast majority of crude oils are lighter than Arctic Ocean water, which has an approximate density of $1029 kg/m^3$. The only crude oils with the potential to be heavier than this are extra-heavy crude oils, defined by the World Energy Council to have a density between that of freshwater ($1000 kg/m^3$) and $1045 kg/m^3$, and a reservoir viscosity greater than 100 Poise. The WEC's 2010 Survey of Energy Resources reports no known offshore deposits of extra-heavy crude oil, and the most recent 2013 edition makes no mention of new discoveries (WEC, 2010). Therefore all in-reservoir oil will be considered to be buoyant in water here.

After removal from the reservoir, the density of oil may change due a number of influences. Oil that is exposed to sunlight will partially evaporate, increasing the density of the remaining fraction. Evaporation rates vary by oil type and are affected by the presence of snow and ice. For example, Wang et al. (2003) gives the evaporation rate of Alaska North Slope Crude under no influences other than the sun's radiation as,

$$\%Ev = (2.86 + 0.045T)\ln t \tag{3.14}$$

Here %Ev is the weight fraction that is evaporated, T is the oil surface temperature in °C, and t is the elapsed exposure time. Buist et al. (2009) presents general equations to account for the effects of ice and snow on evaporation rates. In general, evaporation will increase both the density and viscosity of the remaining oil. For the case of ANS crude, density at 0 °C increases from $877.7kg/m^3$ for in-reservoir oil to $945.7kg/m^3$ for 30.5% evaporation. Viscosity increases from 0.232 Poise to 42.3 Poise (Wang et al., 2003).

Ambient temperature also has a significant effect on the physical properties of an oil. In general, density and viscosity of the oil increase with decreasing temperature. The magnitude of this increase depends on oil type and degree of evaporation and general mathematical relationships to predict this are not easily formulated. An interesting feature of crude oil that significantly affects its spreading properties is the 'pour point', or temperature at which oil ceases to flow under gravitational force. At or below this temperature, oil can essentially be considered to behave as a solid that is transported only by advection with currents or ice (Drozdowski et al., 2011). The pour point of oil also varies with degree of evaporation. For ANS crude, the pour point in-reservoir is -32 °C, however this increases up to -6 °C for oil that is 30.5% evaporated (Wang et al., 2003).

When crude oil is released in water, water-in-oil emulsions may form, which alters the physical behaviour of the spill significantly (Fingas, 2009). Emulsions are characterized based on their water content, which determines the stability of the emulsions, i.e. the time required for it to break down. Emulsification also depends on the type of oil and degree of evaporation. Wang et al. (2003) reports that ANS crude only forms emulsions with significant stability when the degree of evaporation reaches 30.5%. Generally, emulsification increases the density and viscosity of an oil (Drozdowski et al., 2011), and will cause the oil to behave in a non-Newtonian fashion, i.e. the viscosity becomes dependent on the shear rate (ASCE, 1996). It is therefore a process that must be considered in order to accurately forecast the trajectory of an oil spill.

The final method by which the characteristics of spilled oil may change is interaction with sediment, or other particles, in the water. This is also used as a cleanup method, by addition of mineral fines to a surface oil slick. Oil will coat the fine material, forming so-called OSA's (Oil-Suspended Particulate Matter-Aggregate), thereby reducing the size of oil droplets and preventing the re-formation of a slick. This serves to enhance dispersion and re-entrainment into the water column which increases biodegradation of the oil (SL Ross, 2010). Formation of OSA's is also a concern for trajectory modelling in areas where sediment concentration is high, such as the Mackenzie Delta. In these locations significant quantities of oil may be re-entrained into the water column, especially when turbulent mixing energy is high, for example due to a storm. It is also because of this principle that most oil spill trajectories cease the simulation when oil comes in contact with a shoreline, or seafloor, though the review by ASCE (1996) suggests that this approach may be too simplistic (Drozdowski et al., 2011).

Both intentional OSA formation and dispersant application are intended to clean up oil spills by dispersing slicks into small droplets. This, as well as the possible increases in density mentioned above, increases potential for vertical movement of the oil. OSA's may sink simply because their density is greater than that of the surrounding water. Surface oil with a relatively high density may also be re-entrained by vertical currents due to strong wind and wave action, or even deep convection if the density of the oil is less than that of one of the involved waters. Oil with a relatively high density at depth, for example due to emulsion formation after a well blowout, may be trapped in the subsurface and be advected by currents different from those on the ocean surface. It is therefore important that the vertical distribution of the oil be accurately modelled for such cases, for example through use of a plume modelling suite like ADMS (Advanced Deepwater Modelling Suite), formulated by Poojitha Yapa and colleagues.

### 3.3.5 Arctic Considerations

Since many of the above processes are directly or indirectly a function of temperature, spills in the Arctic will behave differently than spills at more temperate latitudes. Details of interactions of spilled oil with the Arctic ice cover are discussed in the next section, but even where ice is not present, the cold temperatures of the Arctic will serve to increase the density and viscosity of spilled oil. The reduction in viscosity, as well as the formation of a wax layer at the oil-water interface, serves to slow the gravitational spreading of oil, and in the case of extreme temperatures can even reduce oil transport to purely advective processes. Due to conservation of mass, the reduction in slick area implies that a thicker slick is formed (Drozdowski et al., 2011). The effect of evaporation is also lessened, by the sheltering effect of ice and snow as well as the lack of sunlight during the Arctic winter (SL Ross, 2010; Fingas et al., 2006).

### 3.4 Behaviour of Oil in Ice-Infested Waters

The purpose of this section is to give insight into the small scale processes through which oil may interact with ice. As mentioned previously, the length scales of these processes cannot be resolved using currently available numerical atmosphere-ice-ocean and oil spill trajectory models, due to limitations in available computing power. The parameterizations used by current models, as well as the present study, to represent these processes are discussed in Section 4.1. However, the processes of the actual interaction will be introduced here to facilitate inclusion in future models. First, interaction and transport with mobile drift ice is discussed, followed by a review of the potential interaction with landfast ice and the possible impact on shorelines that may result from these interactions.

#### 3.4.1 Interaction with Mobile Drift Ice

Khelifa (2010) reports that a summary of one of the most thorough literature reviews of the behaviour of oil in ice-infested waters is given in Fingas & Hollebone (2003). The information presented in this section is drawn from this work, with updated information added as required from the reviews of Drozdowski et al. (2011) and Khelifa (2010).

If the ice cover is only partial when the oil is introduced at the ocean surface, the oil may be trapped in areas of open water, also known as leads. Due to its buoyancy, oil under the ice will migrate towards the area of open water and collect there, forming slicks that are thicker than those in open water. Oil slicks up to 150mm thick were observed during an actual spill event in broken ice conditions. Leads hence serve to contain the oil and limit the spread of the spill, however only until the ice cover either closes or breaks up, or the oil is swept out of the leads by strong surface currents. It has been found that if the ice cover closes, only part of the oil will be encapsulated in the ice sheet, and the remainder will be displaced. MacNeill & Goodman (1987) proposed that if leads close sufficiently quickly, the oil may be 'pumped' to the surface of the ice sheet. However, the closure rate required for this phenomenon to occur, reported as $\sim$12 cm/s, is unlikely in a natural setting and therefore the oil will likely be forced under the ice surface instead (Fingas & Hollebone, 2003). Cammaert (1980) studied the displacement of oil trapped in leads by surface ocean currents. The findings showed that this was possible in a laboratory setting, but no data on field tests confirming these results has been found.

In denser ice covers, it is likely that much of the oil will become trapped under ice sheets. Fingas & Hollebone (2003) summarize several laboratory studies aiming to establish relationships for the movement of oil under an ice sheet. However, these studies were conducted under smooth ice sheets, which are unlikely to occur in a natural setting, and therefore the derived relationships are unlikely to apply to actual oil spill scenarios and will not be considered further here. Instead focus will be on two field studies conducted to study the movement of oil under first-year sea-ice in the Beaufort Sea.

NORCOR (1975) studied the spread of oil under ice with nine releases between the end of October and the end of May. The tests were conducted in a bay, sheltered from large-scale circulation, in six to ten meters of water under ice thicknesses ranging from 38 to 195cm. The oil was found to form a slick under the ice sheet and migrate towards the nearest under-ice cavities. Once the nearest cavity was filled, the oil would 'overflow' into the next cavity. Glaeser & Vance (1971) had also observed this phenomenon in some of the first experiments conducted on oil spreading in an Arctic environment, four years earlier. Buist et al. (2009) conducted testing to determine the surface currents required to re-mobilize oil from these under-ice cavities and found the following empirical equation.

$$U_{th} = C_i(\frac{305.79}{88.68 - \mu_0}) \tag{3.15}$$

Here, $U_{th}$ is the 'stripping' velocity in cm/s, $\mu_0$ is the viscosity of the oil in Poise, and $C_i$ is an under-ice roughness factor (1=smooth, freshwater ice, 2=saline ice, 3=freshwater ice with cavities, 4=saline ice with cavities, 6=refrozen, rubble ice). This may be an important consideration for future modelling efforts, since a volumetric approach quantifying under-ice roughness is a good way to parameterize transport of oil trapped under ice sheets in the absence of high-resolution ice profiles. However, the under-ice oil slicks were found to only remain under the ice briefly, and were encapsulated in the growing ice sheet within days. Drozdowski et al. (2011) gives encapsulation times ranging from 18-72 hours, based on a number of studies done in the 1980's. Once encapsulated the oil was found to remain in place, until brine channels started to form with the onset of melting. Brine channels are vertical channels that form when the saline layer at the top of the ice sheet melts, and the denser, saline meltwater migrates downward through the ice sheet (Martin, 1979). Vertical movement of the oil was first noticed in February, with the rate of movement increasing until April, when the oil rapidly reached the ice surface. A lens of oil moving upward through 150cm of ice in less than hour was reported for this rapid, final phase.

Dickins et al. (1981) performed similar testing, but released compressed air along with oil to simulate a release of natural gas, as would occur during a well blowout. This is an important consideration since Purves et al. (1978) found, using laboratory methods, that the presence of gas during an oil spill significantly enhances spreading of oil under an ice sheet. In the modelling effort by Wotherspoon et al. (1985) this was accounted for by multiplying the area of the under-ice oil slick by a factor of seven, based on field observations during an actual spill. Dickins et al. (1981) found that the release of gas caused heaving and fracturing of the ice sheet, which facilitated venting of the gas. This process was less severe during the melt season, when more fractures and vertical channels were already present in the ice. As in the study by NORCOR (1975), vertical movement of encapsulated oil was insignificant until the ice began to melt. Oil released in December surfaced in early June, and oil released in April and May surfaced in mid-June.

Buist et al. (2009) also studied vertical movement of oil encapsulated in ice sheets. Here, oil as well as water-in-oil emulsion were encapsulated in first-year ice. As previously, the oil migrated to the surface through brine channels, however the emulsion did not migrate, and did not reach the surface until the ice melted to the level where it was encapsulated.

It's notable that little testing has been done on oil behaviour in multi-year ice. Fingas & Hollebone (2003) reports that Comfort et al. (1982) conducted such testing in the Canadian high Arctic. Oil was found to migrate here as well, though at a slower rate since there are fewer interconnected brine channels (Drozdowski et al., 2011).

It has been found that oil encapsulated in, or trapped on top of, an ice sheet also affects the thermodynamic properties of the ice. NORCOR (1975) postulated that the encapsulated oil may have accelerated ice melt by one to three weeks.

Any oil that is trapped in leads, on the ice surface, in cavities under the ice, or encapsulated in the ice sheet will be advected with the ice, rather than the ocean currents. Due to the inhibition of momentum transfer from the atmosphere to the ocean by the ice sheet, oil moving with ice will likely be advected farther than oil moving with ocean surface currents.

### 3.4.2 Interaction with Landfast Ice

The general properties of landfast ice were introduced in Section 3.2.4. While all considerations for drift ice also apply to landfast ice, the lack of mobility of landfast ice, as well as it's higher roughness due deformation caused by interaction with drift ice, must be considered. Allen & Nelson (1981) report on field and laboratory testing done on oil spills in the landfast ice zone in 1979/80 and found that oil on or under landfast ice will be largely immobilized and confined to a relatively small area. On ice, spreading of the oil will be inhibited by snow, and any oil that does reach open leads will collect to an appreciable thickness in these leads before migrating underneath the ice surface. Any oil that is released under the landfast ice, or migrates there will be contained in the signficant under-ice cavities. Allen & Nelson (1981) cite a study by prepared by Nortec that gives water currents relative to landfast ice as being slow to non-existent, with values ranging from 0-10 cm/s. A 'worst-case' comparison with Equation 3.15 for fresh ANS crude at 15°C ($\mu_o$=0.115 P) with an under-ice roughness factor of 6 yields a 'stripping' velocity of 20.7 cm/s. This required velocity increases significantly as temperatures decrease and the oil is weathered. Currents are unlikely to be strong enough to mobilize oil trapped in under-ice cavities. Any oil that is mobilized would eventually be prevented from reaching the open ocean by the Stamukhi, the inverted dams formed by extensive deformation at the landfast ice edge. However, the oil will only remain immobilized while the landfast ice is stable, and may quickly be released to the open ocean once the melt season begins, or it may retreat with the landfast ice and reach the coast at this time (Drozdowski et al., 2011).

# CHAPTER 4
# Literature Review of Spill Modelling

The general physical principles that require consideration in a thorough oil spill trajectory model for ice-infested waters have now been established. The first section of this chapter will review the methods by which these processes have been represented in past oil spill trajectory models. Confidence in these modelling efforts cannot be established without evaluation against tests or observed spills of opportunity in the natural environment, since as Fingas & Hollebone (2003) established, laboratory testing is unlikely to fully reproduce the conditions encountered by an oil spill in ice-infested waters. The second section of this chapter is dedicated to summarizing significant results of such evaluation studies. The chapter is concluded by a summary of two recent modelling efforts for potential oil spills in the Canadian Beaufort Sea and a brief discussion of the advantages and disadvantages of the utilized modelling approaches.

## 4.1 Oil Spill Trajectory Modelling in Ice

An ideal oil spill trajectory model for ice-infested waters would consist of a physical and chemical fates model for the oil which considers all processes described in Section 3.3, coupled to a robust, field-verified atmosphere-ice-ocean circulation model that is able to resolve features in the ice field at a scale of 1-10m. Thereby the model would be able to explicitly account for the oil-ice interactions described in Section 3.4, using analytical equations derived from first principles of dynamics to model the physical interactions. However, given current computational limitations, such a model is not likely to be produced in the foreseeable future. Until such a model becomes computationally feasible, processes occurring at the sub-grid scale must be parameterized. Some of the parameterizations employed in existing oil spill models for ice-infested waters will be presented in this section. As Gjosteen et al. (2003) noted, information on the exact algorithms used in many widely utilized oil spill trajectory models can be very difficult to obtain. A good example of this is the commercial OILMAP software, the manual for which was available for public consultation until at least 2013. After a re-structuring of the developer's website, this manual is no longer available for review. Therefore much of the information presented below is taken from review papers on the subject, with original publications referenced where possible. For these detailed reviews of oil spill in ice modelling, the reader is referred to the reviews of Khelifa (2010), who presents an excellent treatment of the algorithms used to calculate oil advection, Yapa & Dasanayaka (2006), who present a thorough treatment of the modelling of oil spreading in the presence of ice, as well as the reviews of Drozdowski et al. (2011), SL Ross (2010), Gjosteen et al. (2003), Reed et al. (1999), and ASCE (1996).

### 4.1.1 Representation of Oil

Drozdowski et al. (2011) gives an excellent summary of the three different ways that oil has been represented in numerical models in the past. Essentially an oil slick can be described by a collection of Lagrangian particles, by Eulerian consideration of grid cells, or a hybrid of these two methods.

In the Lagrangian approach each particle is assigned an initial location and mass. All particles are considered independent and are subjected to advection as well as random 'kicks' to simulate spreading and dispersion due to turbulence (Gjosteen, 2004). In this approach it is important to realize that the end result is a statistical description of the spill extent and therefore it must be ensured that the number of particles used in the simulation is adequate to provide realistic statistics for the area occupied by the slick.

For the Eulerian tracer approach, the model domain is divided into fixed grid cells and the extent of the spill is represented by the number of grid cells it occupies at any given time. Fluxes between the cells are calculated based on the velocity field in addition to the spreading and dispersion algorithms. The oil properties in each cell are updated based on ambient conditions and empirical formulae describing weathering processes. Since high spatial resolution is required to accurately represent the extent of the spill this approach is considered to be more computationally expensive than particle-based approaches. An example of this formulation can be found in the OILBRICE model, developed by El-Tahan and colleagues in the 1980's.

The third approach utilizes 'spillets' to represent the oil slick. These spillets can be considered to be particles with additional degrees of freedom. The extra degrees of freedom can be used to represent thickness or spreading of the spillet. Gjosteen et al. (2003) reports that the spillet and particle approaches are the most widely used (Drozdowski et al., 2011).

### 4.1.2 Advection

As described in Sections 3.3.2 and 3.4.1, oil slicks at the ocean surface are advected by the ocean currents, and sea ice where it is present. The majority of currently available models for predicting oil spill trajectories in ice derive the ocean currents from offline runs of 3-D hydrodynamic models. Since circulation models cannot resolve the current component due to Stokes' drift from waves with a wavelength shorter than two grid spaces, some spill trajectory models, such as the one proposed by Johansen et al. (1995), calculate this component separately using a high-resolution wave model. The Stokes' drift contribution to surface current is then added to the component calculated by the main hydrodynamic model prior to calculating the oil spill trajectory (Khelifa, 2010). Where the hydrodynamic model does not consider the surface layer of the ocean, a fraction of the wind speed is added at a specified Ekman veering angle, as discussed in Section 3.3.2.

Advection with mobile drift ice has been treated in several different ways by different models. When the need for oil spill trajectory modelling in sea ice first became apparent in the 1980's, some existing open-water trajectory models were adapted for use in ice-infested waters by adding rules for interaction with ice to the model formulation. The most commonly used rule is to assume that oil at the water surface begins to be advected with the sea ice when the ice concentration exceeds 30%. Oil is assumed to be unaffected by the presence of ice at lower ice concentrations. Venkatesh et al. (1990) justifies this assumption by examining observed data from two spills of opportunity as well as the observations of SL Ross & DF Dickins (1987). This approach is also used to parameterize spreading and weathering behaviour of oil in ice, as will be discussed in the following section. Some models that utilize this approach to parameterizing advection are OILMAP as developed by Applied Science Associates, OILBRICE as described in Venkatesh et al. (1990), the modelling work of Hirvi et al. (1992) for an oil spill in the Gulf of Finland in 1987, the model developed by Petit (1997) for the Weddell Sea in Antarctica, and the model by Gastgifvars & Koponen (2001). Some of these models, namely OILBRICE and Petit (1997), where formulated specifically for use in ice-infested waters and therefore account for more detailed oil-ice interactions, such as encapsulation. However the principles used in partitioning drift with ocean currents and ice are still based on ice concentration (Khelifa, 2010).

Several models have also attempted to model the transport of oil with sea ice by statistical means. Examples of this approach are the work of Colony (1986) and Johansen (1989); Johansen et al. (1995) as described in Khelifa (2010). The approach taken by Colony (1986) models ice motion as a sequence of successive, independent, random events. Because of this assumption the model can only be considered applicable over large length and time scales, since at small scales these events become dependent. Johansen (1989); Johansen et al. (1995) describes a model in which oil is modelled as particles, and the interaction of the particles with ice is treated by assigning a state of interaction with the ice, such as 'trapped under ice', 'on ice floe', etc. At each time step a probability for transferring between states is assigned based on the particles history, position, and state of weathering. This approach is similar to the approach of the OSCAR model developed by SINTEF and described in Aamo et al. (1997) and Reed et al. (1995) (Gjosteen et al., 2003; Drozdowski et al., 2011).

The most recent model development effort discussed in Khelifa (2010), is one supported by the Engineering Advancement Association of Japan, with the goal of developing a spill trajectory forecasting system for ice-covered waters in Japanese territory. The approach used here is to compute ice concentration and velocity in a coarse grid and use the results of this as boundary conditions for a nested, finer grid in which oil spill behaviour and trajectory are computed. All oil behaviour is based on the solution of the momentum equations, which is promising for calculating spreading behaviour, and this will be elaborated on in the next section, however the authors assume that drift of the oil slick is the same as the ice drift, i.e. all oil moves with the ice at all times. This supports the conclusion of Reed et al. (1999) that oil drift with ice must be parameterized, even at length scales considered to be very small for an ice-ocean model (maximum resolution here was 2km x 2km). Reed et al. (1999) suggests that accurately modelling the interaction of oil and ice is not possible until model resolutions can be reduced to 1-10m. Until then an approach based on ice concentration is likely best, however improvements can be made on existing algorithms, for example by accounting for encapsulation and oil migration to the ice surface by considering oil mass present in a model cell, ice growth rates, and ice concentrations. Partitioning of oil moving with ice and ocean currents can also be improved by considering oil masses trapped in under-ice cavities and surface currents required to mobilize this oil, given by relationships such as Equation 3.15. This process could also be scaled based on ice coverage.

### 4.1.3 Spreading

Few complete formulations of the spreading algorithms used in models for oil spill trajectories in ice have been published and it is likely that the detailed approaches used in existing models vary significantly, based on the vast number of theories that have been formulated. Again, since spreading is not a focus of this study implementation will only be discussed in broad terms here. Essentially spreading can be treated in three possible ways: empirically, analytically, or parameterized.

Empirical formulations, such as models fitted to the relationships proposed by Fay (1969, 1971), based on various field and tank tests make up the majority of spreading algorithms employed in trajectory models to date. Advantages of this approach are the relative simplicity and light computational demands, as well as the ability to represent a variety of ice conditions by varying the formulation and tuning parameters. For example, as SL Ross & DF Dickins (1987) found, oil spreading behaviour changes drastically in the presence of slush or brash ice, compared to open-water or broken ice conditions. On the other hand, this variety of formulations and sensitivity to tuning parameters also brings the ability of the empirical method to produce accurate forecasts into question. Choosing the correct formulations is highly dependant on accurate forecasts of ice conditions and formulations must be derived with use in Arctic environments in mind, since the spreading behaviour changes drastically in ice and cold temperatures, as is emphasized in the description of the OILBRICE model by Venkatesh et al. (1990).

The analytical approach is based on treating oil as a viscous fluid and calculating its spread in ice based on conservation of mass and momentum. Examples of this can be found in Yapa & Chowdhury (1990), Gjosteen (2004), and the Japanese forecasting work by Rheem & Yamaguchi (2004); Ano et al. (2005); Hara et al. (2008); Kawauchi et al. (2010) (Khelifa, 2010). While this approach likely has a lot of potential and a strong appeal in terms of physical correctness, the demands it places on the quality of the ice forecast are likely excessive at this time. Since the ice provides physical boundary conditions for the oil slick, features of the ice must be well-resolved which is not feasible on significant geographic scales with the current generation of atmosphere-ice-ocean models. In the absence of well-resolved ice features, boundary conditions of the slick would need to be parameterized in order to apply this approach in a natural setting. It is doubtful that the accuracy gained by this approach with parameterized boundary conditions is significant enough to warrant the added computational expense when compared to skillful application of empirical methods. However, research on these methods must be continued so that they may be implemented when ice forecasts are available at a resolution that renders it feasible to do so.

The third approach referred to, parameterized spreading, was encountered in the recent modelling effort by Nudds et al. (2013), which will be discussed further in Section 4.3.1. Here spreading is modelled simply by increasing diffusivity of the tracer in the utilized ice-ocean model, which allows for an approximation of spreading without requiring any input parameters. However, since the diffusivity is seemingly independent of any of the physical properties of the spill, this should be considered to be a qualitative description of spreading behaviour only.

## 4.2 Field Verification

Reproducing Arctic environmental conditions within a laboratory setting is difficult at best. Fingas & Hollebone (2003) showed that often empirical relationships for oil spreading in ice-infested waters which are developed in a laboratory/test tank, do not hold in natural environments. Studying the advection and spreading of crude oil in an Arctic field setting is not easily done due to regulatory and logistical difficulties, however several tests have been carried out since the 1970's. Dickins (2011) lists all known field experiments on oil in ice up to 2011. Of these tests, most focused on the spreading behaviour of oil and detailed interactions with the ice, such as NORCOR (1975), rather than advection with the ice. Since the focus of this study is on advection, these tests will not be described in detail here. The most relevant, and well-cited field experiment of modelling oil spill trajectories in ice with modern tools is the work of Reed & Aamo (1994). This work will be described in detail later. Several other experiments are also worthy of a brief mention.

Trites et al. (1986) attempted to hindcast the trajectory of the oil spill from the *Kurdistan* in Cabot Strait, NS in 1979, using a particle approach that only considered advection and spreading. While the results of the modelling were approximate at best when compared to recorded observations, an important conclusion could be drawn. Trites et al. (1986) found that wind is the governing factor in oil spill advection, and storms can cause significant advection. Background currents play only a secondary role, though it is suggested that their role may become more significant with increasing spill duration.

SL Ross & DF Dickins (1987) studied the behaviour of oil in drift and slush ice with three $1m^3$ spills of Alberta crude offshore from Cape Breton Island. The oil was only tracked for 5 hours, and moved ~5 km during that time, and therefore should be considered too short for detailed studies of the advection behaviour of oil in ice. Some useful general observations were made though. SL Ross & DF Dickins (1987) used a vector addition of the mean currents plus 3% of the wind speed with a 10° rotation to the right to predict the trajectory. Venkatesh et al. (1990) used a dynamic approach, solving the equations of motion with measured and calculated currents and wind as forcing inputs, to hindcast the observed trajectory. They reported that the method of SL Ross & DF Dickins (1987) produces a trajectory that is oriented too far to the left. Their results are either to the right, or the left of the observed trajectory as well, depending on whether measured or calculated currents were used, though the bearing is generally more accurate than that produced by SL Ross & DF Dickins (1987). The method of Venkatesh et al. (1990) overpredicted the magnitude of advection of the oil spilled in slush ice, highlighting the strong influence of ice conditions on drift trajectories.

Sørstrom et al. (2010) also conducted extensive field testing in drift in near Svalbard, however this work focused on the effectiveness of countermeasures and no trajectory models were tested.

### 4.2.1 MIZ '93

MIZ '93 was a field oil spill experiment conducted by SINTEF in the Barents Sea marginal ice zone (MIZ) in April 1993. 26 tonnes of crude oil were released from a research vessel at a location determined through prior OILMAP modelling to result in oil spill trajectories that minimized environmental impact while maximizing potential to study oil spill behaviour in partial ice covers. Reed & Aamo (1994) performed the initial modelling and attempted to forecast the trajectory of the released oil throughout the experiment using the OILMAP software. Forecasts were compared to the trajectory of a surface drifter released with the oil in the ice pack.

The initial modelling was done by manually inputting an averaged ice field for the study area in April, as well as fifty randomly selected wind velocity fields for the area for the month of April, taken from a data set covering the years 1981-1990. The resulting fifty trajectories were then used to compute probability distributions for the trajectory from each potential release site. Reed & Aamo (1994) also note that a mean background and tidal current field for the area were input for these runs, however the mean background current did not seem to affect the trajectories. They concluded that the surface currents in this area are driven primarily by winds and tides, confirming the conclusion of Trites et al. (1986), and they therefore neglected background currents in their forecasting model.

For the forecasting process the authors report that the model performed well during the first three days of the experiment, with ice concentrations of 60 - 90% and relatively low winds (3-7 m/s) directed 'off-ice'. Setting the tuning parameters of wind contribution to surface layer drift to 2.5% of wind speed at an Ekman veering angle of 35° to the right reproduced the actual trajectories quite well. On the fourth day the winds were reported to strengthen to ~10 m/s and shift direction 'on-ice'. At this point the model results diverged from observations and the tuning parameters were changed to 1.5% of wind speed and 60°. Forecasting was carried out continuously throughout the experiment, with the model being updated whenever new wind forecasts or ice data from helicopter observations became available. Tuning parameters for forecasting were established each day by hindcasting the trajectory using observed wind data. Through comparisons of forecasts and hindcasts Reed & Aamo (1994) show that the input wind fields have a significant effect on model accuracy and hence accurate wind forecasts are essential for accurate oil spill trajectory forecasts.

On the fourth day of the experiment, when the winds shifted 'on-ice', it was observed that the winds caused sea ice to pile up, forming a keel that extended vertically into the water column. Reed & Aamo (1994) report this as the reason for the required change in tuning parameters at this time, since the piled up ice caused the wind stress to be distributed over a deeper portion of the water column, which caused a decrease in wind contribution to velocity and increase in Ekman veering angle.

From their forecasting experiment, Reed & Aamo (1994) conclude that simple parameterizations for oil weathering and advection in ice provide reasonable trajectory models, however accurate wind forecasts and an ice rheology model that is able to treat ridging and pile-up are critical to providing accurate forecasts.

Johansen et al. (1995) also attempted to reproduce the spill trajectory from this experiment with their model. They concluded that their model did not adequately represent the decrease in dispersion and weathering effects observed for an oil slick in ice, compared to open water. Other conclusions were that wave damping by the ice cover was not well accounted for and that the spatial resolution of the model was too coarse (Khelifa, 2010).

## 4.3 Recent Arctic Modelling Efforts

To conclude this literature review, two recent modelling studies on oil spill trajectories in the Canadian Beaufort Sea will be summarized. These studies will later serve as comparisons to the results of the modelling effort undertaken in this study. The first study by Nudds et al. (2013) follows an approach similar to the one in this study, using a coupled atmosphere-ice-ocean model to track particles representing the oil spill. The second study by Gearon et al. (2014) follows a more 'traditional' approach to trajectory modelling, using user-specified environmental data to calculate the trajectory and weathering of the spilled oil. It is desirable to fully incorporate such an oil fates model into a coupled atmosphere-ice-ocean model, however given current limitations this is not yet feasible. Hence both approaches have significant advantages and disadvantages at this time and both require consideration here.

### 4.3.1 Nudds *et al.* 2013

Nudds et al. (2013) modelled potential spill trajectories from the offshore oil and gas exploration lease in the Canadian Beaufort Sea described in Section 2.1.1. Results of the present study will be compared to those obtained by Nudds et al. (2013) in Section 7.1.1. Spills were initialized at the beginning of January, April, July, and October and tracked for three months in each case. The modelling was done by first deriving the ocean and sea ice velocity fields using the ARC118 atmosphere-ice-ocean model. Oil trajectories were then computed separately for the ocean and ice using an offline, Lagrangian particle tracking scheme for an arbitrary number of particles.

No mention is made of the physical properties of these particles, i.e. whether they are passive or active, buoyant tracers. 3D current fields are used to compute the ocean trajectory, however no mention is made of buoyancy effects.

Spreading is simulated by assigning a diffusion coefficient to each particle. The diffusion coefficient was varied with season/temperature to represent the retardation of spreading by cold temperatures. The diffusion coefficients used in the ice trajectory calculation were 10-50% of those used for the ocean trajectory to represent the inhibited spreading behaviour of oil in ice. However, no clear indication of how the diffusion coefficients were chosen with respect to oil volume and spreading properties is given, and the authors acknowledge that more research is needed in this area. Until this research is completed and a clear mathematical relationship for formulating such a spreading coefficient can be given, this method should only be considered as a qualitative representation of spreading behaviour. A valuable conclusion drawn from this representation of spreading behaviour is that spreading can influence advective trajectories, if the oil spreads far enough to encounter a current shear, i.e. currents flowing in different directions, like those found at the interface of the eastward Pacific inflow and the westward Beaufort Gyre circulation off Alaska's North Slope.

The ARC118 atmosphere-ice-ocean model used in computing the velocity fields in this study is derived from the general circulation model NEMO (Nucleus for European Modelling of the Ocean). It is set up to cover the Arctic Ocean basin at an $\sim$6 km spatial resolution, though the authors note that the resolution increases away from the North Pole and is $<$6 km in the Canadian Beaufort Sea. The difference between the velocity fields calculated by this model and those of a $1/6^{\circ}$ model are compared and it is shown that increasing the spatial resolution resolves prominent eddies near the Alaskan coast and produces higher local currents near the Alaskan Continental Slope. The potentially significant impact of these features on oil trajectories leads to the conclusion that high resolution is necessary for accurate oil spill trajectory forecasting. The authors also state that Arctic atmosphere-ice-ocean models often overestimate the sea ice velocity. In this study the sea ice velocity was adjusted to observations by tuning the air-ice drag coefficient.

Forcing was provided by the Common Ocean-Ice Reference Experiments (CORE2) data set. First, the model was spun up for 10 years using the 'normal-year', i.e. averaged, forcing of this set. Runs were then completed using this 'normal-year' forcing as well as records for the years 1998-2000, in order to show interannual variability. It was concluded that interannual variability is significant, with little overlap in the trajectories, and therefore the use 'normal-year' forcing is not adequate for risk assessment.

In general, the study concludes that oil trajectories in ice are significantly shorter than in water during the winter months and only become comparable when ice floes become more mobile at the onset of summer. The trajectories in water and ice were found to not be co-located. For the Winter, Spring, and Summer scenarios the oil was advected eastwards, towards Banks Island, though it did not reach the coast in any of the 3-month simulations. In the Fall scenario advection occurred westwards towards Alaska. The authors attribute this to a weakening Pacific inflow during this time of year which increases the influence of the Beaufort Gyre.

Since using coupled atmosphere-ice-ocean models for oil spill trajectory modelling has only recently become computationally feasible, these models are still in a very early stage of development. Other than stating that evaporation, weathering, and emulsification are not considered, which would likely cause an overestimation of the quantity of oil at the ocean surface, Nudds et al. (2013) make no mention of the oil-ice interaction algorithms or the physical representation of oil through the particles, so no comment can be made on the treatment of many of the processes described in Sections 3.3 and 3.4 by this model. The argument for the utilized spreading algorithm could be improved significantly by establishing a clear relationship between the diffusion coefficient and the properties of the oil, as well as environmental conditions such as temperature and ice presence. A grid spacing of 6km with an assumed equilibrium slick thickness of 1 mm, based on the observations presented in Table 1 of Venkatesh et al. (1990), corresponds to an oil volume of ∼226,400 bbl of oil per grid cell. This is significantly more than most of the probable discharges identified by the literature review of Gearon et al. (2014). Based on their reported volumes, this volume of oil could only be exceeded in one grid cell in the case of a complete tanker spill, or a worst-case discharge well blowout with little to no advection away from the spill site. Therefore it cannot be clearly established that spreading is a significant process at the grid spacing used in this study.

#### 4.3.2 WWF 2014

Gearon et al. (2014) performed a modelling study of four hypothetical oil spills in the Canadian Beaufort Sea for the World Wildlife Fund. The study considered four generalized spill scenarios; a shipping accident in the eastern Beaufort, a spill resulting from a shipping accident or pipeline leak near the Canada - US border, a well blowout in shallow water on the continental shelf, and a well blowout in deep water on the continental slope. For each scenario individual trajectories were computed based on likely release times and durations, volume and type of oil spilled, and likely countermeasures to be implemented. These trajectories were then grouped and used to produce probability distributions of contamination for each set of release conditions under varying environmental conditions. Evolution with time and mass balances were also presented for a representative trajectory for each set of conditions. Probability distributions for the deep well blowout scenario are compared to the results of this study in Section 7.1.1.

The oil spill trajectory model used in this study is the Spill Impact Modelling Application (SIMAP), developed by RPS Applied Science Associates (RPS ASA). The model utilizes user-specified environmental conditions to compute Lagrangian trajectories of spillets, resulting in an output of oil mass per unit area at the ocean surface and oil concentration in the subsurface. It includes a physical fates model which considers advection and spreading of the surface slick, as well as entrainment into the water column and movement at depth. To compute initial vertical distribution for the deep well blowout scenario, SIMAP was coupled to RPS ASA's plume model, OILMAPDeep. SIMAP's physical fates model also considers oil weathering and natural degradation, as well as shoreline interaction, Oil-Suspended Particulate Matter-Aggregate (OSA) formation, and re-suspension. Common oil spill countermeasures such as in-situ burning and dispersant application can also be considered.

In this study the extent of the oil slick was defined by two different sets of concentration thresholds. The first set, said to represent oil concentrations having an impact on human activities and requiring cleanup, was defined by concentration thresholds of $0.1g/m^3$ for oil in a slick at the ocean surface, and $1g/m^3$ for oil impacting a shoreline. The second set, said to describe concentrations posing a significant threat to wildlife, was given by concentrations of $10g/m^3$ for surface oil and $100g/m^3$ at shorelines. Gearon et al. (2014) also include biological impacts in their study, however this is beyond the scope of this review and will not be described here.

SIMAP has reportedly been extensively validated against field observation, though Gearon et al. (2014) do not list any examples of verification against spills which occurred in ice infested waters. Here, interaction with ice was treated by parameterizations described earlier. Surface oil is assumed to be advected completely with ocean currents for ice concentrations less than 30% and completely with the ice field for ice concentrations greater than 30%. Changes to spreading and weathering behaviour are also determined based on ice concentration. These processes are assumed to be unaffected by ice presence at ice concentrations less than 30%. For intermediate ice concentrations between 30% and 80% weathering effects are decreased linearly and the equilibrium thickness of the oil slick is increased proportionally to the ice concentration in the spreading calculation. At ice concentrations greater than 80% neither spreading nor weathering occur. The model also considers landfast ice, by immobilizing any oil that comes in contact with the landfast ice in water depths less than 2 m, and storing it at the contact location until the ice retreats. If the water depth is greater than 2 m, the averaged thickness of landfast ice, the oil may be advected underneath the landfast ice with the specified currents. The authors acknowledge that the parameterizations for oil-ice interaction are approximate and may not be fully accurate.

The input environmental data for this study, which considered the period between April 2008 and March 2013, was gathered from several sources. Daily mean three-dimensional current fields, as well as ice velocity and concentration, are provided by TOPAZ4, which is a coupled ice-ocean data assimilation project by the Nansen Environmental and Remote Sensing Center (NERSC). The authors acknowledge that the resolution of this data is too coarse to represent some near-shore features such as the counter-current to the Beaufort Gyre at the Alaskan Coast, which is also mentioned in Nudds et al. (2013), and the freshwater plume in the Mackenzie Delta. It is also noted that studies have found the sea ice velocities provided by TOPAZ4 to be too fast by $\sim$3 km/day. The vertical density structure of the ocean is taken from the World Ocean Atlas. Mean monthly landfast ice extent is derived through a synthesis of two data sets by the Bureau of Ocean Energy Management (BOEM) and Mahoney with the National Snow and Ice Data Center (NSIDC). Wind data was taken from the ERA-40 data set, which is a re-analysis on a 0.75° grid undertaken by the European Center for Medium-range Weather Forecast. The contribution of wind to oil drift is parameterized for ice concentrations less than 30% by adding 3.5% of the wind speed to the ocean currents at an Ekman veering angle of 20°. For ice concentrations greater than 30% the contribution of wind to oil drift is neglected.

Gearon et al. (2014) presented many results on the trajectories of oil from each scenario, possible environmental impacts, and countermeasure effectiveness. In the interest of brevity, only the general findings pertaining to the trajectories of oil advection will be repeated here. It was found that transport of oil over long distances is possible for the considered time frames. The shipping, and trans-boundary scenario spills were both tracked for 90 days. The shallow blowout scenario considered release durations between 30 and 90 days, with tracking for 60 to 120 days. Due to the difficulties inherent in responding to a blowout in deep water, this scenario considered releases between 60 and 120 days, which were tracked for 120 to 180 days. For each case the probability densities revealed that transport to the western boundary of the model domain, set at the international date line in the Chukchi Sea, is possible. Depending on the currents and winds some eastward trajectories into the Canadian Archipelago were also observed, as well as some north/south movement, though this was small compared to east/west movement.

Long transport distances generally correlated well with low oil concentrations, below the threshold for significant wildlife impacts. These potential low concentrations were observed over large areas of the probability distribution. The footprint of the higher threshold was much smaller, though observed to increase significantly for larger volumes of spilled oil.

Ice effects were summarized by stating that ice presence limited the spreading of oil, which is particularly evident in the deep blowout scenario as this release location is the furthest offshore. The authors also noted that the slowed weathering of oil in the presence of ice increased the spill's residence time at the ocean surface.

The major advantage of the approach taken in this study is the ability to model the physical properties of different oils and their change over time very well, due to the computational advantages of using a Lagrangian approach with user-specified environmental impacts. This can have significant effects on the extent of contamination, as is well demonstrated by the results of the shipping analysis. Two oils were considered, a heavy, viscous fuel oil and lighter diesel. The diesel evaporates more readily and hence the extent of the diesel spill was significantly less than the extent of the fuel oil spill for an equivalent volume.

Some criticisms of this approach are the way that ice interaction is treated, particularly spreading under ice, the parameterization of wind contribution to drift, and the resolution issues mentioned by the authors. As was demonstrated in Section 3.4.1, spreading does occur under ice sheets and should not be neglected in a numerical model if the equilibrium thickness, which may be estimated using the literature cited in this review, multiplied by the area of one grid cell exceeds the volume of spilled oil. That being said, under ice storage can lead to large oil thicknesses and for spatial resolution on the scale of kilometres a very large oil spill may be required before spreading becomes numerically significant. Since the authors do not state the grid spacing used in this study it cannot be concretely established here that neglect of under ice spreading lead to significant errors. Regarding the parameterization of wind drift, it was found by Reed & Aamo (1994) that the percentage of wind speed and Ekman veering angle are unlikely to remain constant over time in the presence of ice. From this it can be concluded that using a constant value of these parameters for a long simulation is likely to introduce error.

# CHAPTER 5
# Methods

Clearly, the concept of using a coupled atmosphere-ice-ocean to forecast oil spill trajectories in ice-infested waters has potentially significant advantages over using a traditional offline scheme. While offline schemes are currently far more advanced in the realistic representation of oil characteristics, it is thought that with a fully integrated, coupled model significant gains in accuracy are possible, especially for long-term simulations such as would be required for worst case evaluation of an Arctic spill scenario. These gains are realized through direct inclusion of wind drift in the hydrodynamic model, the potential for realistic representation of interaction of oil with evolving ice fields, and uniform resolution of ambient environmental conditions.

Until the ideal model described in Section 4.1 can be achieved, it is possible to work towards it by modelling the oil's behaviour within the framework of existing atmosphere-ice-ocean models and parameterizing the processes of Sections 3.3 and 3.4 by the methods of Section 4.1, or improved parameterizations as they become available.

This study is intended to be a step in this direction, by modelling the evolution of oil spills from the sites identified in Chapter 2 within the framework of the MITgcm. Modelling is done to the extent possible without modifying the MITgcm source code, as such modifications would not be feasible within a reasonable time frame. Additional offline calculations are performed in MATLAB as required to complete the trajectory modelling, and sea ice trajectories are validated by comparison with historical observations available through the IceTracker tool (Pfirman et al., 2013; Fowler & Tschudi, 2003).

Spills are initialized on November 1 of each year from 1980 to 2010 and tracked for one year. Oil is continuously added at the initialization location to represent a worst-case scenario. Here the worst-case scenario is considered to be a well blowout at the end of the drilling season that continues to release oil. Given that the well blowout in the Gulf of Mexico in 2010 took five months to cap (Weber, 2010), a year-long release is deemed justifiable considering that any efforts at capping the well during the winter months would be severely hindered by ice presence and harsh environmental conditions.

This chapter begins by introducing the procedure used in the modelling and the parameterizations and assumptions inherent in this procedure. Next, the MITgcm model is introduced in general terms, building on the discussion of the equations in Sections 3.1.2 - 3.2.3, and including the observational data-assimilated setup and historical wind forcing used. A spatial resolution of 18km was used to compute the advection of oil trajectories in the ocean, as well as the sea ice velocities and concentrations. The computational expense of higher resolution was found to be prohibitive within the scope of this study. The IceTracker tool used to validate these contaminated sea ice trajectories is briefly discussed in the next section. MATLAB routines were used to process the MITgcm output and and compute trajectories of contaminated sea ice and these are discussed in the final section.

## 5.1 Assumptions

Modelling oil spill trajectories at coarse resolution using the above procedure without modifying the MITgcm source code required several significant assumptions to be made. These assumptions, along with their justification and effects, will be described in this section, starting with assumptions in the advection calculations. These explanations will be illustrated with references to ANS crude oil, the properties of which were introduced in Section 3.3.4. The major assumption required here was to model oil as a passive tracer in the ocean, which does not allow for representation of the oil's density and viscosity. This in turn made it difficult to accurately consider spreading processes, though the neglect of these is shown to be acceptable at coarse resolutions. Finally, since density and viscosity were not represented in the model, weathering could not be represented since the effect of weathering is a change in density and viscosity. Because of the uncertainty introduced by the assumptions made, oil is not modelled quantitatively, but rather each grid cell is assigned a state of oil present/absent at each time step.

The tracer was initialized at the ocean surface, both because of the inaccuracies in subsurface oil behaviour introduced by the passive tracer assumption, and since attempting to represent the vertical stratification resulting from the complex plume dynamics of an oil and gas well blowout within the constraints of MITgcm and the utilized vertical resolution was deemed to introduce a computational effort that is unnecessary for the time being. It is unlikely that the horizontal deviation between the well location and the oil surfacing location would be significant compared to the spatial resolution of the model. In their field study of underwater oil and gas plume dynamics in the Norwegian Sea, Johansen et al. (2003) observed a horizontal deviation of ∼600 m, much less than one grid spacing.

To simulate a continuous release of oil at the spill site the tracer concentration in the corresponding grid cell is re-set to 1000 'units' at every time step. Presence of oil in a grid cell is defined by a specified tracer concentration threshold. Since it is difficult to objectively and accurately quantify the exact threshold of tracer corresponding to a quantity of oil which causes appreciable impacts, the contamination extents corresponding to three different thresholds (5, 50, and 200 'units') are investigated in this study. The lowest threshold, 5 'units', was chosen by visual examination of results from test runs to remove seemingly unphysical/noisy results, such as isolated small patches of oil presence and extremely small tracer concentrations that cannot reasonably be said to constitute oil presence. This is illustrated in Figure 5–1.

The higher thresholds were chosen to study the extent of areas of higher oil concentration, analogous to the procedure used by Gearon et al. (2014). The results of this analysis are given in Section 6.1.2.

### 5.1.1 Advection

The advection of the spilled oil was calculated using the passive tracer package of MITgcm. In this package the tracer is assumed to be neutrally buoyant, and the tracer evolution in each grid cell is calculated in an Eulerian fashion by Equation 3.6. Since ANS crude oil is lighter than water, with a density of $\sim 900kg/m^3$, the neutral buoyancy assumption will clearly introduce errors. Specifically, the residence

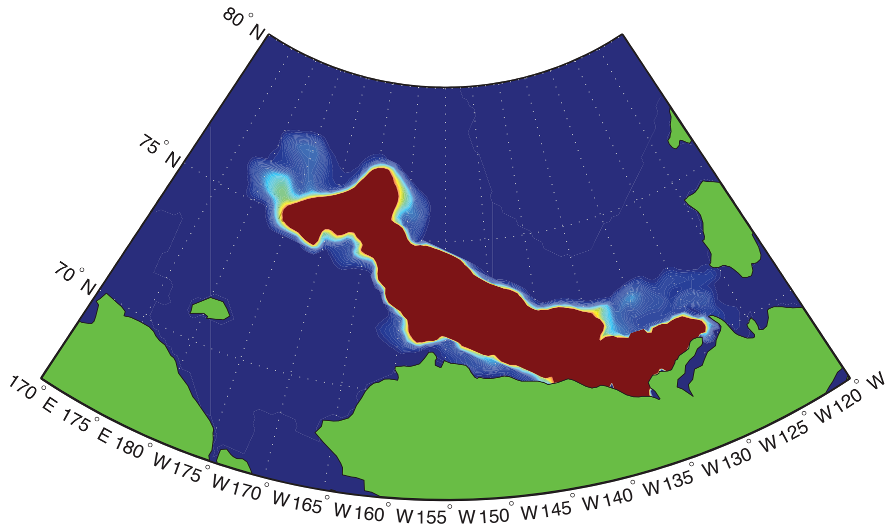


Figure 5–1: Area of oil presence defined by 5 'units' of passive tracer (burgundy) and removed, smaller tracer concentrations (contoured) for the Canadian Beaufort Continental Slope location. Note the small area of high tracer concentration near the threshold for oil presence at ∼135°W, 72°N.

time of an oil slick at the ocean surface will be underestimated, since the tracer will be more susceptible to entrainment into the water column than fresh oil would be.

The ocean component of advection includes currents induced by wind, interior circulation patterns, density gradients, and Stokes' drift caused by waves with wavelengths greater than two grid spaces, 36 km in this case. It is desirable for future works to reduce the error produced by the neglect of shorter wavelengths, either through utilizing higher spatial resolution, an appropriate parameterization, or both.

Advection of oil with ice is parameterized based on ice concentration, after Venkatesh et al. (1990) and Drozdowski et al. (2011). However since the proposition of Venkatesh et al. (1990) that oil is generally advected with broken ice fields of ice concentration greater than 30% has not been explicitly proven, three different ice concentration thresholds for advecting surface oil (20%, 30%, and 50%) are investigated in this study in order to evaluate the sensitivity of the results. In general, if the ice concentration in a cell is greater than the threshold mentioned above and oil is present in the ocean surface layer in this cell, the ice will be assigned a state of 'oil present'. However the ice does not remove oil from the ocean surface since it is unlikely that all oil in one grid cell will be trapped in the ice simultaneously at intermediate ice concentrations. The advection of the ice in this cell is then tracked in a semi-Lagrangian fashion until the ice concentration drops below the threshold and the oil is released back into the ocean. The algorithms used to calculate the advection by ice are described in more detail in Section 5.4.2.

This parameterization of oil advection with ice could certainly be improved, since it does not include any detailed oil-ice interactions such as encapsulation, under-ice storage, or trapping in leads. However employing more detailed parameterizations for these processes at coarse resolution is unlikely to result in significant gains in accuracy and is therefore left until higher resolution modelling is computationally feasible.

### 5.1.2 Spreading

The spreading of spilled oil into a thin slick at the ocean surface is not considered in this study. From the field observations summarized in Table 1 of Venkatesh et al.

(1990), a slick thickness of 1 mm is chosen as a conservative, representative oil slick thickness in waters where ice is present. At this thickness a slick that spreads over one 18km x 18km grid cell in open water conditions would contain a volume of oil of 324,000$m^3$ or ∼2,000,000 bbl. Such a volume of oil is deemed highly unlikely to be present in one grid cell, based on the literature review of Gearon et al. (2014). It is approximately four times the volume of the largest tanker considered by Gearon et al. (2014) and much larger than the worst-case discharge for a well blowout, identified as 60,000 bbl/day.

It is possible that spreading becomes important within the parameters of this study, if an extremely large quantity of oil is released under an ice sheet in an area that is very sheltered from currents, or if a slick is advected into an area of high ice concentration and oil is confined to the leads between ice floes. Neither of these cases were deemed likely enough to warrant explicit consideration in this study. In the first case the thickness of the formed slick would likely be larger than 1 mm due to under-ice roughness and cold temperatures under the ice sheet and therefore an even larger volume would be required to cover one grid cell. The second case would only represent a temporary condition since, as both Fingas & Hollebone (2003) and Hara et al. (2008) show, the oil would tend to migrate underneath, or potentially on top of, the ice sheet and therefore increase the area available for spreading.

It is thereby concluded that the neglect of the effects of oil spreading represents a trajectory error that is smaller than the spatial resolution of the model used in this study. By this analysis, gravitational spreading of oil will not become a significant process until the spatial resolution of the model is increased.

### 5.1.3 Weathering

Weathering of oil through interaction with the environment is not considered in this study. The neglect of changes to density and viscosity does not introduce additional error in the context of this study, since the oil is modelled as a passive tracer and spreading is not considered. The primary error introduced by neglecting weathering effects is overestimation of oil present at the ocean surface due to lack of evaporation. Under laboratory conditions the evaporation of ANS crude oil can be estimated by Equation 3.14. Using this equation with a oil surface temperature of -1°C, roughly 30% of oil mass evaporates in three months. As shown in Section 3.3.4, ANS Crude oil is still lighter than water at this degree of weathering Wang et al. (2003). When considering this, coupled with the slowing of weathering effects through sheltering by ice and snow, cold temperatures resulting in thicker oil layers, and lack of sunlight in the winter months (SL Ross, 2010; Fingas et al., 2006), it can be concluded that this error is acceptable for the time being, especially since oil is only represented in a qualitative manner. Loss of surface oil due to evaporation likely won't be significant until the latter part of the tracking period. The error must be acknowledged though, and certainly should be considered in future work.

## 5.2 MITgcm

The governing equations of the ocean and ice dynamics, as used by the MITgcm model, have been introduced in Sections 3.1.2 - 3.2.3. The model will now be introduced in more general terms. MITgcm is a numerical, finite volume model that may be used to study both oceanic and atmospheric processes. The usage of general 'r' coordinates allows one dynamical kernel to drive both sets of equations. It's ability to model complex bathymetry well, using volume-conserving partial cells, as well it's capability to run an adjoint simulation for a particular setup makes it very suitable to oceanic data assimilation studies, such as ECCO2. Model formulation began at the Massachusetts Institute of Technology in 1995 and has been carried on by a global user community since then. Packages allowing the study of sea-ice dynamics, tracer problems, and biogeochemical cycles have been added over time along with more general additions, such as different eddy parameterizations and vertical mixing schemes, and boundary condition types. It is set up to study a wide variety of problems of different scales, from local phenomena on a length scale of ~100m to global circulation patterns (Adcroft et al., 2014).

To obtain oceanic dynamics at each time step the model solves finite-volume discretizations of the horizontal components of Equation 3.4, Equation 3.5, the continuity equation, as well as the equation of state and the buoyancy relation contained in the second equation of 3.2. The model steps these discretizations forward in time using the Adams-Bashforth scheme. At every time step the sea-ice dynamics are solved using the result of the oceanic dynamics and specified external atmospheric forcing via the method proposed in Zhang & Hibler (1997). The tracer advection is also calculated using the oceanic dynamics and a user-specified numerical advection scheme. Details on the numerical schemes used can be found in Adcroft et al. (2014).

The model input parameters, except those described in Section 5.2.1, as well as the boundary conditions used to conduct this study were obtained from the work of the consortium Estimating the Circulation & Climate of the Ocean (ECCO). ECCO is a scientific partnership between the Massachusetts Institute of Technology, Jet

Propulsion Laboratory, Scripps Institute of Oceanography, and Atmospheric and Environmental Research. It's mandate in the current, second phase (ECCO2) is to work towards a fully-coupled state estimation of the ocean, sea-ice, biogeochmistry, and atmosphere, with a resolution high enough to resolve the length scale of mesoscale eddies (~5-200km) and ocean re-stratification processes. Essentially, this work involves development of the MITgcm model with continuing comparison of computational results with observations. Data syntheses are obtained by least-squares fitting of available satellite and in-situ data to the MITgcm model. As part of its results, ECCO has made various configurations of the MITgcm model available to the scientific community, and improved, higher-resolution configurations are becoming available with time (ECCO, 2007). The configurations are optimized by tuning control parameters to available observations of mean sea level, sea level anomaly, temperature and salinity profiles, sea surface temperature, and sea ice concentration, motion, and thickness. Control parameters are initial temperature and salinity conditions, atmospheric boundary conditions, background vertical diffusivity, vertical viscosity, bottom drag, albedo coefficients for ice, ocean, and snow, drag coefficients for the air-ice, ice-ocean, and air-ice interfaces, and the critical Richardson number for the Nonlocal K-Profile Parameterization (KPP) scheme, as formulated by Large et al. (1994), employed by this configuration of MITgcm to calculate vertical mixing in the ocean (Menemenlis et al., 2008).

The specific ECCO2 configuration used in this experiment is the 18km cubed-sphere grid formulation for the Arctic Ocean. In this configuration, the initial distributions of temperature and salinity in the model are taken from the publicly available

World Ocean Atlas 2005 (NODC, 2005). For all simulations no-slip bottom, free-slip lateral, and ocean free surface boundary conditions are used. At the in-/outflows, boundary conditions of potential temperature, salinity, ocean currents, and sea surface elevation are prescribed based on a the integration of a global circulation model, also based on the data of WOA05 (Menemenlis et al., 2005). Monthly averaged inputs from runoff are specified from the database of Lammers et al. (2001).

Atmospheric forcing to drive the model, via the external forcing package, for the study period was provided by the Japanese 25-year Reanalysis project (JRA-25). In this project, undertaken by the Japanese Meterological Agency, atmospheric conditions described by 42 variables were re-created on a 6-hour interval for the period 1979-2004. The analysis has since been carried on until 2014. This was done by analyzing satellite imagery and observational data from agencies around the world, and fitting the resulting data to a grid (Onogi et al., 2007). Seven of the available variables were adopted for use in this study, namely temperature and specific humidity two meters above the ocean surface, zonal and meridional winds 10 meters above the ocean surface, as well as incoming precipitation, longwave and shortwave radiation. To initialize the runs, the model was spun up for 14 years using a random permutation of this data from the years 1979-1992. These years were chosen to ensure that the resulting initial conditions were representative of conditions in the 1980's.

### 5.2.1 Customizations

For this study MITgcm needed to be modified to represent tracers continuously released from the locations described in Chapter 2, with properties as close to those of ANS crude oil as possible. This was accomplished through use of the passive tracer (PTRACER) and relax boundary conditions (RBCS) packages.

Setup of the PTRACER package required the choice of three parameters for the tracers, these being the numerical scheme used to solve for advection using Equation 3.6, and the horizontal and vertical diffusion coefficients. MITgcm offers six choices of numerical scheme for solving the tracer advection equation, ranging from relatively simple formulations like centered second-order space differencing with Adams-Bashforth time stepping to more complex methods like the non-linearly interpolating third-order direct-space-time (DST) method with limited flux and forward time stepping. Figures 2.14-2.16 in Adcroft et al. (2014) show that the four schemes which do not employ flux limiters are prone to producing false extrema, especially at large Courant numbers, i.e. high velocities with large time-to-space-step ratios. Since the computational savings achieved by these schemes do not justify introducing such errors, they will be disregarded from this point on. The two remaining schemes are second-order flux limiter, which is the MITgcm default, and third-order direct-space-time with limited flux. Both schemes are described in detail in Adcroft et al. (2014). To aid in the choice of an appropriate scheme calculations of a tracer being advected from two different locations were carried out for each scheme with otherwise identical parameters. The results are shown in Figure 5–2.

The schemes produce graphically very similar results. The only significant, noticeable difference is the longer extent of higher tracer concentration near Point Barrow, AK ($\sim$155°W) that is produced by the second-order flux limiter, which is likely more realistic than the sharp curve produced by the third-order limited

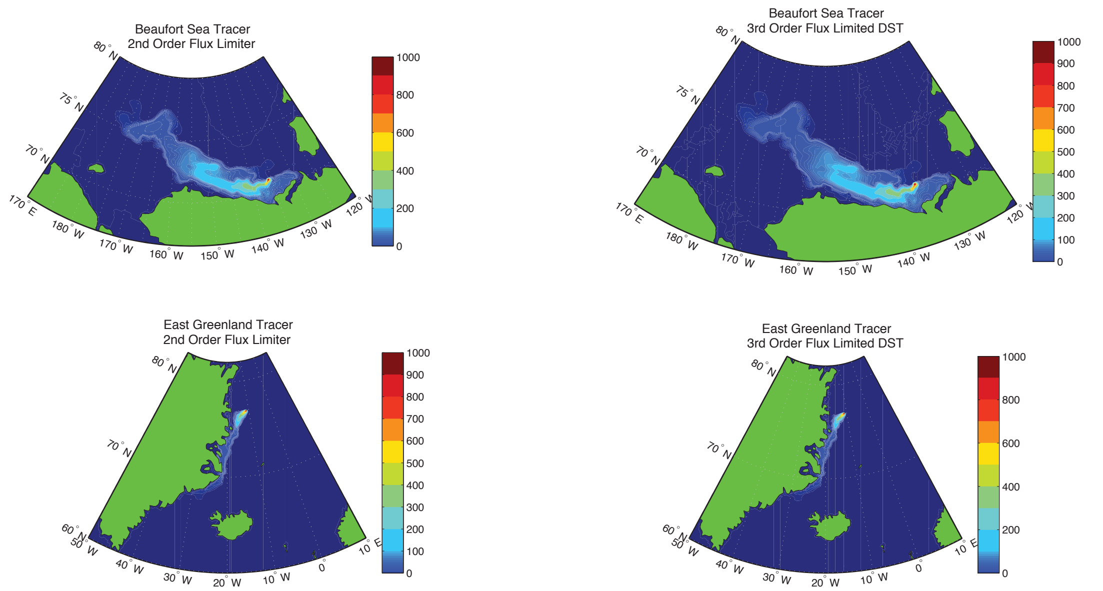


Figure 5–2: Comparison of performance of $2^{nd}$-order flux limiter (right) and $3^{rd}$-order flux limited DST (left) for tracer advection in Beaufort Sea (top) and East Greenland (bottom)

flux DST scheme. Examination of the numerical results also shows unrealistically extensive regions of low tracer concentration produced by the third-order scheme, which are far below any of the chosen concentration thresholds and too minute to be reproduced graphically. These sometimes occur independently in regions well away from the tracer source and are considered to be numerical noise. Lastly, the second-order scheme is less computationally expensive. For these reasons the second-order flux limiter scheme is chosen to compute the tracer advection in this study.

Since the passive tracer assumption overestimates the vertical movement of oil it was deemed desirable to limit vertical movement by any means possible. For this reason the vertical diffusion coefficient for the tracer was set to zero for this study.

As the gravitational spreading of oil is not considered, for reasons given in Section 5.1.2, no further horizontal diffusion was added to the tracer calculation. Adding diffusion to account for the effects of eddies which are not resolved by the 18km resolution, but are resolved by lower resolutions such as the 4.5km grid spacing setup, was considered. However, it was determined that numerical diffusion in the model is at a level that would render addition of further diffusion physically unrealistic (Jean-Michel Campin and An Nguyen, personal communication, 2014). Hence the horizontal diffusion coefficient in the tracer calculation is also set to zero.

Constant tracer values at the source required use of the RBCS package to set up a restoring layer, which specified the re-set initial tracer value at each time step, and a mask layer which restored the value of the tracer to that specified by the restoring layer and removed any tracer near the periodic open boundary conditions, to avoid re-introduction elsewhere in the domain. The sponge layer specified that any tracer entering the the outer two grid cells of the domain be reduced according to the following decay expression.

$$\frac{d\tau}{dt} = \frac{d\tau}{dt} - \frac{e^{-0.8x}}{T_\tau}(\tau - \tau_{RBC}) \tag{5.1}$$

Here x is the distance from the boundary in grid cells, zero at the boundary, and $T_\tau$ is the timescale associated with the reduction, here set to the model timestep, 1200 sec. $\tau_{RBC}$ is the value specified by the restoring layer, zero at the boundaries, and 0.8

is an arbitrarily chosen constant. All other values are as defined previously (Adcroft et al., 2014). This gradual reduction is done to avoid numerical instabilities caused by sharp tracer gradients at the boundary grid cell.

## 5.3 IceTracker

The IceTracker software is an interactive tool that shows the historical movement of sea ice from user-specified locations in the Arctic Ocean Basin for the period 1981-2012. It can be freely accessed online (thepolarhub.org/interactive/arctic-basin-ice-tracker). The software is described in Pfirman et al. (2013) and is based on the gridded sea ice velocity data of Fowler & Tschudi (2003). The data set of Fowler & Tschudi (2003) uses satellite and buoy ice motion data from a variety of sources to compute daily ice motion vectors for the period November 1978 to December 2012 on the domain 48.4°N to 90°N for the Arctic Ocean Region. An Antarctic data set is also included. This data is projected onto the 25km EASE-grid developed by Brodzik & Knowles (2002). The data set also gives yearly, monthly, and weekly means.

This data is used to calculate backward and forward Lagrangian trajectories of sea ice from any location in the domain for a specified period between 1981 and 2012. Trajectories are output at a user-specified timestep of 1, 3, or 5 days, and endpoints are interpolated linearly at each timestep if they do not coincide with a grid point. The IceTracker algorithm considers significant amounts of sea ice to be present in a grid cell if the sea ice concentration exceeds 50%. Cells with lower ice concentrations are disregarded as essentially ice free. The calculation of the sea ice trajectory from the user-specified location begins when the sea ice concentration in the corresponding grid cell first exceeds 50%. This sea ice is then tracked as a

Lagrangian parcel until the sea ice concentration of the parcel drops below 50%. The final location of the parcel is recorded and tracking is resumed from this location if the sea ice concentration increases to exceed 50% again during the remainder of the study period. (Bruno Tremblay, personal communication, 2014).

## 5.4 MATLAB Code

### 5.4.1 Basic

In the offline MATLAB calculations, first the binary data output by MITgcm describing the ocean tracer, ice concentration, and sea ice and ocean surface velocity fields, as well as the observed data from IceTracker are read into MATLAB arrays. For here the contaminated ice trajectory calculation, as described in detail in Section 5.4.2, is performed. Once this is completed the areas affected by contaminated ice and water are calculated. The area affected is approximated by summing the grid cells containing oil in the ocean, ice, or both and multiplying this sum by the area of one grid cell, 324 $km^2$. This calculation is only approximate, as not all of a cell might be covered in oil, however it is the best estimate achievable at the utilized resolution.

For the final presentation of results the occurrences of 'oil present' in the ice and ocean are counted for all 31 years and used to calculate probability distributions for the likelihood of contamination in each medium. From these the maximum potential transport distance is approximated by finding the 'great circle' distance between the spill site and the farthest point showing a potential for contamination. The 'great circle' distance was chosen to represent the shortest distance response crews could reach the far extent of the spill by. It does not necessarily represent the total distance the oil has travelled.

### 5.4.2 Ice Trajectory Calculation

As mentioned in Section 5.1.1, sea ice in a grid cell is assigned a status of 'oil present', or contaminated with oil, when the sea ice concentration in this cell exceeds the specified threshold, either 20%, 30%, or 50%, and oil is present in the ocean surface layer at a concentration greater than the specified threshold of 0.5%, 5%, or 20%, of the concentration at the source of the spill.

The trajectories of sea ice contaminated by oil are tracked in a semi-Lagrangian fashion from the cell where the ice first became contaminated. Once contamination has occurred the weekly averaged ice velocity vectors are used to calculate the latitude and longitude of the ice in the cell at contamination via the 'reckon' function provided by MATLAB's Mapping Toolbox. This function uses the distance travelled at a given azimuth from a specified location to calculate the final location on a spherical, global grid. Once the coordinates are obtained, they are mapped back to the MITgcm grid cell with the nearest center.

If the sea ice in a cell is contaminated with oil and the ice concentration drops below the specified threshold, the sea ice in this cell is assigned a new state of 'oil absent', and an oil concentration equal to the specified threshold used to define spill extent is assigned to the ocean surface layer cell below, in order to signify qualitative 'oil presence' in this cell. This 'oil presence' is then tracked using a procedure analogous to contaminated sea ice advection until the simulation ceases.

# CHAPTER 6
# General Results & Discussion

To better understand the scope and limitations of the results produced by this study it is necessary to discuss some general findings and analyses before presenting location-specific results. These are the sensitivity of the results to the investigated parameters, sources of error other than the errors inherent in the utilized parameterizations, agreement with historical ice drift data, as well as some general observations regarding the evolution of an oil spill in ice-covered waters as predicted by this modelling approach.

## 6.1 Parameter Sensitivity

As part of this study, the sensitivity of the results to two parameters, the ice concentration required for oil to be advected with ice fields, and the MITgcm tracer concentration defining the state of 'oil present', were evaluated. The results of this evaluation are presented in this section and the combination of 30% ice concentration required for advection with ice and 0.5% of initial tracer concentration defining 'oil present' is identified as being most representative.

### 6.1.1 Ice Concentration for Advection

In Section 4.1.2 the notion that oil is advected with sea ice fields for ice concentrations greater than 30% was introduced. To date this is still the primary parameterization used when modelling oil trajectories in ice-covered waters. The earliest explicit mention of this criterion was found in Venkatesh et al. (1990), who arrive at this conclusion by examining the results of the field tests by SL Ross & DF Dickins (1987) and a field test in Prudhoe Bay in 1983, as well as incorporating the general observations made on a spill of opportunity in 1977. Both field tests used in this derivation were carried out in ice concentrations of 40-60%. Hence the 30% ice concentration criterion should be viewed as a rough guideline, rather than a thoroughly tested empirical method. As stated in Section 5.1.1, this criterion was used in this study, however due to the uncertainty associated with it the results were also computed for oil being advected with ice at ice concentrations of 20% and 50%. To illustrate the sensitivity to this parameter, results obtained for oil contamination in ice at the Beaufort Continental Slope location after one year of tracking are shown in Figure 6–1.

From Figure 6–1 it is clear that the analysis is not sensitive to the exact value of this parameter. The only noticeable difference is a slight decrease in the area of high probability of contamination for the cases requiring higher ice concentration for oil transport with ice. However the overall contaminated area does not change significantly. For this reason, the cases corresponding to the traditionally used value of 30% are used to present the trajectories computed in this study.

### 6.1.2 Tracer Concentration Cutoff

The qualitative nature in which the area affected by the oil spill is delineated in this study required setting an MITgcm passive tracer concentration defining a state of 'oil present'. As was noted in Section 5.1, results were computed using a cutoff concentration of 0.5%, 5%, and 20% of the tracer concentration at the source.

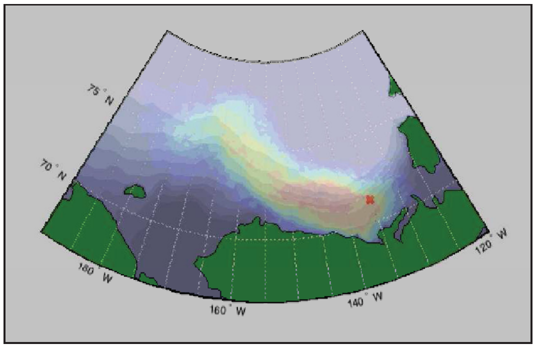

(a) 20% Concentration

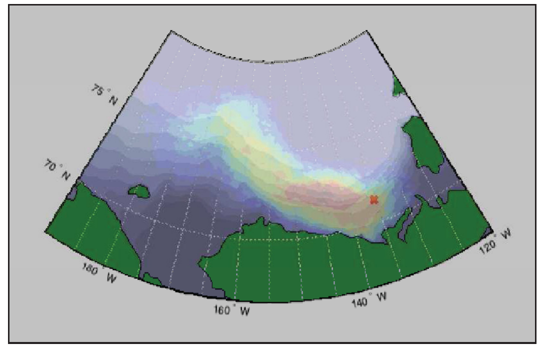

(b) 30% Concentration

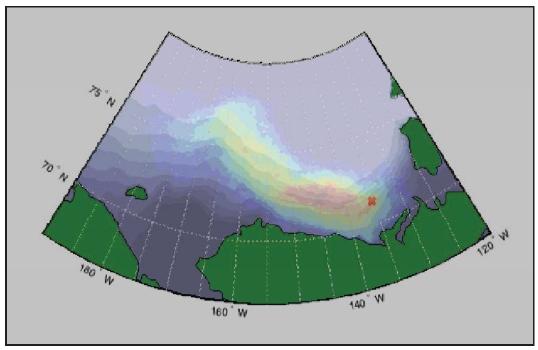

(c) 50% Concentration

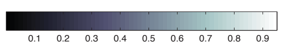

(d) Ice Concentration

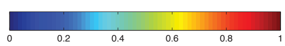

(e) Oil Probability

Figure 6–1: Sensitivity to the ice concentration criterion, illustrated by probability density of oil contamination in ice for a representative spill with 0.5% of concentration at the source representing oil presence.

Very rough estimates of volumes of oil corresponding to these quantities may be obtained by scaling the total 'units' of tracer in the domain at the end of the tracking period to a volume of oil spilled. Given the behaviour of crude oil in cold environments it is likely that small quantities oil will be found in amalgamations such as pockets of oil in or under an ice sheet, small but thick oil slicks, or tarballs that may re-form into oil slicks as mentioned by Gearon et al. (2014) and described in Fingas et al. (2006). This makes for a very difficult comparison of small volumes of oil calculated to correspond to low tracer concentrations by such a scaling to concentration thresholds, such as the ones given by Gearon et al. (2014). For example, an oil volume of $0.5m^3$ would correspond to a concentration of $2x10^{-7}g/m^3$ if distributed throughout the cell, which would indicate no significant adverse effects. However the same volume of oil could also approximately be contained in a 20m x 20m x 1mm oil slick that is trapped between ice floes. Such a lead in the ice pack would see significant wildlife activity and therefore the oil would pose a significant risk. Due to these complexities the exact concentration of oil representing significant impacts should be evaluated by the end-user of this risk assessment.

To illustrate the sensitivity to this cutoff concentration, the total area affected by the oil spill for the Canadian Beaufort Sea Continental Slope location is shown for the various cutoffs in Figure 6–2.

Clearly, the area affected by low concentrations of tracer is much larger than the area affected by high concentrations. Gearon et al. (2014) also found large areas of low contamination surrounding an area of higher contamination.

Continuing with the notion that in dense ice packs the extent of contaminated ice delineates the maximum spill extent, it follows that the most accurate representation is given by the case which corresponds best to the historical ice drift data. Figure 6–3 shows comparison of these results to historical drift data at the end of April for three locations where landfast ice does not influence historical drift data. The influence of landfast ice on historical drift data will be discussed in more detail in Section 6.3.2.

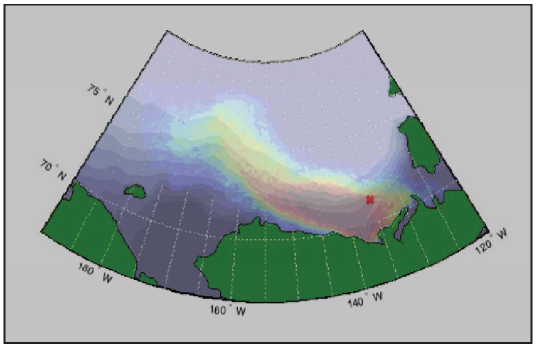


(a) 0.5% Cutoff

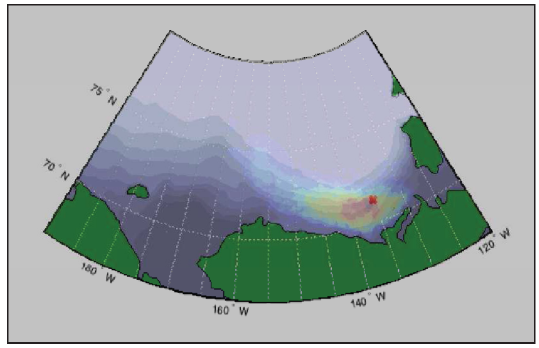


(b) 5% Cutoff

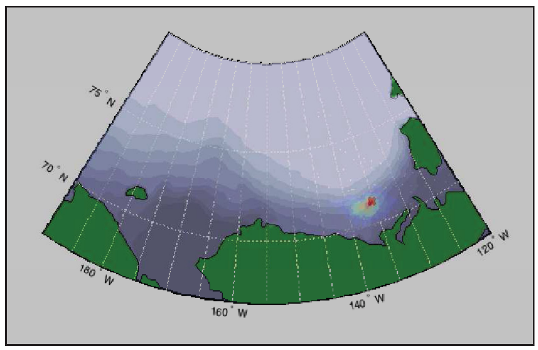


(c) 20% Cutoff

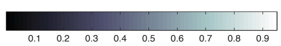


(d) Ice Concentration

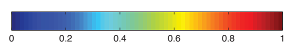


(e) Oil Probability

Figure 6–2: Sensitivity to tracer concentration defining 'oil present', illustrated by probability density of oil contamination for a representative spill using a 30% ice concentration criterion for oil advection.

By this reasoning Figure 6–3 clearly shows that the 0.5% cutoff tracer concentration provides the best delineation of the area affected by the spill.

### 6.2 Error Analysis

In addition to the errors introduced by the parameterizations used in this study, the model setup and inherent assumptions introduced several errors which will be discussed, and quantified where possible, in this section. The first issue discussed is

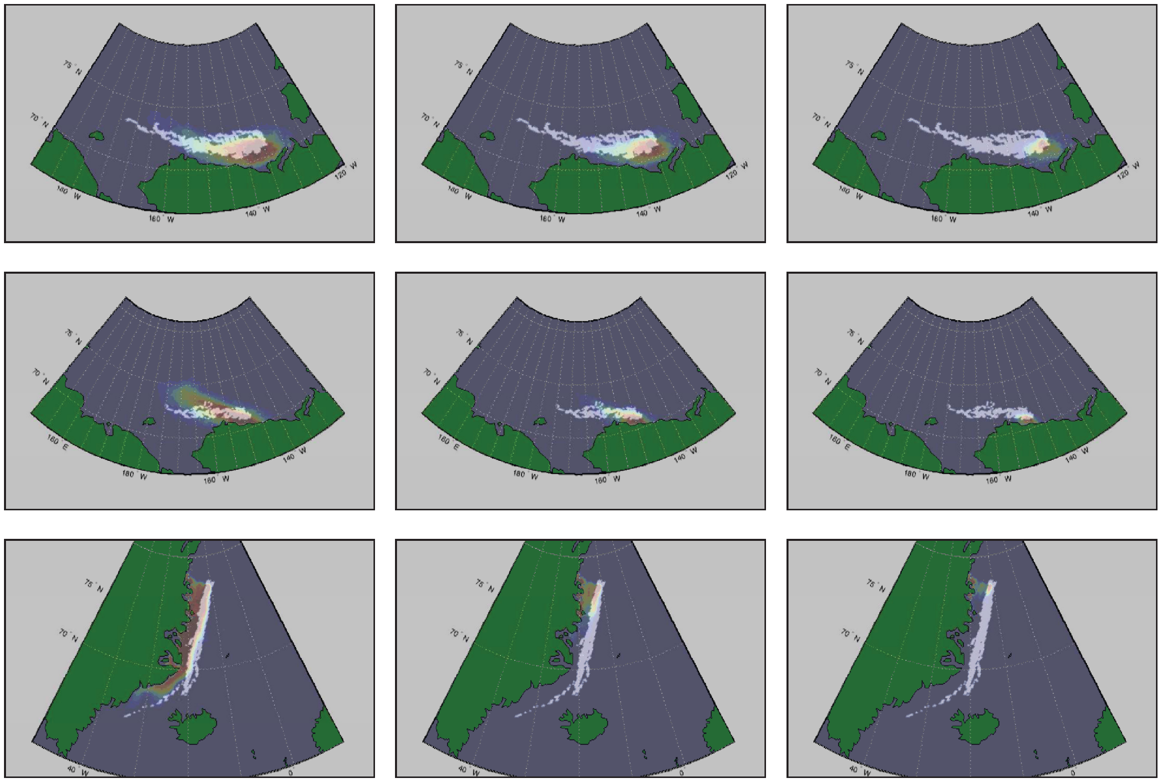

Figure 6–3: Total probability of oil contamination at the end of April at Beaufort Sea Continental Slope (top), US Beaufort Sea (middle), and East Greenland (bottom) sites delineated by 0.5% (left), 5% (centre), and 20% (right) of initial tracer concentration defining 'oil present', with historical ice drift superimposed in white.

unrealistic vertical entrainment and loss of surface oil due to the misrepresentation of the buoyancy of oil as a passive tracer. This is found to be only of minor importance in the context of this study. The next issue considered is the averaging error introduced by vertical discretization of the steep velocity gradients at the ocean surface. Finally, it is recognized that the relatively coarse resolution used in this study introduces error in the representation of the velocity field. This is discussed to conclude the error analysis, though computational limitations did not permit quantification of this error.

### 6.2.1 Vertical Advection of Passive Tracer

The assumption of modelling oil as a passive, non-buoyant tracer means that vertical entrainment of oil will be more significant than if the density difference was properly accounted for. However, naturally occurring vertical entrainment due to OSA formation and density increases of weathered oil is not considered here, also because of the passive tracer assumption. Therefore it would be erroneous to consider all oil travelling at the subsurface to be an error. Because of this, the error in vertical movement associated with the passive tracer assumption cannot be quantified with reasonable accuracy. Some magnitudes of vertical transport are shown in Figure 6–4 as examples for comparison with results of future studies which include buoyancy and weathering effects, but no quantitative error estimate will be attempted.

Since oil is represented as neutrally buoyant, vertical movement could be significant in regions of deep convection. Therefore the Baffin Bay and East Greenland locations are considered here. Additionally, the site in the Barents Sea is considered since it is ice-free year round and therefore vertical entrainment due to wave action is higher than at ice-covered sites. Finally, vertical transport at the Mackenzie Delta site is evaluated, since the site is in relatively shallow water and vertical movement due to OSA formation may be considered in future studies. For each site, tracer concentrations in the ocean up to 5 'units', or 0.5% of the original concentration, are mapped after 1, 4, 12, 26, 39, and 52 weeks for the run starting in 1993. This year was arbitrarily chosen. Tracer concentration decreases sharply with depth, and no more than 44% of the initial tracer concentration is present subsurface for any case. For all cases except the Barents Sea, subsurface tracer concentrations are less than 30% of the initial concentration. It is unlikely that this would cause a depletion of tracer at the ocean surface at a level that would lead to erroneous delineation of oil presence.

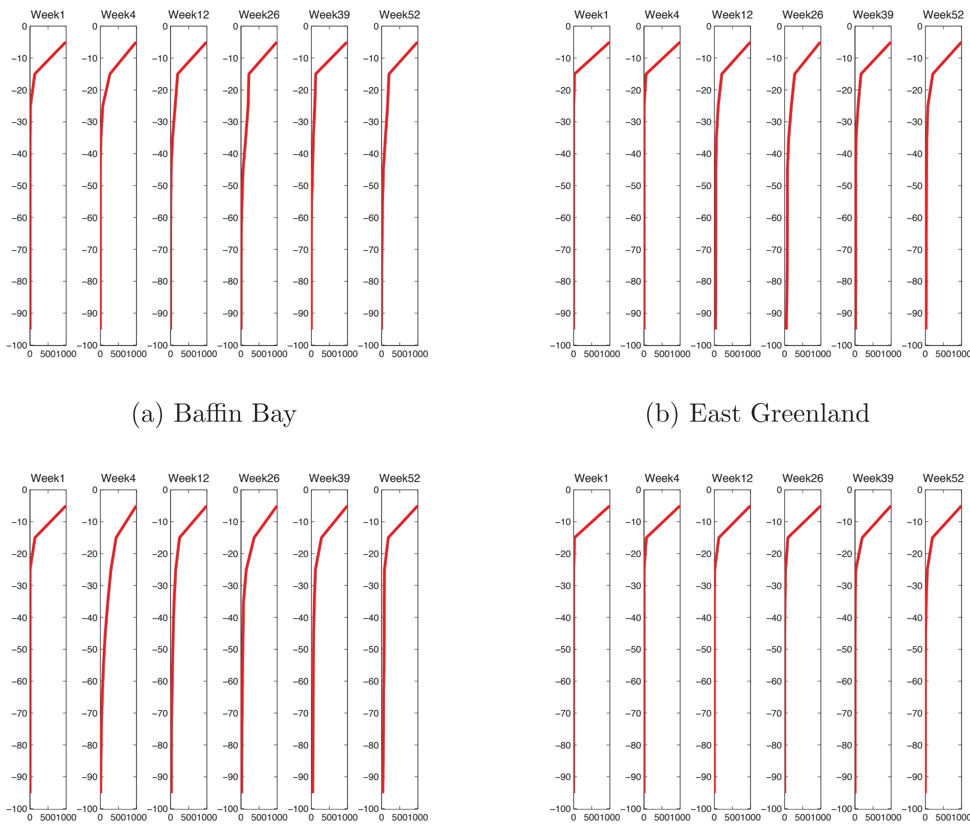


(a) Baffin Bay

(b) East Greenland

(c) Barents Sea

(d) Mackenzie Delta

Figure 6–4: Vertical profiles of maximum tracer concentration by layer. Snapshots taken 1, 4, 12, 26, 39, and 52 weeks after release in 1993.

Vertical movement is not consistently downward. For the deep convection cases, an increase in tracer concentration in the second layer of the ocean, indicating downward vertical movement of tracer, is noted during the winter months however the concentration decreases in the summer months. For the Barents Sea, significantly higher tracer concentration in the second layer is noted in December compared to other months. This is perhaps due to increased storm activity in this area in the winter. It is also interesting to note that vertical entrainment was much more significant in the Barents Sea than in other cases, which suggests that entrainment induced by wind and waves in open water conditions is more effective than deep convection. In general it is concluded that loss of tracer from the ocean surface due to the passive tracer assumption does not introduce a significant error within the parameters of this study. However the density difference between crude oil and water will need to be accurately accounted for in a quantitative analysis of oil spill trajectories.

### 6.2.2 Underestimate of Surface Stress Contribution to Velocity

Drozdowski et al. (2011) points out that most hydrodynamic circulation models underestimate the actual water velocity at the ocean surface since this is an area of steep velocity gradients which are not well resolved by the vertical discretization employed in most models. This error is illustrated graphically in Figure 6–5.

This is especially applicable for models which are applied over a large domain and long time scales, such as the one employed in this study. In order to assure numerical stability, a balance must be struck between resolving the steep velocity gradients in the surface layer and ensuring that vertical layers are thick enough to not cause unrealistically large horizontal velocities at the maximum sea surface elevation

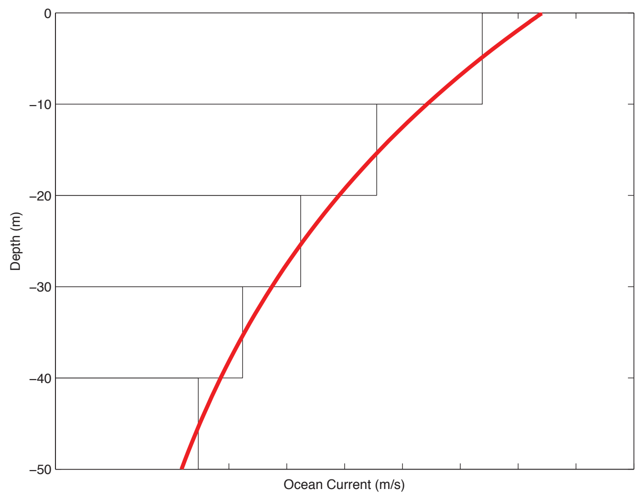


Figure 6–5: Generalized profile of wind-induced ocean surface velocity as calculated by Equation 6.1 (red) and as represented in MITgcm (black).

difference. When layers become very thin, vertical accelerations occur and therefore horizontal accelerations must also occur in order to satisfy conservation of mass. These large accelerations can lead to numerical instability.

The overall contribution of wind to the free drift speed of an object at the open ocean surface is generally said to be ∼3% of the wind speed (Tsahalis, 1979). The contribution of surface stress, either wind stress or ice-ocean interface stress, is included in the currents calculated by MITgcm. It is accounted for by the forcing term in Equation 3.4 and can be clearly seen as a change of gradient in the vertical velocity profile, such as the example shown in Figure 6–6. Therefore it can be reasoned that the error introduced by coarse resolution is much less than 3% of the wind speed.

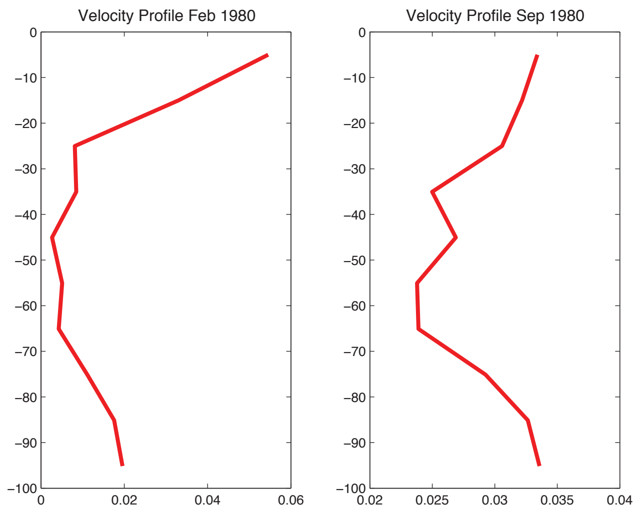


Figure 6–6: Vertical Velocity Profile at the spill location on the Beaufort Sea Continental Slope. Profile of a snapshot taken during completely ice-covered conditions in February 1980 on the left, and during open water conditions in September 1980 on the right. Influence of ocean surface stress is clearly seen by the change in velocity gradients at ∼30m depth.

Furthermore, the free drift speed of ice under the influence of wind is known to be ∼2% of the wind speed (Nansen, 1902; Weiss, 2013). In dense icepacks, where ice is not free-drifting, the ice absorbs momentum from the atmosphere which would normally be transferred to the ocean. From this, and the fact that the model output sea ice velocities contain additional components due to currents, Coriolis force, internal ice stress, and sea surface potential height, it is concluded that the error introduced in the ocean surface trajectory by coarse vertical resolution is bounded by the extent of contamination in the ice. Therefore this error does not lead to an underestimate of the contaminated area where ice is present.

In open water conditions, the magnitude of this error can be approximated by a basic model of the atmosphere-ocean interface, following Chapter 6 of McWilliams (2006). For the northern hemisphere, such a model is described by the following equations.

$$\begin{aligned}
\tau_s^x &= \rho_{atm}\sqrt{\frac{f\nu_{e,atm}}{2}}(u_{geo} - v_{geo}) \\
\tau_s^y &= \rho_{atm}\sqrt{\frac{f\nu_{e,atm}}{2}}(u_{geo} + v_{geo}) \\
\lambda &= \frac{1}{\sqrt{\frac{2\nu_{e,oc}}{f}}} \\
u_{oc} &= \frac{e^{\lambda z}}{\rho_{oc}\sqrt{2\nu_{e,oc}f}}[(\tau_s^x + \tau_s^y)\cos\lambda z + (\tau_s^x - \tau_s^y)\sin\lambda z] \\
v_{oc} &= \frac{e^{\lambda z}}{\rho_{oc}\sqrt{2\nu_{e,oc}f}}[(-\tau_s^x + \tau_s^y)\cos\lambda z + (\tau_s^x + \tau_s^y)\sin\lambda z]
\end{aligned} \tag{6.1}$$

$\tau_s^{x,y}$ is the zonal and meridional wind stress on the ocean surface. $\rho_{atm/oc}$ is the density of the atmosphere and ocean, taken as 1.225 $kg/m^3$ and 1029 $kg/m^3$. $\nu_{e,atm/oc}$ is the eddy viscosity of the atmosphere and ocean, taken approximately as $\sim 100m^2/s$ and $\sim 0.1m^2/s$ after Vallis (2005). f is the Coriolis parameter, $2\Omega\sin\phi$, with $\Omega$ being the angular velocity of the earth, $0.73x10^{-4}$rad/s, and $\phi$ being the latitude, taken as a worst-case 90°. $u_{geo}$ and $v_{geo}$ are the geostrophic wind speeds, i.e. the wind speeds due to the Earth's rotation. $\lambda$ is the inverse of the oceanic boundary layer depth and z is the depth at which the wind-induced currents are being calculated, decreasing from zero at the ocean surface. This approximation yields a difference of ~12.5%, or ~0.5% of the wind speed, between the wind-induced currents at the very ocean surface and their average over the thickness of the ocean surface layer in

MITgcm, 10m. It should be stressed that this approximation does not take currents from sources other than wind into account, and all constants are general, commonly used values.

### 6.2.3 Coarse Resolution Velocity Field Errors

Nudds et al. (2013) demonstrated the difference between the velocity fields produced by models of differing resolution by comparing the velocity field in the Beaufort Sea as calculated by models with a $1/6°$ and $1/18°$ resolution. To gain an understanding of the significance of this error within the context of this study, model runs with the same forcing and initial conditions as the production runs, but at a higher resolution, are required. Unfortunately spinup files giving the same initial conditions for both setups were not available at the time of modelling and the computational cost of creating such files was prohibitive. However, from the finding that adding horizontal diffusion to account for unresolved eddies is not physically realistic due to high numerical diffusion (Jean-Michel Campin and An Nguyen, personal communication, 2014), it is reasoned that the mean velocity fields are not significantly misrepresented. However as mentioned throughout this study, increased resolution is desirable and resolution of small-scale features in the velocity field will certainly improve local trajectory predictions.

## 6.3 General Conclusions

To conclude the general discussion of the results, some common observations about the behaviour of a spill throughout the tracking period are made and the general agreement between the calculated results and historical ice drift data is discussed, highlighting the significance of landfast ice presence.

### 6.3.1 Spill Evolution

General findings about the evolution of an oil spill in ice-infested waters are well illustrated by examination of a time series of the probability distribution of contamination of ocean surface and sea ice. Here the probabilities of contamination will be shown for the Canadian Beaufort Sea Continental Slope location after 1, 3, 6, 9, 10.5, and 12 months. The parameters used in the creation of these distributions were the parameters identified as most representative in the previous section. To illustrate the influence of sea ice, all plots will show 'normal-year' sea ice distribution for the area, obtained by averaging sea ice concentration for all 31 years.

Figure 6–7 confirms that after one month, transport of oil with sea ice is already more significant than transport with the ocean. As mentioned previously, this is due to the dense sea ice cover inhibiting momentum transfer from the atmosphere to the ocean.

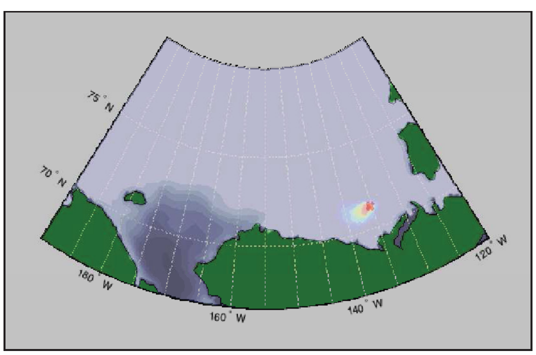


(a) Ocean

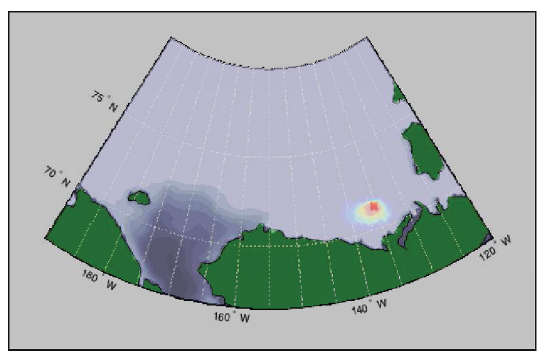


(b) Ice

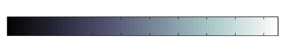


(c) Ice Concentration

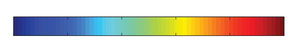


(d) Oil Probability

Figure 6–7: Probability distribution of oil contamination in ocean and sea ice one month after spill initialization.

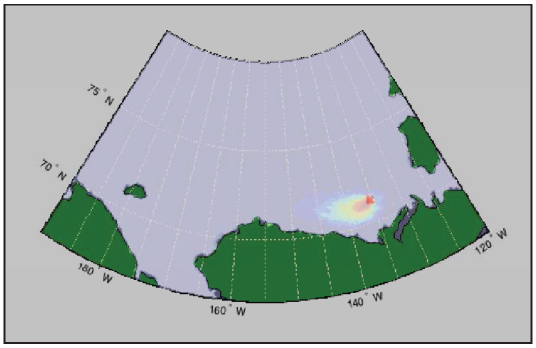


(a) Ocean

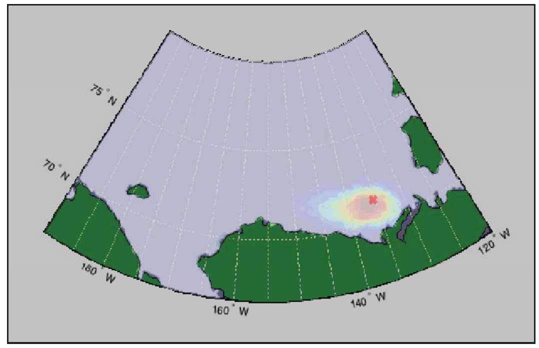


(b) Ice

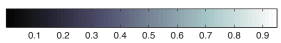


(c) Ice Concentration

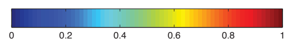


(d) Oil Probability

Figure 6–8: Probability distribution of oil contamination in ocean and sea ice three months after spill initialization.

Figure 6–8 shows the evolution of this spill after three months. From the fact that the area of high probability of contamination in sea ice is much larger than in the ocean, and that the sea ice contamination probability distribution exhibits significantly steeper gradients, it can be inferred that oil transport with sea ice over long distances occurs more consistently than transport in the ocean. Conversely, areas of low contamination probability in the ocean west of the spill site, with relatively low gradient indicate higher interannual variability.

Examination of Figure 6–9 shows by the end of a winter season there is significant potential for oil transport away from the spill site. In this case the oil has moved ∼1,400km westward. This is significant since effective cleanup is unlikely in the near-complete ice cover that is present at most chosen sites during the winter months. Much of the oil is either moving at the bottom of the ice, or is encapsulated in it, making it very difficult to recover mechanically, by ignition, or by dispersion and

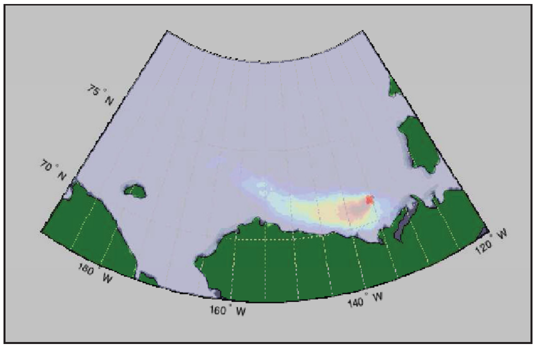


(a) Ocean

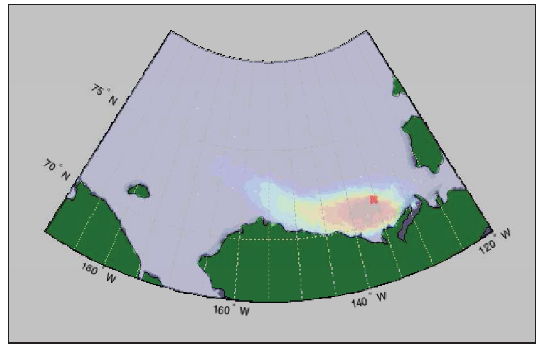


(b) Ice

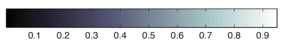


(c) Ice Concentration

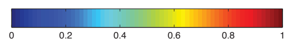


(d) Oil Probability

Figure 6–9: Probability distribution of oil contamination in ocean and sea ice at the end of the winter, six months after spill initialization.

natural degradation. It is also notable that there is a high probability of oil being transported towards the coastline by ice.

Figure 6–10 shows the effect of the receding ice cover on oil distribution. Here it is noted that the area of ocean surface affected by the spill increases significantly once the ice cover recedes, allowing direct wind contribution to the ocean surface currents. Ocean surface contamination near the coast also increases significantly, due to increased wind forcing as well as release of oil from the receding ice cover. Ice coverage is very low at most sites during the summer, meaning that the ice edge will pass through the site in both Spring and Fall. This presents additional hazards for drilling activities since lower ice concentrations near the ice edge are generally associated with greater drift velocities of ice floes.

The significant result obtained from Figure 6–11 is that oil being transported at the ocean surface during the summer months is restrained by the ice edge and moves

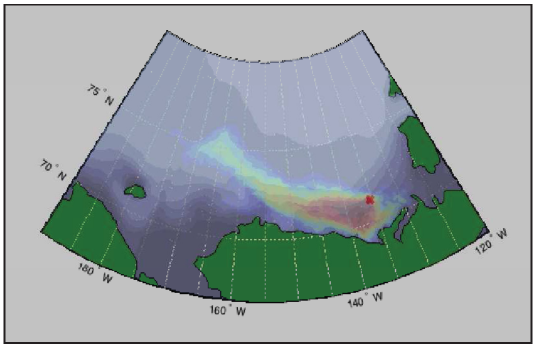


(a) Ocean

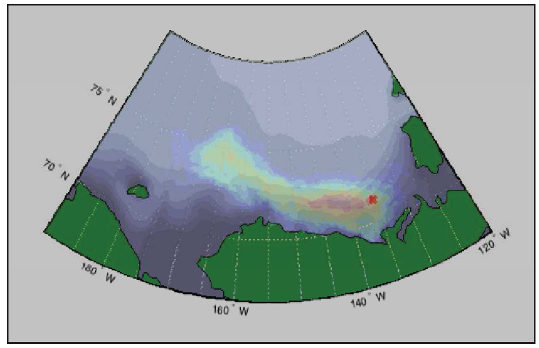


(b) Ice

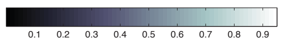


(c) Ice Concentration

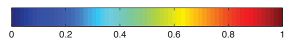


(d) Oil Probability

Figure 6–10: Probability distribution of oil contamination in ocean and sea ice in mid-summer, nine months after spill initialization.

with currents parallel to it. At this ice coverage, which is the lowest encountered during the tracking period, the shape of the oil distribution in the ocean closely matches that of the ice edge and little transfer of oil is observed into the ice field. This finding is supported by the observation made by Sørstrom et al. (2010) that in ice concentrations greater than 20% ice can act as a boom which confines the oil, as well as by the field observations summarized in Venkatesh et al. (1990) which lead to the conclusion that at ice concentrations greater than 30% there is little relative movement between oil and ice.

Figure 6–12 shows the probability distribution of ocean and ice contamination at the end of the tracking period. The significant increase in potential ice contamination from Figure 6–11 suggests that maximizing cleanup of oil before the onset of ice formation is crucial. It is much easier to remove oil on open water than in

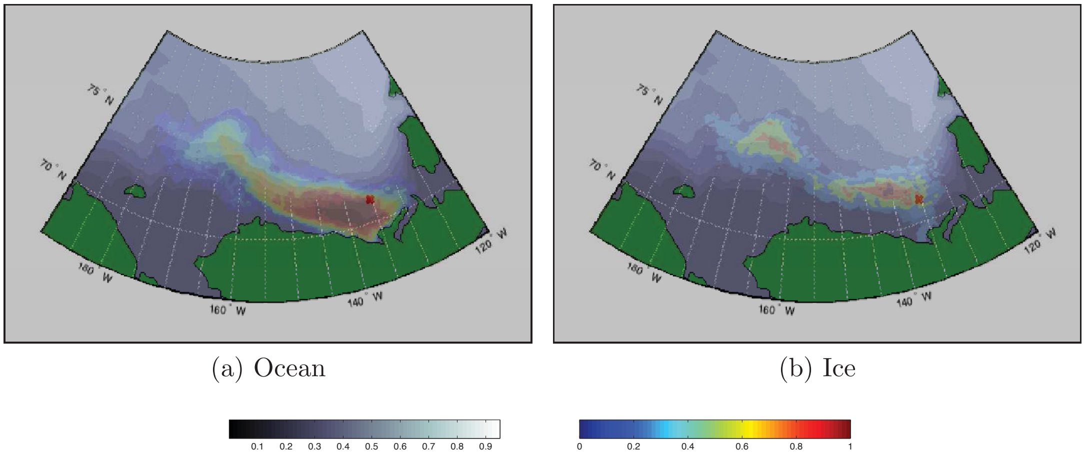


(a) Ocean (b) Ice

(c) Ice Concentration (d) Oil Probability

Figure 6–11: Probability distribution of oil contamination in ocean and sea ice at the end of the Arctic summer in mid-September, 10.5 months after spill initialization.

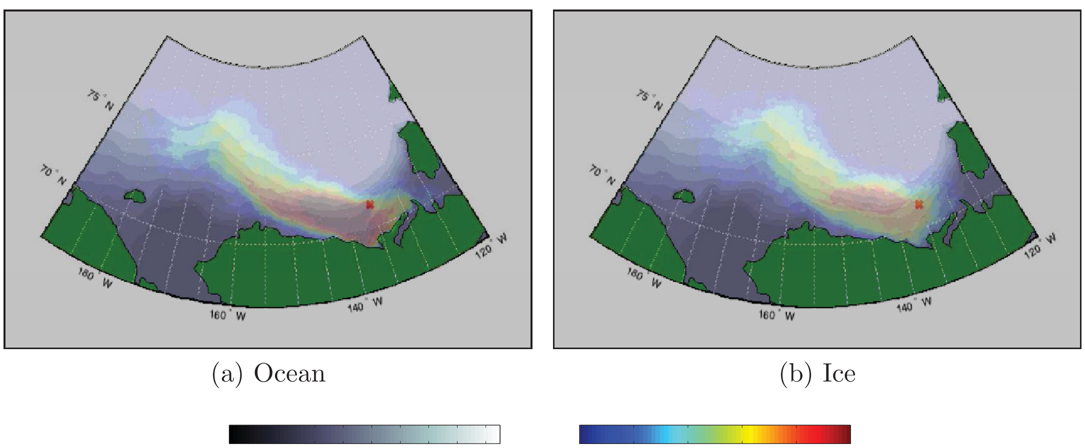


(a) Ocean (b) Ice

(c) Ice Concentration (d) Oil Probability

Figure 6–12: Probability distribution of oil contamination in ocean and sea ice at the end of the tracking period (end of October), twelve months after spill initialization.

significant ice concentrations, especially considering that the majority of ice contamination shown in Figure 6–12 will be comprised of oil encapsulated in newly formed ice which is very difficult to remove until it surfaces through brine channels in the following spring.

### 6.3.2 Historical Data Verification

To verify the calculated oil trajectories, historical ice drifts from the chosen spill sites were reproduced for the applicable time period (1981-2010) using the IceTracker software described in Section 5.3. Drifts for the year 1980 were not included since it is outside of the domain of available data in IceTracker. In comparing these trajectories it must be kept in mind that the historical drifts only show the superposition of trajectories from the actual spill site and do not include drift from locations that oil is transported to by ocean currents. Therefore the calculated trajectories are expected to be more expansive than the historical trajectories, but both are expected to move in the same direction for similar distances.

Comparison generally yielded good results, as has been illustrated in Figure 6–3, provided that landfast ice is not consistently present at the spill site. In these cases there is a mismatch between the calculated and observed trajectories since the drift of landfast ice throughout a winter is insignificant except for a few potential events during formation and breakup (Mahoney et al., 2007) and landfast ice is not considered in MITgcm. This mismatch is observed at the Sverdrup Islands and Baffin Bay locations in Canadian territory, as well as the Pechora Sea location in Russian waters. Results are shown in Figure 6–13.

The water depths at the Canadian locations are 384m and 891m, respectively. Landfast ice is generally found in water depths of 10-180m (Mahoney et al., 2007) and therefore it cannot be said with absolute certainty that the actual spill locations

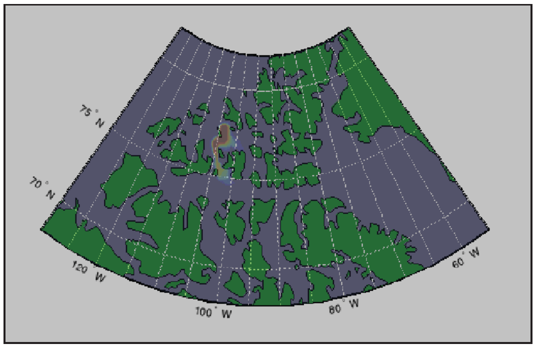


(a) Sverdrup Islands

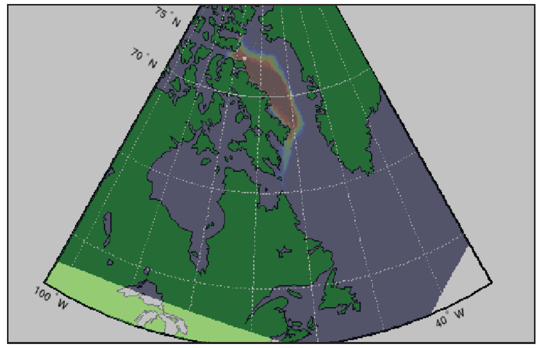


(b) Baffin Bay

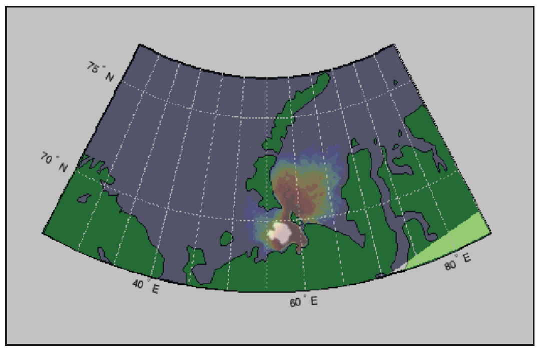


(c) Pechora Sea

Figure 6–13: Comparison of calculated (contoured) and historical (white) ice drifts at the end of April in areas with consistent landfast ice coverage.

will consistently be covered by landfast ice. Both locations exhibit relatively steep bathymetry and therefore it is possible that the identification of landfast ice by IceTracker is due to a mismatch in resolution. However both locations are certainly near the edge of the landfast ice zone and therefore landfast ice should be considered in future modelling efforts for these locations.

The water depth in the Pechora Sea location is only 20m and hence it is very likely that this location is covered by landfast ice during the ice season and the trajectories from this location are hence overestimated.

Historical ice drifts in the Mackenzie Delta and Kara Sea locations, which are also in relatively shallow water, also suggest that these locations are susceptible to landfast ice influence in some years. As Figure 6–14 shows, some historical trajectories from these locations exhibit significantly farther drift than the majority. This farther drift is closer to the calculated results which suggests that it is from years in which the site was in the mobile drift ice zone. For the Kara Sea location farther historical drifts are observed closer to the east coast of Novaya Zemlya which is an area that is deeper than the majority of the Kara Sea. This observation supports the notion that short historical trajectories are due to landfast ice.

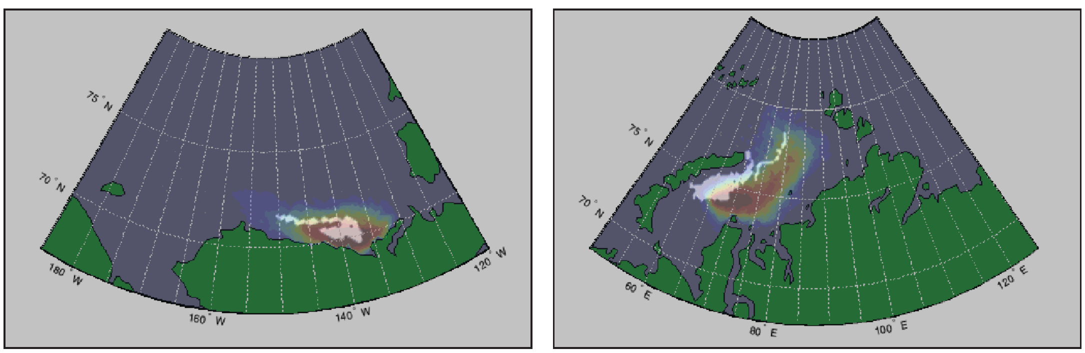


(a) Mackenzie Delta (b) Kara Sea

Figure 6–14: Comparison of calculated (contoured) and historical (white) ice drifts at the end of April in areas with annually varying landfast ice coverage.

A more thorough comparison of calculated and historical trajectories for each location is given in Chapter 7.

# CHAPTER 7
# Location-specific Results

Keeping in mind the general results and analysis from Chapter 6, this chapter discusses results specific to each assessed location, commenting on quantitive measures such as the total area affected and maximum transport distance, which are summarized in Tables 7–1 and 7–2. Since landfast ice is not accounted for in MITgcm, discussing shoreline effects in a quantitative manner would imply a greater degree of accuracy than the study provides. These effects will be qualitatively summarized for each case. Other topics discussed are interannual variability, cleanup considerations and more general observations such as transboundary legal issues arising from oil drifting across national borders. As in Chapter 6, all results will be presented for the case of oil being advected with ice fields at 30% ice concentration and 0.5% of the MITgcm tracer concentration at the source defining the state of 'oil present' in the ocean surface.

## 7.1 Canada

### 7.1.1 Beaufort Sea Continental Slope

Spills from this location present a risk of significant contamination, with potential for contamination over an area of 1,130,112 $km^2$ at the end of the tracking period. Figure 7–1 shows the potential contamination in ice and ocean at the end of the winter, end of the summer, and the end of the tracking period.

Table 7–1: Maximum area of ocean, ice, and total contamination by location by the end of winter and end of the tracking period.

| **Location** | **Area Affected ($km^2$)** | | | | | |
|---|---|---|---|---|---|---|
| **Time** | End of Winter | | | End of Tracking | | |
| **Medium** | Ocean | Ice | **Total** | Ocean | Ice | **Total** |
| Beaufort Sea Continental Slope | 287,064 | 468,180 | **473,688** | 962,280 | 842,400 | **1,130,112** |
| Mackenzie Delta | 154,224 | 238,788 | **238,788** | 495,396 | 579,960 | **594,540** |
| Sverdrup Islands | 34,344 | 40,824 | **40,824** | 190,188 | 175,932 | **257,256** |
| Baffin Bay | 309,420 | 526,824 | **533,304** | 1,272,672 | 592,920 | **1,288,224** |
| US Beaufort Sea | 206,064 | 430,920 | **434,160** | 623,052 | 812,916 | **878,364** |
| US Chukchi Sea | 167,184 | 315,576 | **322,380** | 560,520 | 777,276 | **826,200** |
| East Greenland | 232,956 | 289,656 | **311,364** | 637,632 | 346,680 | **641,196** |
| Barents Sea | 173,016 | 64,476 | **219,024** | 337,608 | 69,984 | **337,608** |
| Pechora Sea | 133,812 | 172,692 | **183,384** | 258,228 | 172,692 | **258,228** |
| Kara Sea | 204,444 | 325,944 | **331,128** | 500,580 | 489,240 | **561,168** |

Table 7–2: Maximum area of ocean, ice, and total contamination by location by the end of winter and end of the tracking period.

| **Location** | **Transport Distance (km)** | |
|---|---|---|
| **Time** | End of Winter | End of Tracking |
| Beaufort Sea Continental Slope | 1,431 | 1,988 |
| Mackenzie Delta | 1,424 | 1,971 |
| Sverdrup Islands | 463 | 1,656 |
| Baffin Bay | 1,705 | 3,549 |
| US Beaufort Sea | 1,185 | 1,815 |
| US Chukchi Sea | 887 | 1,603 |
| East Greenland | 1,624 | 2,416 |
| Barents Sea | 736 | 981 |
| Pechora Sea | 1,159 | 1,408 |
| Kara Sea | 984 | 1,681 |

The trajectories in Figure 7–1 show a general westward drift with the circulation of the Beaufort Gyre, with transport towards the coast by sea ice during the winter.

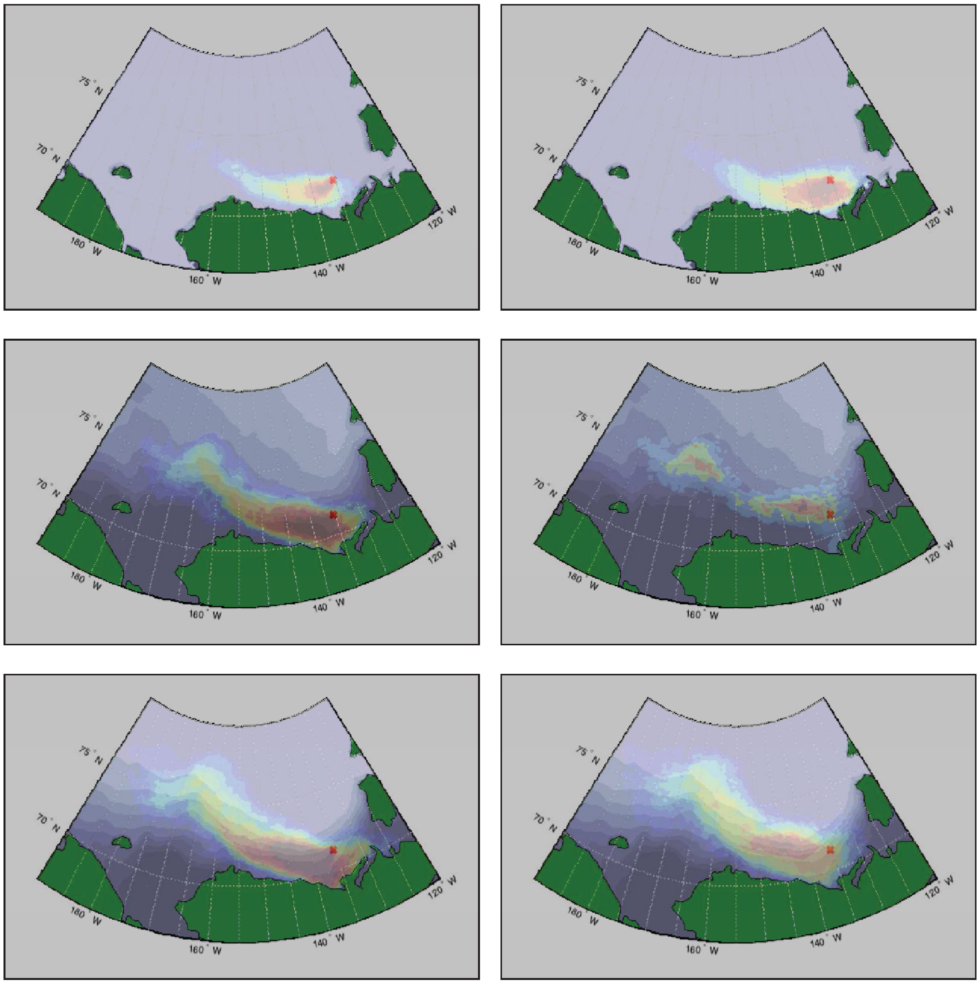


Figure 7–1: Probability of contamination in ocean surface waters (left) and sea ice (right) for the Canadian Beaufort Continental Slope location at the end of April (top), mid-September (middle), and end of October (bottom).

During the summer months transport with ocean surface currents increases as expected, showing potential for appreciable, but annually variable northwest-ward drift from $\sim 155°$W and a greater meridional spread. Due to this spread the coastline from the Amundsen Gulf in the eastern Canadian Beaufort Sea to Point Barrow on the Alaskan North Slope may be impacted by oil, depending on the distribution of landfast ice in the area.

Historical trajectories of sea ice from this site agree well with these findings, as is illustrated in Figure 6–3.

During the summer potential for contamination in sea ice decreases considerably as ice concentrations drop rapidly below 30% and release oil. However, this only provides a brief window for simplified cleanup of oil on relatively open water, as the ice advances significantly again by the end of October and encapsulates much of the surface oil in the open water. This encapsulated oil is very difficult to remove until the ice melts again, and therefore it is critical that cleanup be maximized while open-water conditions persist.

This site is the furthest offshore site in the Canadian Beaufort Sea and located in waters much deeper than those previously explored in ice-covered areas. For these reasons the site is novel in this study and trajectories from two locations within the lease area were computed to study potential effects of distance offshore and water depth on oil spill trajectories. However the two calculated sets of trajectories did not differ significantly. Trajectories from the location in deeper water and further offshore are displayed in this section. Trajectories from the second location followed a slightly more southern trajectory and the affected area was slightly smaller, as seen in Table 7–1, but variation was not significant considering the uncertainties associated with these trajectories. Plots analogous to Figure 7–1 for the second location are shown in Appendix A.

This location has received much recent attention from the spill trajectory modelling community, due to the significant water depth at the site and relatively far distance from the coast. It was studied in both Gearon et al. (2014) and Nudds et al. (2013). The most closely matching time periods considered in these studies were a 3-month release initialized in August in Gearon et al. (2014) and tracked for four months, and a 10-day release, tracked for three months, in Nudds et al. (2013). Figure 7–2 shows the results of Gearon et al. (2014) and Figure 7–3 shows the applicable results of Nudds et al. (2013). To allow for comparison with the results of this study, the probability of contamination in ice and ocean after three months is shown in Figure 7–4, however since the time frames are not closely aligned enough with the spill initialization date used in this study to account for the highly variable ice conditions at this time of year, a close match between the results is not necessarily expected.

All studies exhibit a westward drift from the spill site. The trajectories obtained by Nudds et al. (2013) are comparable to the results from this study, though less extensive. This is expected, as Nudds et al. (2013) only simulated a ten day release of tracer, whereas the tracer release in this study is continuous. General trajectory lengths match reasonably well and both results agree that transport towards the coast is more significant in sea ice.

The probability distribution obtained by Gearon et al. (2014) is much more extensive, which is also to be expected as a different modelling approach, described in Section 3.3.2, was used and the spill was initialized during low ice concentrations in August and tracked for one additional month.

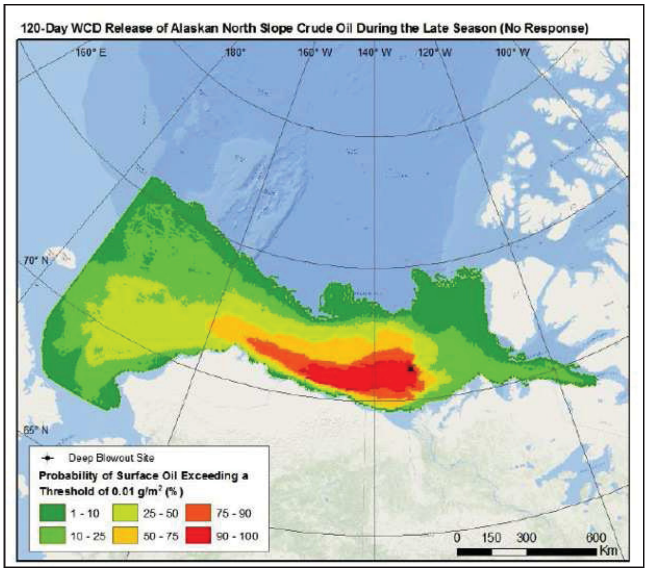


Figure 7–2: Total probability of contamination for Canadian Beaufort Continental Slope location obtained by Gearon et al. (2014) for a well blowout releasing oil from Aug.-Oct. and tracked for 120 days. Source: Gearon et al. (2014)

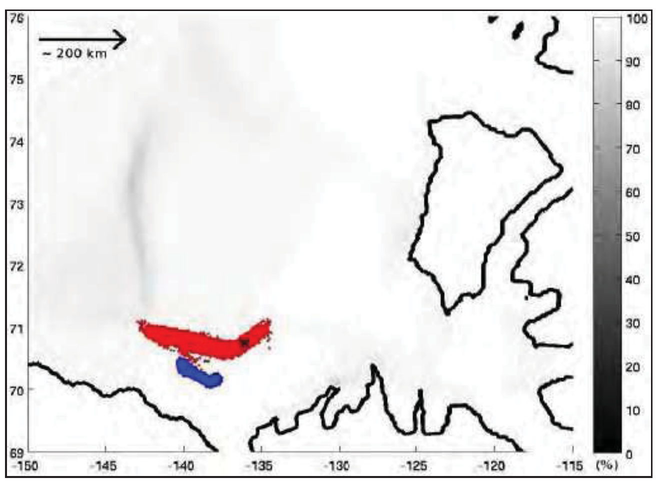


Figure 7–3: Oiling in ocean (red) and sea ice (blue) for Canadian Beaufort Continental Slope location obtained by Nudds et al. (2013) for a well blowout releasing oil for 10 days, tracked from Oct.-Dec. Ice concentration is shown as grayscale. Source: Nudds et al. (2013)

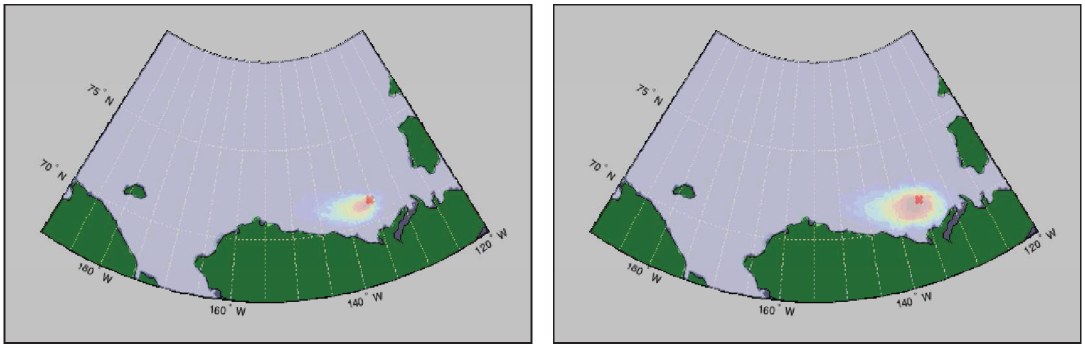


Figure 7–4: Probability of contamination in ocean surface waters (left) and sea ice (right) for the Beaufort Sea Continental Slope location after three months.

The results of both the present study and Gearon et al. (2014) show that oil spilled from this location will be transported into US waters.

### 7.1.2 Mackenzie Delta

The evolution of an oil spill from this location is given in Figure 7–5. Most conclusions drawn from this figure, regarding general trajectory, shoreline effects, and transboundary issues, are the same as for the Beaufort Sea Continental Slope location. However, as the probability distributions and Table 7–1 show, the area affected by this spill is appreciably less due to more significant meridional transport occurring at the previous, further offshore location. Maximum drift distance from the release location is very similar to the previous location.

Comparison with historical ice drift trajectories from this location shows that landfast ice presence is possible, but not consistent. This is illustrated in Figure 6–14. Ice drift data from years where the location is within the drift ice zone agree well with calculated trajectories of contaminated sea ice.

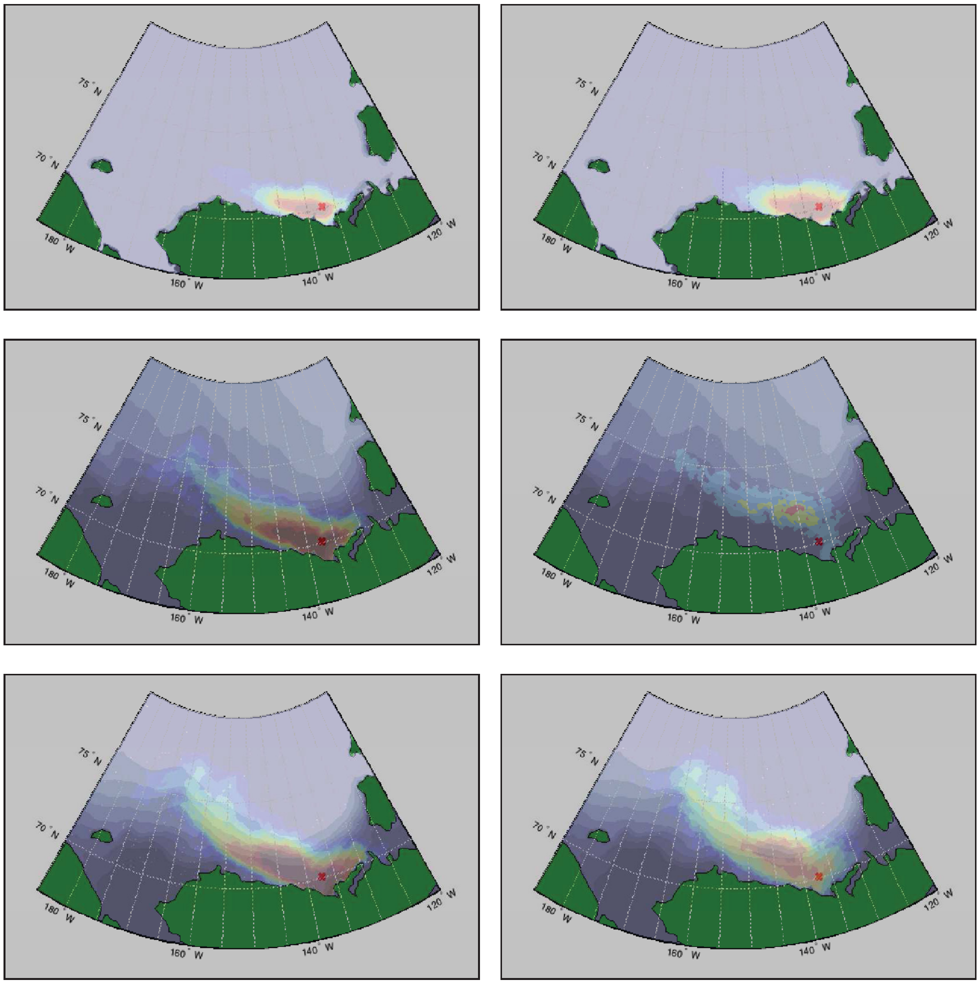


Figure 7–5: Probability of contamination in ocean surface waters (left) and sea ice (right) for the Mackenzie Delta location at the end of April (top), mid-September (middle), and end of October (bottom).

The location of this site at the mouth of the Mackenzie River suggests that a significant quantity of oil may be removed from the water surface by OSA formation, since the Mackenzie River is one of the largest point sources of sediment into the Arctic Ocean, importing $\sim 65x10^6$ tonnes/year (MacDonald et al., 1998). A detailed study of potential OSA formation and environmental impacts from this is recommended as part of the risk assessment for hydrocarbon exploration at this site.

### 7.1.3 Sverdrup Islands

As is shown in Figure 6–13, ice conditions at this location are influenced significantly by landfast ice, which covers the site or its immediate vicinity all year. Therefore the calculated oil trajectories from this site are likely an overprediction and must be verified once MITgcm includes a landfast ice component. The calculated trajectories, shown in Figure 7–6, do however reproduce the general pattern that would be expected at this site.

Oil drifts southeast-ward with water flowing out of the Arctic Ocean into Baffin Bay. During the winter there is negligible transport of oil by sea ice and the only contamination of ice occurs by oil moving under relatively static ice. This transport of oil under ice may be overpredicted since in order for such transport to occur ocean surface currents must be greater than those given by Equation 3.15 for the ice type in the area. Once the ice cover retreats during the summer, oil in the southern parts of the affected area is transported more easily with ocean currents and may reach Baffin Bay by the end of the tracking period.

Even though the overall area potentially affected by a spill from this location is relatively small, potential environmental impact is significant should oil move as predicted by these trajectories after a spill, as hypothesized in Section 2.1.3. This is because a significant length of shoreline on various islands would be exposed. The degree of exposure is also highly dependent on landfast ice presence though, which

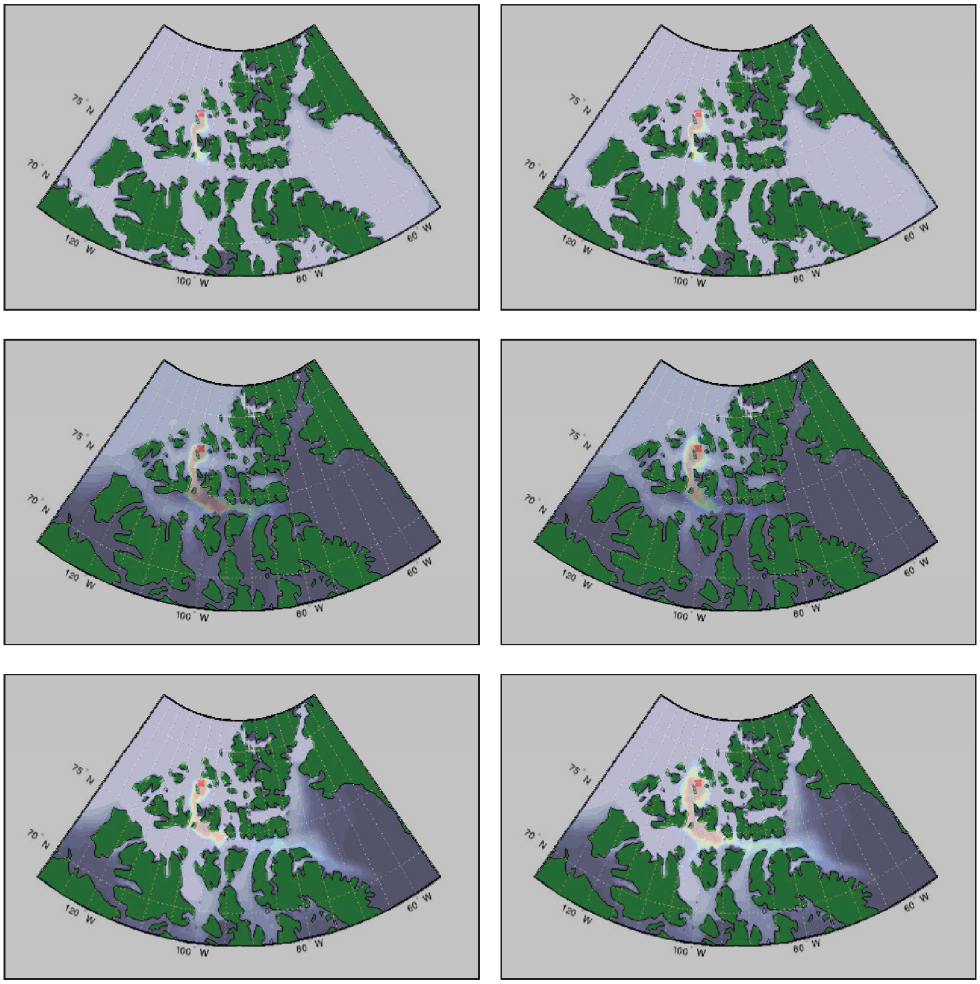


Figure 7–6: Probability of contamination in ocean surface waters (left) and sea ice (right) for the Sverdrup Islands location at the end of April (top), mid-September (middle), and end of October (bottom).

may be year-round in this area (Mahoney et al., 2007), and is therefore subject to further verification.

### 7.1.4 Baffin Bay

The location of this site within the Labrador Current, which transports water out of the Arctic Ocean into Baffin Bay, presents a significant potential for transport of oil spilled here. Like the previous location, historical data suggests that ice drifts at this site may be influenced significantly by landfast ice presence, as shown in Figure 6–13. However, for reasons described in Section 6.3.2, and because the regions east of this site are almost certainly within the mobile drift ice zone this influence is not certain and likely less than at the Sverdrup Islands location. Again the results obtained during the winter are subject to further verification once landfast ice can be considered within MITgcm.

As seen in Figure 7–7. the ice inhibits transport of oil in the ocean and serves to protect parts of the coast of Baffin Bay during the winter. Contamination is contained by the ice edge, however oil is still transported 1,705km from the spill site by the end of April.

During the summer the ice edge retreats well past the spill site and transport in the ocean surface is increased significantly under the influence of wind. The zonal extent of the potentially contaminated area increases until it reaches the western shore of Greenland, and oil is potentially transported south to Newfoundland, 3,549km from the spill site, by the end of the tracking period. Due to this increased transport there is a risk of contamination on shorelines of Baffin Bay, Newfoundland, Labrador, and western Greenland. These shorelines contain a significant number of bay, fjords, and inlets, which pose increased difficulties for cleanup.

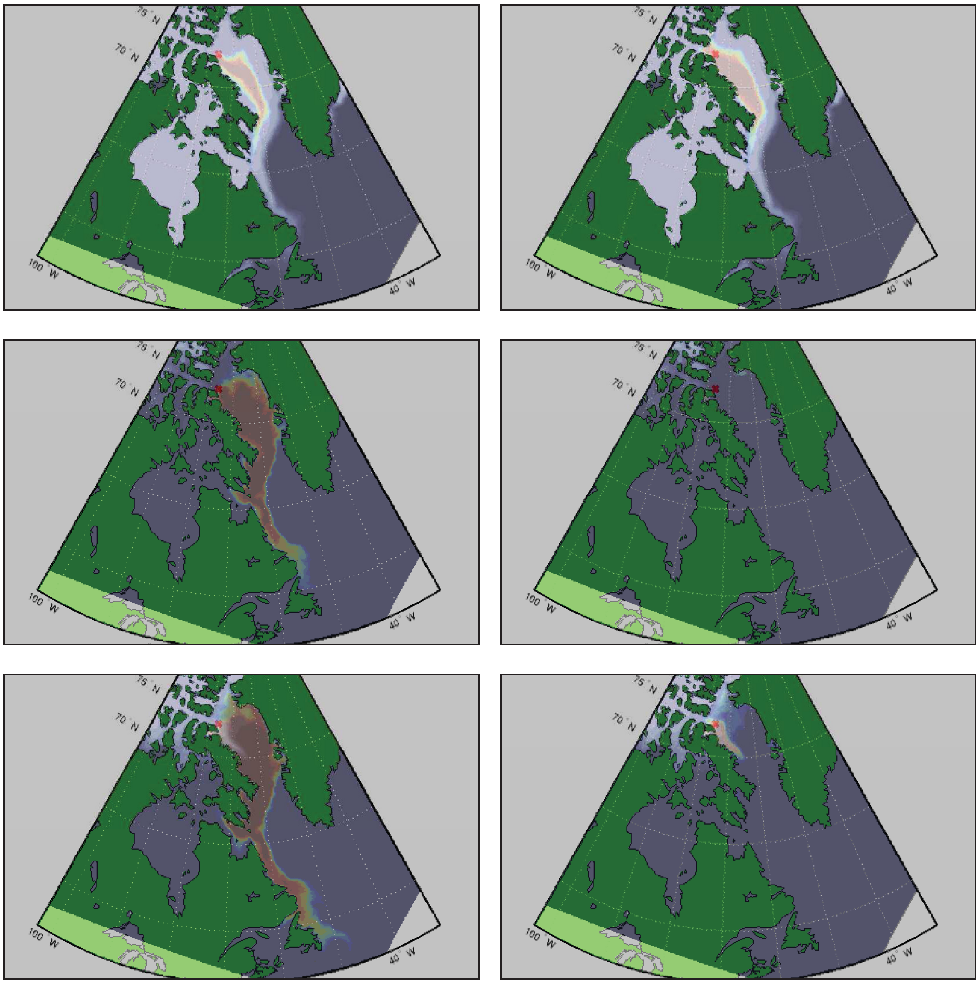


Figure 7–7: Probability of contamination in ocean surface waters (left) and sea ice (right) for the Baffin Bay location at the end of April (top), mid-September (middle), and end of October (bottom).

The trajectories calculated here do not show significant transport of oil into Lancaster Sound.

Overall, contamination from this site could potentially reach an extent of 1,288,224$km^2$, the largest potential extent of the sites considered in this study. However, as is the case at all sites, a significant portion of the potentially affected area contains low concentrations of oil, which were discussed in Section 6.1.2. This is shown graphically in Figure 7–8.

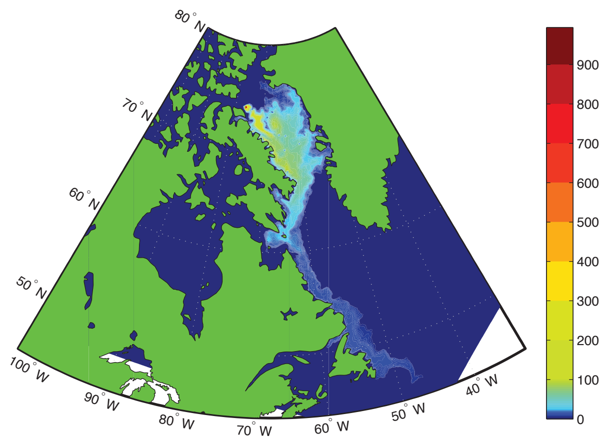


Figure 7–8: MITgcm passive tracer concentration in ocean surface for the Baffin Bay location at the end of the tracking period for an arbitrary year, 1998. High concentrations of oil are found on the east coast of Baffin Island. The remainder of the area contains low concentrations of oil.

## 7.2 USA

### 7.2.1 Beaufort Sea

This location is in shallow waters on the continental shelf, but outside of the landfast ice zone, as shown by the historical ice drifts in Figure 7–9. The historical ice drifts match the computed trajectories well, especially during the winter when ice cover is dense. During the summer the oil in the ocean surface waters follows the ice edge and hence the trajectory of the oil changes slightly, veering north from the winter trajectory. The evolution of the spill is shown in Figure 7–10.

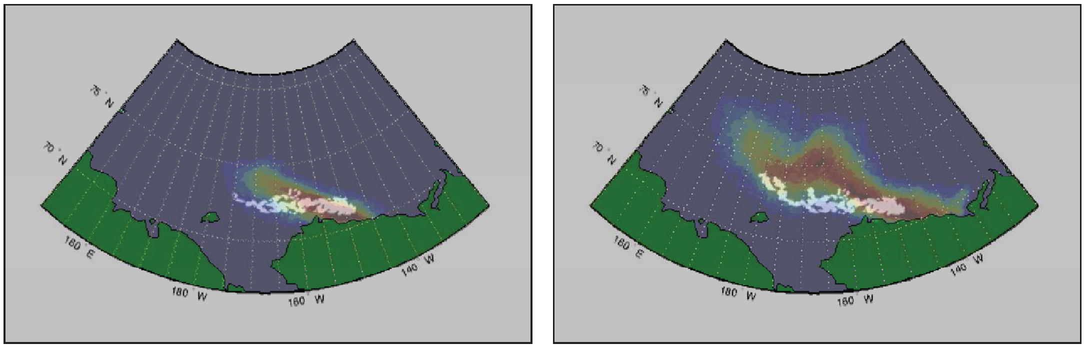


Figure 7–9: Comparison of historical ice drifts (white) and total probability of contamination trajectories (contoured) at the US Beaufort Sea location at the end of April (left) and the end of October (right).

Generally the oil drifts west with the circulation of the Beaufort Gyre, however some eastward drift is observed from the spill site. This eastward drift is especially strong during the summer months and likely due to the inflow of water from the Pacific moving east along the Alaskan coastline. Under the combined influence of these two systems, potential for contamination of coastlines is shown westward along the North Slope of Alaska and eastward into the Canadian Mackenzie Delta. In the open ocean, oil also drifts into Russian territories by the summer.

### 7.2.2 Chukchi Sea

Shell's ill-fated 2012 exploration well, described in Section 2.2.2, is located in an area of complex interaction between the inflow of warm, Pacific water through the Bering Strait and the anticyclonic circulation of the Beaufort Gyre. This influence can be seen clearly in the evolution of a spill from this site, as shown in Figure 7–11. The oil first is transported north with the inflow from the Pacific and drifts northwest-ward with the Beaufort Gyre once north of the Alaskan coastline. Oil is

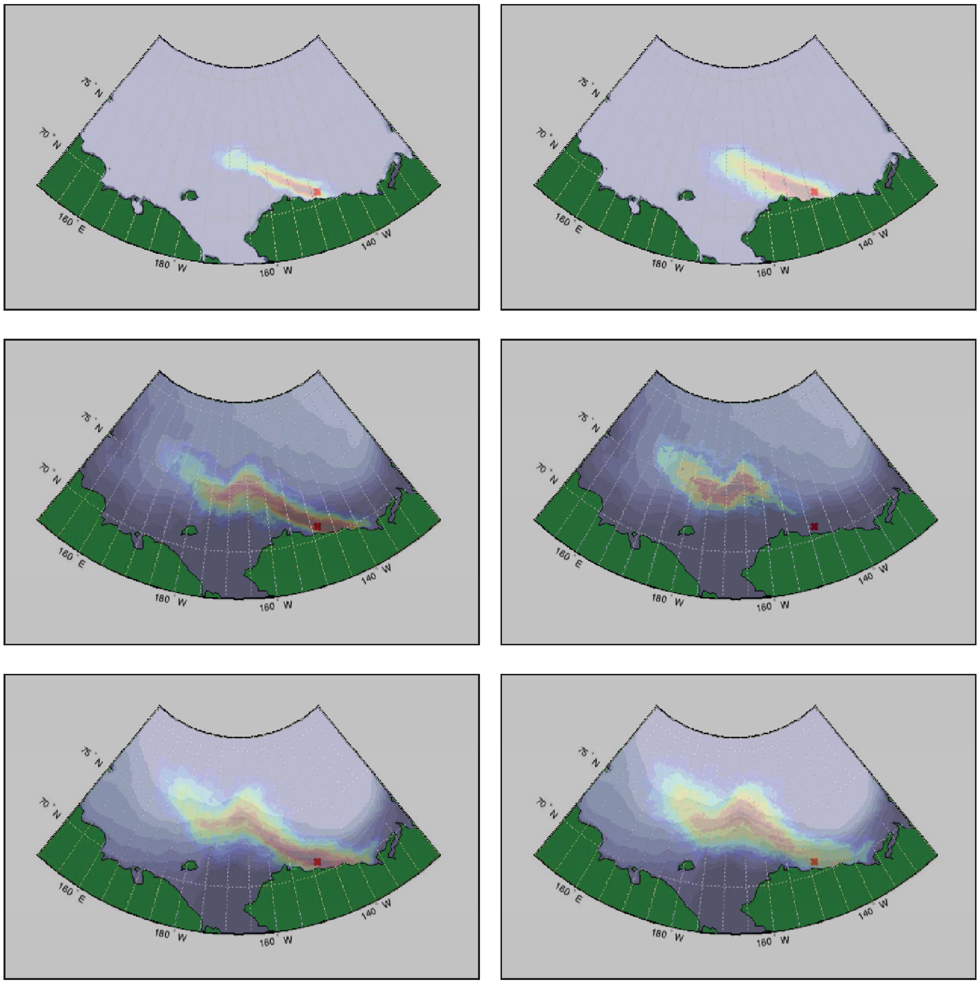


Figure 7–10: Probability of contamination in ocean surface waters (left) and sea ice (right) for the US Beaufort Sea location at the end of April (top), mid-September (middle), and end of October (bottom).

also transported east along the Alaskan coastline, though not quite as far as from the US Beaufort Sea location. Similar to the US Beaufort Sea, oil also drifts westward into Russian waters from here.

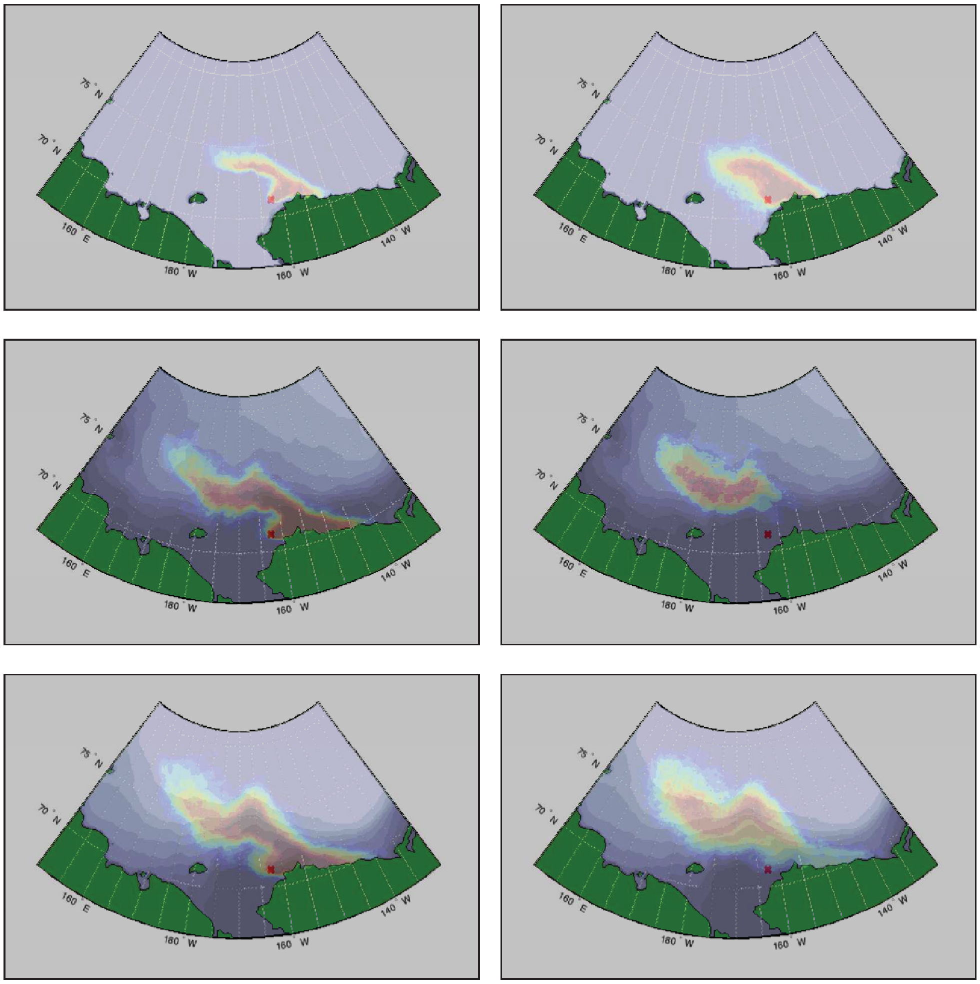


Figure 7–11: Probability of contamination in ocean surface waters (left) and sea ice (right) for the US Chukchi Sea location at the end of April (top), mid-September (middle), and end of October (bottom).

In general, similar conclusions can be drawn for both locations in US waters. It is notable that both locations are relatively close to the coast, in the shallow waters of the continental shelf, however there is a significantly higher potential from transport away from the spill site and overall contamination from these sites than from the shallow continental slope site in the Canadian Mackenzie Delta. Drift distances from these sites are comparable to the results for the further offshore location on the Canadian Beaufort Continental Slope, though the affected area is slightly less. This is consistent with the observation that the circulation of the Beaufort Gyre intensifies near the Alaskan shelf, made in Section 3.1.

The historical ice drifts from this spill site, shown in Figure 7–12 show the general westward drift seen in the calculated trajectories and generally match the length of the trajectories well. However the historical drifts do not include the northward transport by inflowing Pacific water and show more trajectories heading southwest from the spill site, rather than northwest (as the calculated trajectories show).

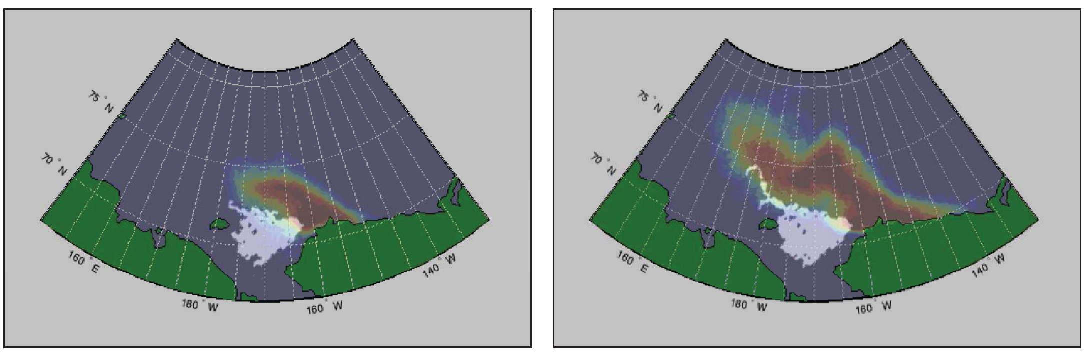


Figure 7–12: Comparison of historical ice drifts (white) and total probability of contamination trajectories (contoured) at the US Chukchi Sea location at the end of April (left) and the end of October (right).

This is likely due to the ice concentration at the site not being significant at the beginning of the simulation, due to the warming influence of Pacific water. Consistent presence of intermediate ice concentrations could lead to these sorts of mismatches since the historical drifts, as given by IceTracker, only show ice concentrations higher than 50%, rather than the 30% required for ice contamination in the calculated results.

### 7.3 Greenland

The location of this site in the main outflow of water and ice from the Arctic Ocean, as well as it's year-round ice coverage, present a significant risk for extensive contamination after an oil spill from this area. Large extent of potential contamination is confirmed in this study, with transport from the site reaching 2,416km by the end of the tracking period. Calculated trajectories, as shown in Figure 7–13, show oil travelling south along the east coast of Greenland, and transport towards the coast by sea ice.

The calculated trajectories agree very well with historical ice drifts, as is demonstrated in Figure 7–14.

Oil is contained well within the ice edge during the winter, though the majority of transport occurs during this time. At the end of April the oil has reached points up to 1,624km from the spill site. Further transport occurs once the ice retreats in the summer, and some annually variable trajectories following recirculating currents are seen at $\sim 72°$N. Since the transport occurs almost entirely along the east coast of Greenland, which is also marked by many bays, fjords, and inlets, potential for contamination is significant here and cleanup difficulty would be increased.

### 7.4 Norway

Due to the warming influence of the North Atlantic Current, this site is generally ice-free year-round. Some contaminated ice was recorded in eleven of the 31 years considered, however for four of those years ice was only affected in a single model cell

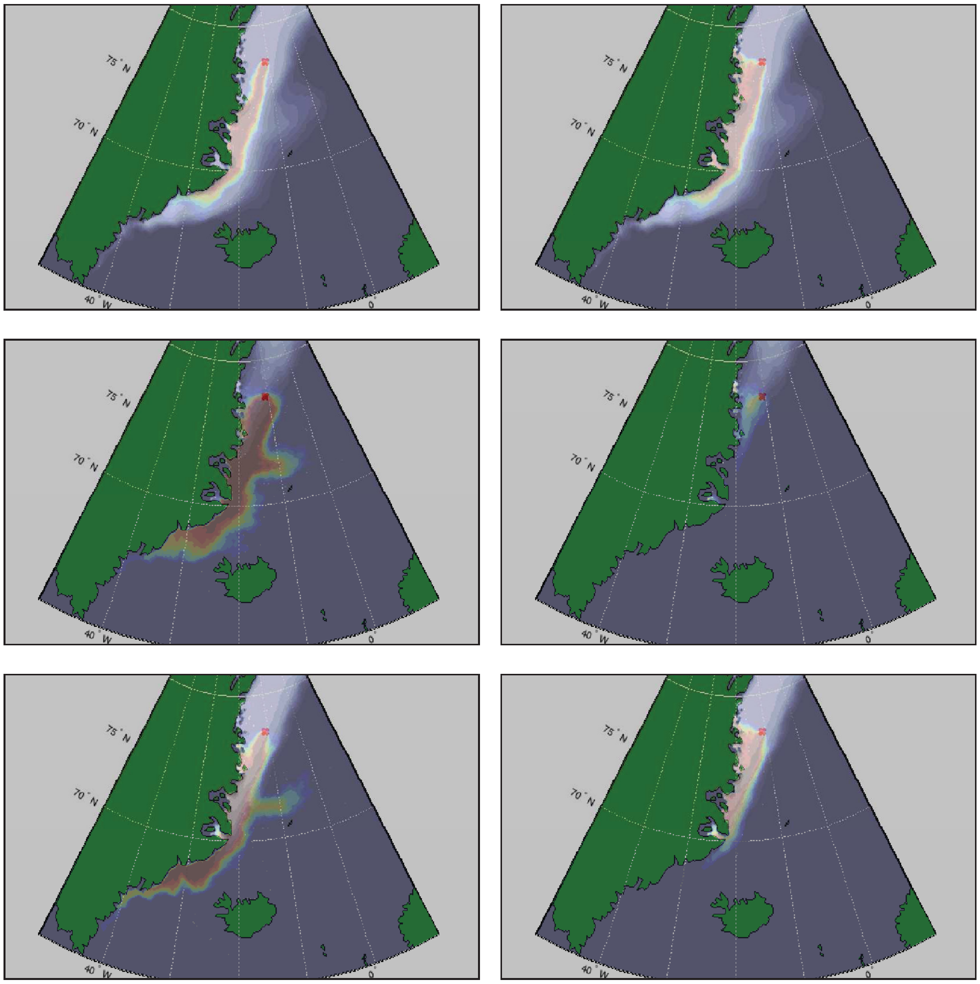

Figure 7–13: Probability of contamination in ocean surface waters (left) and sea ice (right) for the East Greenland location at the end of April (top), mid-September (middle), and end of October (bottom).

and the maximum area of contaminated ice recorded was 69,984$km^2$. This is less than half of the next greatest extent of contaminated ice, found in the Russian Pechora Sea. For this reason no verification against historical ice drift data was available. The evolution of the spill on open water is shown in Figure 7–15. The extent of the

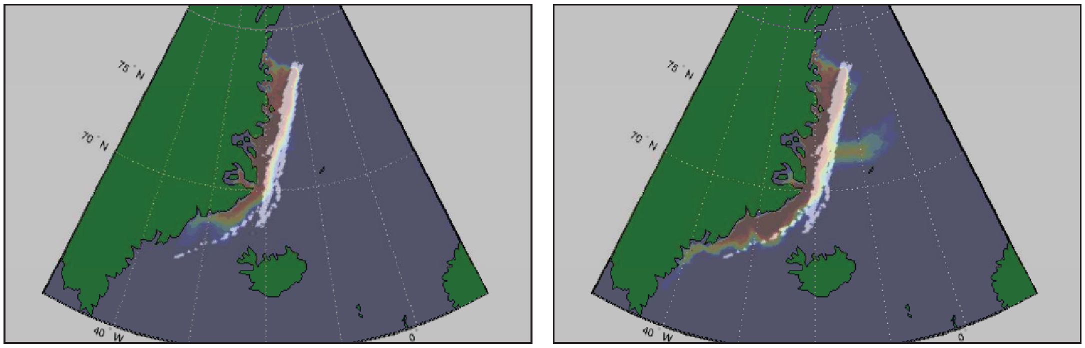

Figure 7–14: Comparison of historical ice drifts (white) and total probability of contamination trajectories (contoured) at the East Greenland location at the end of April (left) and the end of October (right).

'normal-year' ice coverage shown in this figure confirm the general absence of ice in the affected area.

Oil spilled from this site generally drifts east and south, towards the coast, during the winter months. In the summer the oil follows a narrow trajectory along the northern Norwegian coast and into Russian territory, posing a potential for significant contamination in both countries.

While this location is located in the North Atlantic Current, the southeastern parts of the affected area are sheltered from its influence by the landmass of Norway. When compared to locations which are exposed more directly to a large-scale circulation feature, such as the Beaufort Gyre at Canadian and US locations, the area affected by a spill from this location is relatively small, ∼30% of the area which is affected from more exposed locations. This, along with findings from more exposed sites such as East Greenland, suggests that study of mean circulation patterns could

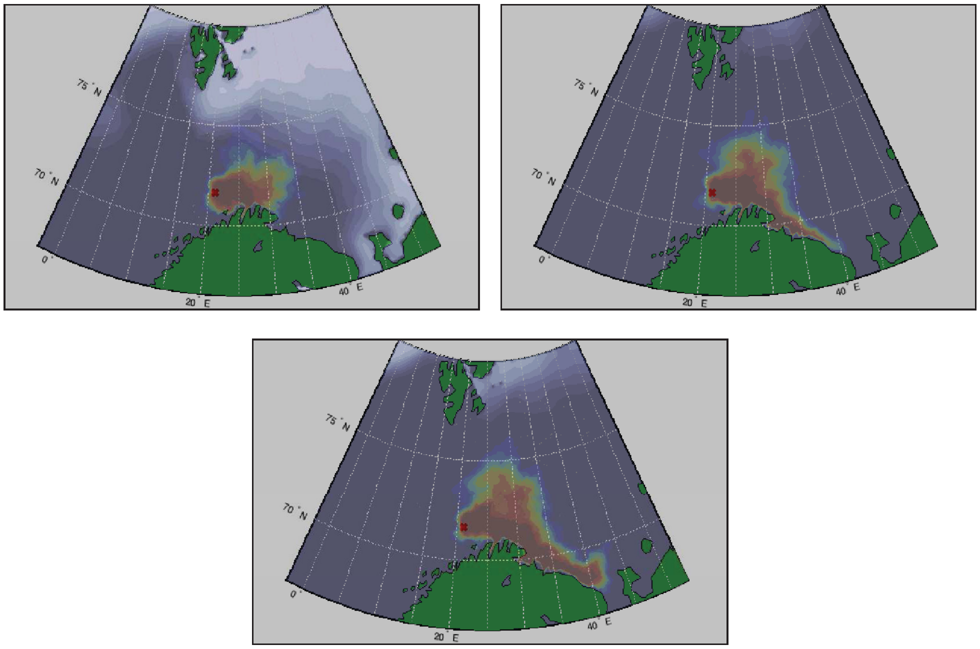


Figure 7–15: Probability of contamination in ocean surface waters for the Barents Sea location at the end of April (left), mid-September (center), and end of October (right).

yield a rough, but indicative assessment of risk for contamination from potential drilling sites.

## 7.5 Russia

### 7.5.1 Pechora Sea

Both due to the shallow water depth and the close proximity to shorelines at this site, landfast ice presence is almost certain. This is evidenced by the historical ice drifts shown in Figure 6–13. Therefore the trajectories shown in Figure 7–16 are likely to overpredict the actual extent of contamination.

As was mentioned in Section 7.1.3, significant transport under landfast ice can only occur with ocean surface currents greater than the threshold given by Equation

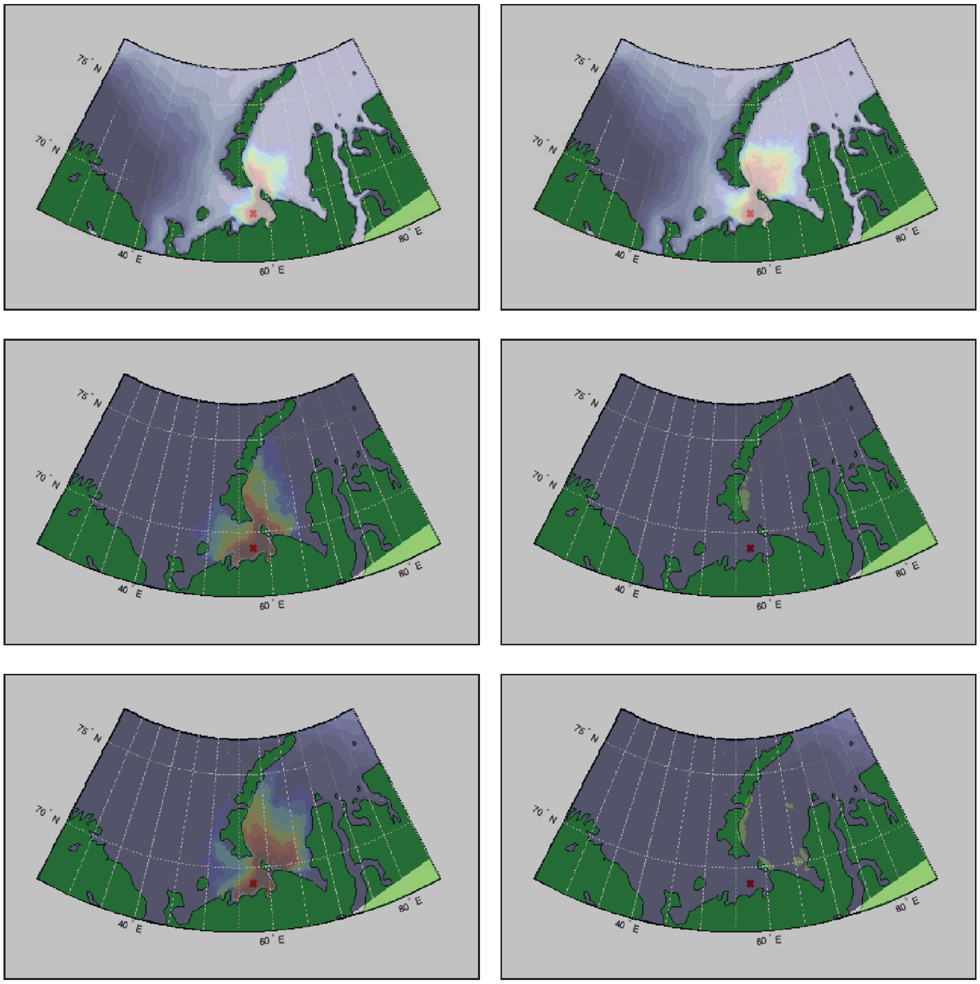


Figure 7–16: Probability of contamination in ocean surface waters (left) and sea ice (right) for the Pechora Sea location at the end of April (top), mid-September (middle), and end of October (bottom).

3.15. For currents weaker than this threshold, movement of oil would be limited to spreading under ice as long as the landfast ice cover is present. Therefore this location must be reconsidered once MITgcm is configured to include landfast ice.

However since the site is only ice covered between December and June, significant impact on surrounding shorelines of mainland Russia and Novaya Zemlya is possible from oil transported on open water during ice-free periods.

### 7.5.2 Kara Sea

This site is more exposed than the Pechora Sea location. As was illustrated in Section 6.3.2, ice dynamics here are likely influenced to some degree by landfast ice, though significant transport with mobile drift ice is possible in the deeper waters on the east coast of Novaya Zemlya. Therefore the southeastern portions of the probability distributions shown in Figure 7–17 are subject to verification once landfast ice is considered in MITgcm.

Periods of significant ice coverage are longer at this site than at the Pechora Sea location, and transport with sea ice is significant during the winter. With the receding ice edge, potential for contamination in sea ice drops to very low levels by the end of the summer. Encapsulation in growing ice during the Fall is shown to vary significantly from year to year, but potential for significant encapsulation, and the associated difficulty in subsequent cleanup exists.

Potential for shoreline impact is somewhat less than at other locations, though is still an issue along the coast of the Taymyr Peninsula and islands in this area. Mahoney et al. (2007) noted that this is an area where multi-year landfast ice has been observed, which may serve to help mitigate shoreline effects, since most of the shoreward transport occurs during the summer months.

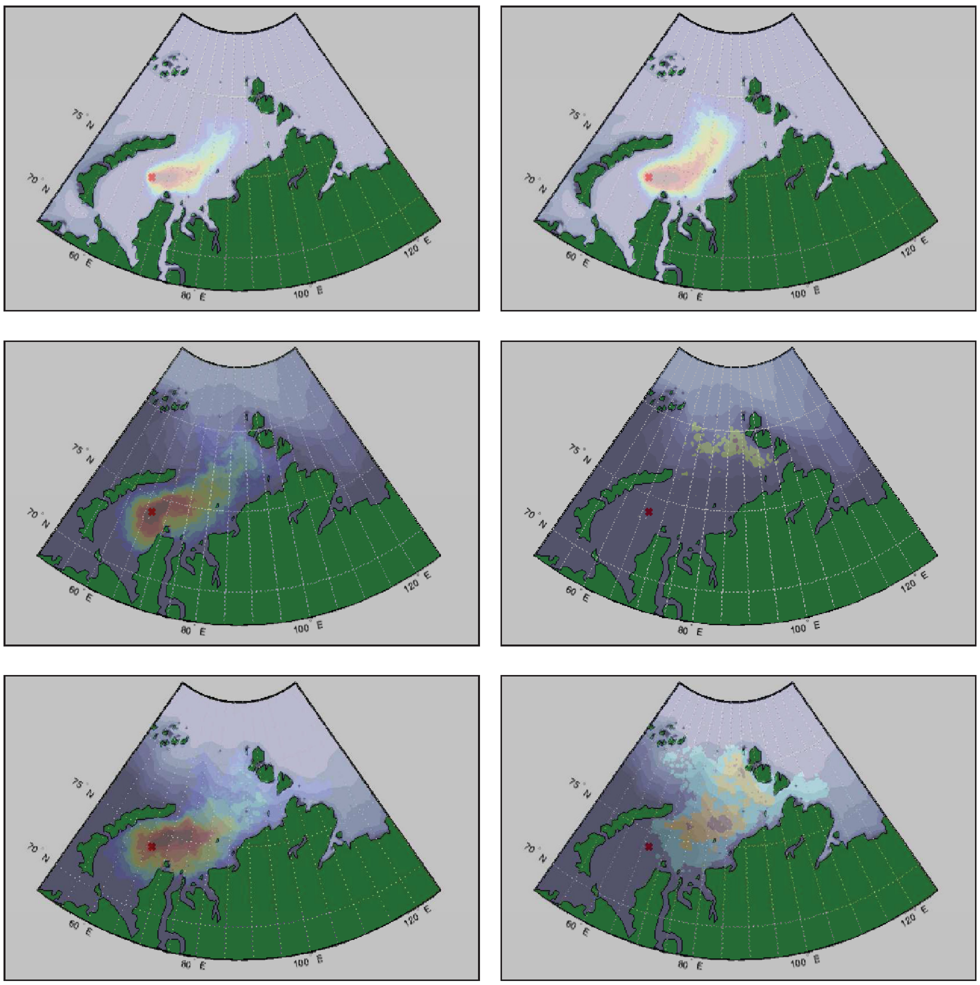


Figure 7–17: Probability of contamination in ocean surface waters (left) and sea ice (right) for the Kara Sea location at the end of April (top), mid-September (middle), and end of October (bottom).

# CHAPTER 8
# Conclusions

## 8.1 Summary

The main circulation patterns in the Arctic Ocean (Figure 3–1) give good first estimates of the trajectory of oil spilled at a given location. This is seen in the North American Beaufort and Chukchi Seas, where the anticyclonic rotation of the Beaufort Gyre and the inflow of Pacific water along the Alaskan shore dominate transport patterns, in the Sverdrup Islands and Baffin Bay, where oil is carried south by water flowing out of the Arctic Ocean into the Atlantic through the Canadian Archipelago, and off the east coast of Greenland, where the strong outflow of water and sea ice through Fram Strait carries oil south into the Atlantic. The influence of the North Atlantic Current, which brings warm water into the Arctic Ocean along the western shore of Norway and over the Russian Continental Shelf, is seen in the Barents, Pechora, and Kara Seas. The magnitude of transport distance depends on the exposure of a site to the mean current, with significantly less transport being observed at sites that are sheltered by landmasses.

The postulate that transport of oil in dense ice packs is greater than transport in ocean waters is repeatedly validated in the results. Table 7–1 shows that the area of contaminated sea ice at the end of winter is consistently greater than the area of contaminated ocean waters. The ice edge restrains oil during the winter, since very strong currents would be required to mobilize oil trapped under ice sheets and carry it out of the ice field. The spread of oil at the ocean surface is also inhibited by the ice edge, as can be clearly seen in Figures 7–1, 7–5, 7–10, and 7–11. In the summer, the areas showing significant probability for oil contamination at the ocean surface are limited to areas of relatively low sea ice coverage and follow the contours of the retreating ice. This is consistent with the observations that ice coverages greater than 20% may act as a natural boom on oil slicks (Sørstrom et al., 2010) and that there is little relative movement between oil and ice at ice concentrations greater than 30% (Venkatesh et al., 1990).

Spills resulting from oil and gas activities in the Arctic Ocean are verified to be an international issue. In five of the ten considered scenarios, simulated contamination resulting from a spill in one nation's territory was transported into another nation's territory within the study period.

As Nudds et al. (2013) and Gearon et al. (2014) noted, sea ice velocities derived from ice-ocean models are often too fast, by ~3km/day in the case of Gearon et al. (2014). Therefore modelled transport of oil with sea ice over long distances should be examined critically. However, since the calculated trajectories of contamination generally show similar, or even slightly shorter transport at the end of winter than the observed sea ice drifts from the corresponding sites, it is concluded that the modelled sea ice velocities are realistic.

For all scenarios, low passive tracer concentrations (<100) are simulated over a significant portion of area where oil presence is indicated. This is consistent with the findings of Gearon et al. (2014). Oil presence in these areas will likely take the form of small, isolated volumes of oil which are either encapsulated in or trapped under the ice or in open leads. In open water, tarballs or small portions of oil slicks which have separated from the main slick may be observed (Gearon et al., 2014; Fingas et al., 2006).

Increased sea ice velocities at the ice edge present a hazard to operations. The ice edge passes most sites during both the spring and fall, rendering ships and drilling platforms susceptible to impact from fast moving ice floes. As the ice edge advances towards the shore, it will transport spilled oil with it, and it may impact shorelines when landfast ice retreats. This is particularly well illustrated in Figures 7–1 and 7–13.

Transport of oil at the ocean surface is much more significant during times of open water, due to increased wind influence. This increased influence is well illustrated by increases in areas showing high probability of contamination from the end of April to the end of October, and from mid-September to the end of October, a period of only six weeks but with frequent high-wind events.

Finally, as is illustrated well in Figures 7–1, 7–5, 7–10, 7–11, 7–13, and 7–17, the area of contaminated ice increases significantly between mid-September and the end of October. Cleanup of oil must be maximized during the summer months, as oil that contaminates ice during the fall will be encapsulated in the ice and extremely difficult to remove until the following spring.

## 8.2 Recommendations for Future Research

Since this modelling approach is still in early stages of development, more work is needed to maximize it's potential. To conclude this report, some future steps towards an optimized, state-of-the-art, operational trajectory forecasting and risk assessment model are outlined.

The buoyant nature of oil requires that it be treated as an active tracer within MITgcm. Section 6.2.1 showed that due to the qualitative delineation of oil spill extents in this study, representing oil as a passive tracer did not introduce significant error, however treating the vertical movement of oil in the water column will become critical for quantitative studies and comprehensive consideration of subsurface releases.

Accurate treatment of vertical movement of oil also requires appropriate treatment of oil weathering processes, using parameterizations from recent testing such as the program described in Buist et al. (2009). Weathering and biodegradation processes will further gain importance once the model is used to study different oil types, since some weather much more quickly than others. For example, light fuels such as diesels are found to completely evaporate quickly compared to crude oils, especially during periods of 24 hour sunlight in the Arctic Summer.

Vertical movement due to OSA formation may be studied in a statistical fashion and such a project would be of particular importance in areas of riverine inflow such as the Mackenzie Delta and the Pechora Sea.

Since the use of weekly averaged data in the offline calculation of contaminated sea ice trajectories does not account for variability on short time scales it is desirable to formulate an algorithm allowing such tracking to be done within MITgcm at the model timestep, 20 min for the 18km resolution. Such an algorithm may be quite similar to the passive area tracer capability that is currently under development

(Gael Forget, communication to MITgcm development forum, 2011) however added flexibility would be required to accommodate algorithms for the parameterization of oil-ice interaction.

Oil-ice interaction would require parameterization until model resolutions reach 1-10m. Increasing model resolutions as available computational power increases is crucial to more accurately account for both the interaction of oil and ice as well as small scale features in the ocean surface velocity field as are often found in nearshore areas.

However, it is recognized that model resolutions of 1-10m are not reasonably achievable on larger domains in the near future. Smaller domains may be employed, however great care must be taken to accurately represent the boundary conditions in this case, especially with respect to the sea ice field. Until such resolutions can be achieved it is desirable to improve the parameterizations used from the basic criterion of 30% ice concentration being required for altered oil and trajectory behaviour. Encapsulation may be reasonably well accounted for within the framework of MITgcm, since mean ice growth rates are known for every cell. Vertical migration within the ice may be parameterized by ablation rates and observations on movement in brine channels such as those found in NORCOR (1975) and Dickins et al. (1981), however more detailed field studies of these behaviours to confirm the available findings and better quantify movement rates are desirable. Oil storage under ice and in leads and potential relative movement in areas of strong ocean surface currents may also be parameterized with greater accuracy using expressions such as Equation 3.15. However this would require more detailed knowledge of the vertical profile of the ice than is currently given by MITgcm. Specifically, the extrema of ridges in ice sheets must be known in order to more accurately quantify storage volume.

As was explained in Section 6.3.2 and Chapter 7, landfast ice has significant potential to impact oil spill trajectories in the Arctic Ocean. Therefore it is critical that MITgcm be configured to account for landfast ice in the future. Such development is already in progress and the capability will be included in future updates to MITgcm (Bruno Tremblay, personal communication, 2014).

Lastly, field testing to verify the accuracy of the model solution is critical to obtaining stakeholder acceptance. Since regulatory requirements for permitting of such tests are a significant hurdle, a first step towards this may be taken by verifying the model against existing observational data, for example from the experiments of Reed & Aamo (1994). However verification over longer time scales is also critical in the Arctic Ocean since spills are likely to persist for some time.

## Appendix A

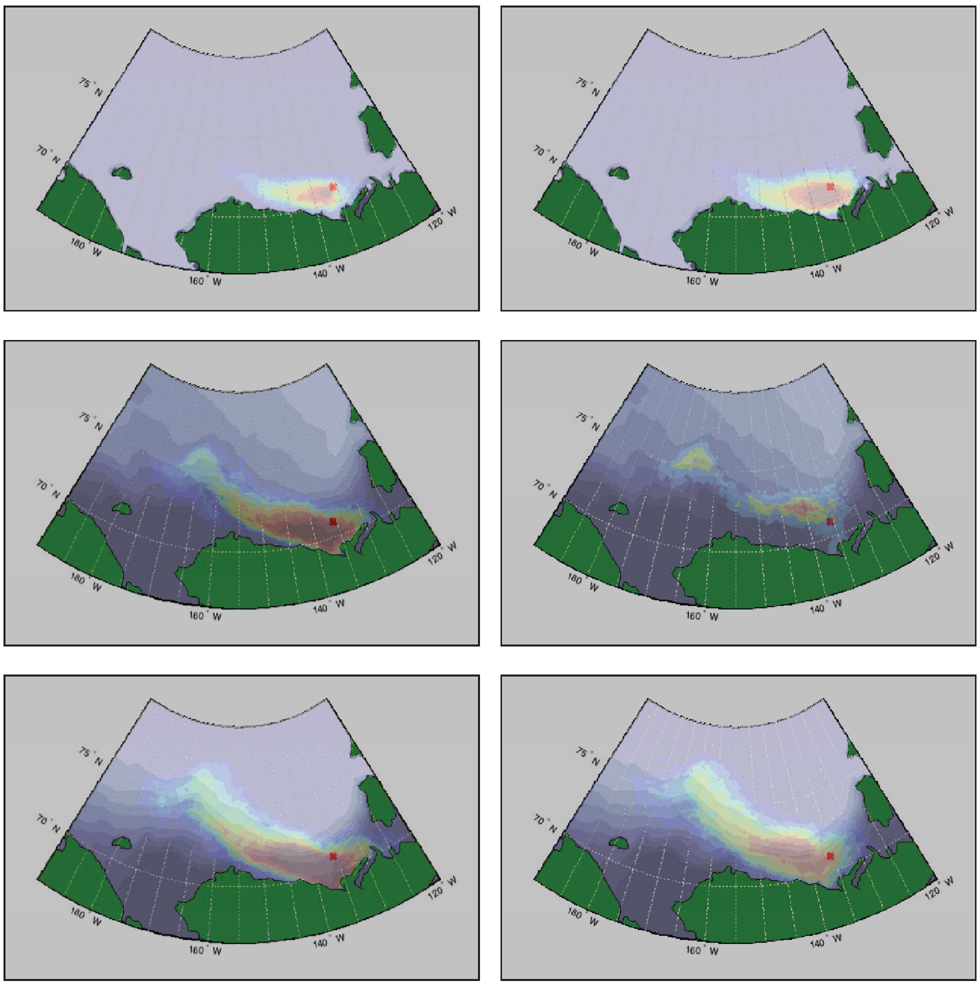


Figure 8–1: Probability of contamination in ocean surface waters (left) and sea ice (right) for the shallow release at the Canadian Beaufort Continental Slope location at the end of April (top), mid-September (middle), and end of October (bottom).

References


Aamo, O. M., Reed, M., & Downing, K. (1997). Oil spill contingency and response (oscar) model system: Sensitivity studies. In *International Oil Spill Conference*, (pp. 429–438).

Aboriginal Affairs and Northern Development Canada (2013). Northern oil and gas annual report. Tech. rep., Department of Aboriginal Affairs and Northern Development.

Aboriginal Affairs and Northern Development Canada: Northern Oil and Gas Branch (2013a). Oil & gas dispositions beaufort sea & mackenzie delta. Web.

Aboriginal Affairs and Northern Development Canada: Northern Oil and Gas Branch (2013b). Oil & gas dispositions eastern arctic offshore. Web.

Aboriginal Affairs and Northern Development Canada: Northern Oil and Gas Branch (2013c). Oil & gas dispositions sverdrup basin. Web.

Adcroft, A., Campin, J.-M., Dutkiewicz, S., Evangelinos, C., Ferreira, D., Forget, G., Fox-Kemper, B., Heimbach, P., Hill, C., Hill, E., Hill, H., Jahn, O., Losch, M., Marshall, J., Maze, G., Menemenlis, D., & Molod, A. (2014). *MITgcm User Manual*. Massachusetts Institute of Technology Department of Earth and Planetary Science.

Allen, A. A., & Nelson, W. G. (1981). Oil spill countermeasures in landfast sea ice. In *International Oil Spill Conference*.

Ano, K., Rheem, C.-K., & Yamaguchi, H. (2005). Numerical simulation of behaviour of sea ice and spilled oil coupled with ocean model. In *Proceedings of the 2nd Joint Japan/Korea Workshop on Marine Environmental Engineering*, (pp. 107–115). Fukuoka, Japan.

ASCE Task Committee on Modeling of Oil Spills of the Water Resources Engineering Division (1996). State-of-the-art review of modeling transport and fate of oil spills. *Journal of Hydraulic Engineering*, *122*, 594–609.

Bradner, T. (2014). Feds aim for revised chukchi eis by march 2015. *Alaska Journal of Commerce*.

Brehmer, E. (2014). Bering straits native corp. seeks land for future arctic port. *Alaska Journal of Commerce*.

British Oceanographic Data Centre (2014). General bathymetric chart of the oceans. Web.
URL www.gebco.net

British Petroleum (2006). Fact sheet: Prudhoe bay. Tech. rep., British Petroleum.

Brodzik, M., & Knowles, K. (2002). Ease-grid: a versatile set of equal area projections and grids. In M. Goodchild, & A. Kimmerling (Eds.) *Discrete Global Grids*, chap. 5. Santa Barbara, CA, USA: National Center for Geographic Information & Analysis.

Buist, I., Belore, R., Guarino, A., Hackenberg, D., Dickins, D., & Wang, Z. (2009). Empirical weathering properties of oil in ice and snow. In *Arctic and Marine Oilspill Program Technical Seminar*, 33.

Cairn Energy (2014). Greenland. Web.
URL www.cairnenergy.com/index.asp?pageid=72

Callow, L. (2012). Oil and gas exploration and development forecast: Canadian beaufort sea 2012-2027. Tech. rep., Beaufort Regional Environmental Assessment.

Cammaert, A. (1980). Oil and gas under ice laboratory study. Tech. rep., Beaufort Environmental Impact Statement.

Campin, J.-M., Marshall, J., & Ferreira, D. (2008). Sea ice-ocean coupling using a rescaled vertical coordinate z*. *Ocean Modeling*, *24*, 1–14.

Canada National Energy Board (2014). Imperial resource ventures limited - same season relief well technical proceeding. Web.
URL www.neb-one.gc.ca/pplctnflng/mjrpp/mprlssrw/index-eng.html

Carmack, E. C. (1990). *Polar Oceanography: Part A, Physical Science*, chap. 4, (pp. 171–222). Academic Press.

Casey, K. (2014). Greenland's new frontier: Oil and gas leases issued, though development likely years off. *The Arctic Institute*.

Colony, R. (1986). The random transport of oil by sea ice. *Water Science Technology*, *18*, 25–39.

Comfort, G., Purves, W., & Canada Environmental Emergency Branch (1982). *The behaviour of crude oil spilled under multi-year ice*. Canada Environmental Emergency Branch.

Dickins, D. (2011). Behaviour of oil spills in ice and implications for arctic spill response. In *Arctic Technology Conference*.

Dickins, D., Buist, I., & Pistruzak, W. (1981). Dome's petroleum study of oil and gas under sea ice. In *International Oil Spill Conference*, 1, (pp. 183–189).

DiPietro, N., & Cox, R. (1979). The spreading of a very viscous liquid on a quiescent water surface. *Quarterly Journal of Mechanics and Applied Mathematics*, *32*(4), 355–380.

Drozdowski, A., Nudds, S., Hannah, C. G., Niu, H., Peterson, I., & Perrie, W. (2011). Review of oil spill trajectory modelling in the presence of ice. Canadian Technical Report of Hydrography and Ocean Sciences 274, Fisheries and Oceans Canada, Bedford Institute of Oceanography, Darthmouth, NS, Canada.

ECCO (2007). Estimating the circulation & climate of the ocean. Web. URL `www.ecco-group.org`

Fay, J. A. (1969). *The spread of oil slicks on a calm sea*, (pp. 53–63). Springer Science + Business Media.

Fay, J. A. (1971). Physical processes in the spread on oil on a water surface. In *Proceedings of the Conference on Prevention and Control of OIl Spills*, (pp. 463–467). American Petroleum Institute.

Fingas, M. (2009). A new generation of models for water-in-oil emulsion formation. In *Arctic and Marine Oilspill Program Technical Seminar*.

Fingas, M., & Hollebone, B. (2003). Review of behaviour of oil in freezing environments. *Marine Pollution Bulletin*, *47*, 333–340.

Fingas, M., Hollebone, B., & Fieldhouse, B. (2006). The density behaviour of heavy oils in water. In *Proceedings of the 29th AMOP Technical Seminar*, vol. 1, (pp. 57–77). Environment Canada.

Fowler, C., & Tschudi, M. (2003). Polar pathfinder daily 25km ease-grid sea ice motion vectors. Web.
URL `nsidc.org/data/nsidc-0116`

Gastgifvars, M., & Koponen, J. (2001). Examples of 3d oil in ice modelling in the gulf of finland. In *Proceedings of Combating Marine Oil Spills in Ice and Cold/Arctic Conditions*, (pp. 195–204). Finnish Environment Institute.

Gautier, D. L., Bird, K. J., Charpentier, R. R., Houseknecht, D. W., Klett, T. R., Pitman, J. K., Moore, T. E., Schenk, C. J., Tennyson, M. E., & Wandrey, C. J. (2008). Circum-arctic resource appraisal: Estimates of undiscovered oil and gas north of the arctic circle. Web.

Gearon, M. S., French-McCay, D., Chaite, E., Zamorski, S., Reich, D., Rowe, J., & Schmidt-Etkin, D. (2014). Simap modelling of hypothetical oil spills in the beaufort sea for world wildlife fund (wwf). Tech. rep., World Wildlife Fund.

Gjosteen, J. (2004). A model for oil spreading in cold waters. *Cold Regions Science and Technology*, *38*, 117–125.

Gjosteen, J., Loset, S., & Gudmestad, O. (2003). The ability to model oil spills in broken ice. In *Port and Ocean Engineering under Arctic Conditions*, vol. 17.

Glaeser, J. L., & Vance, G. P. (1971). A study of the behaviour of oil spills in the arctic. Tech. rep., United States Coast Guard.

Greenland Bureau of Minerals and Petroleum (2014). Bmp license map. Web.
URL `licence-map.bmp.gl`

Hara, K., Yamaguchi, H., & Sagawa, G. (2008). A numerical simulation of spilled oil behaviour of ice-covered sea in sea of okhotsk. In *Proceedings of the 23rd*

*International Symposium on Okhotsk Sea & Sea Ice*, (pp. 108–113). Mombetsu, Hokkaido.

Harvey, F., & Walker, S. (2013). Arctic oil spill is certain if drilling goes ahead, says top scientist. *The Guardian*.

Hibler, W. (1979). A dynamic thermodynamic sea ice model. *Journal of Physical Oceanography*, *9*, 815–846.

Hibler, W. (1980). Modeling a variable thickness sea ice cover. *Monthly Weather Review*, *108*, 1943–1973.

Hirvi, J.-P., Koponen, J., & Vepsa, H. (1992). A case study of m/t antonio gramsci oil accident in ice infested waters: comparison between the observations and results from a coupled 3d-hydrodynamic-oil-spill-model. In *Proceedings of Combating Marine Oil Spills in Ice and Cold Conditions*, (pp. 163–173). National Board of Waters and the Environment.

Hogg, J. R., & Enachescu, M. E. (2013). Reviving exploration in the arctic islands: Opportunities and challenges from an operator's perspective. In *Integration geo-Convention*.

Imperial Oil (2012). Preliminary information package: Beaufort sea exploration joint venture. Web.

Jackett, D. R., & McDougall, T. J. (1995). Minimal adjustment of hydrographic profiles to achieve static stability. *Journal of Atmospheric and Oceanic Technology*, *12*, 381–389.

Johansen, O. (1989). Oil spill in ice simulation model development. In *Proceedings POAC 89: Port and Ocean Engineering under Arctic Conditions*, (pp. 1131–1141).

Lulea, Sweden.

Johansen, O., Rye, H., & Cooper, C. (2003). Deepspill - field study of a simulated oil and gas blowout in deep water. *Spill Science & Technology Bulletin*, *8*(5-6), 433–443.

Johansen, O., Skognes, K., & Sveen, V. (1995). Oil drift in ice model. Tech. Rep. OCN 95026, OCEANOR.

Jones, E. P. (2001). Circulation in the arctic ocean. *Polar Research*, *20*(2), 139–146.

Kawauchi, M., Yamaguchi, H., & Kimura, N. (2010). Numerical prediction of spilled oil behaviour in the sea of okhotsk under ice-covered condition. In *Proceedings of the 25th International Symposium on Okhotsk Sea & Sea Icethe*, (pp. 51–54). Mombetsu, Hokkaido.

Khelifa, A. (2010). A summary review of modelling oil in ice. In *Arctic and Marine Oilspill Program Technical Seminar*, 33, (pp. 587–608).

Lammers, R., Shklomanov, A., Vörösmarty, C., Fekete, M., & Peterson, B. (2001). Assessment of contemporary arctic river runoff based on observational discharge records. *Journal of Geophysical Research*, *106*, 3321–3334.

Large, W. G., McWilliams, J. C., & Doney, S. C. (1994). Oceanic vertical mixing: A review and a model with a nonlocal boundary layer parameterization. *Reviews of Geophysics*, *32*(4), 363–403.

MacDonald, R., Solomon, S., Cranston, R., Welch, H., Yunker, M., & Gobeil, C. (1998). A sediment and organic carbon budget for the canadian beaufort shelf. *Marine Geology*, *144*, 255–273.

MacNeill, M., & Goodman, R. (1987). Oil motion during lead closure. Tech. Rep. 53, Environmental Studies Research Fund.

Mahoney, A., Eicken, H., Gaylord, A. G., & Shapiro, L. (2007). Alaska landfast sea ice: Links with bathymetry and atmospheric circulation. *Journal of Geophysical Research*, *112*(C02001).

Marshall, J., Adcroft, A., Hill, C., Perelman, L., & Heisey, C. (1997a). A finite-volume, incompressible navier stokes model for studies of the ocean on parallel computers. *Journal of Geophysical Research*, *102*(C3), 5753–5766.

Marshall, J., Hill, C., Perelman, L., & Adcroft, A. (1997b). Hydrostatic, quasi-hydrostatic, and nonhydrostatic ocean modeling. *Journal of Geophysical Research*, *102*(C3), 5733–5752.

Martin, S. (1979). A field study of brine drainage and oil entrainment in first-year sea ice. *Journal of Glaciology*, *22*, 473–502.

McWilliams, J. C. (2006). *Fundamentals of Geophysical Fluid Dynamics*. Cambridge University Press, 1 ed.

Menemenlis, D., Campin, J.-M., Heimbach, P., Hill, C., Lee, T., Nguyen, A., Schodlok, M., & Zhang, H. (2008). Ecco2: High resolution global ocean and sea ice data synthesis. *Mercator Ocean Quarterly Newsletter*, *31*, 13–21.

Menemenlis, D., Fukumori, I., & Lee, T. (2005). Using green's functions to calibrate an ocean general circulation model. *Monthly Weather Review*, *133*, 1224–1240.

Morrison, J., Aagaard, K., & Steele, M. (2000). Recent environmental changes in the arctic: A review. *Arctic*, *53*(4), 359–371.

Murphy, D. (2013). Nunavut residents consider future of oil and wildlife in lancaster sound. *Nunatsiaq Online*.

Nansen, F. (1902). *The Norwegian North polar expedition, 1893-1896; Scientific Results*. Fridtjof Nansen Fund for the Advancement of Science.

NODC (U.S. National Oceanographic Data Center) (2005). World ocean atlas 2005. Web.
URL www.nodc.noaa.gov/OC5/WOA05/pr_woa05.html

NORCOR Engineering & Research Ltd. (1975). The interaction of crude oil with arctic sea ice. Tech. Rep. 27, Beaufort Sea Project.

Norway Ministry of Petroleum and Energy (2013). Awards in predefined areas: Apa 2013. Web.

Nudds, S. H., Drozdowski, A., Lu, Y., & Prinsenberg, S. (2013). Simulating oil spill evolution in water and sea ice in the beaufort sea. In *Proceedings of the twenty-third International Offshore and Polar Engineering*, (pp. 1066–1071).

Onogi, K., Tsutsui, J., Koide, H., Sakamoto, M., Kobayashi, S., Hatsushika, H., Matsumoto, T., Yamazaki, N., Kamahori, H., Takahashi, K., Kadokura, S., Wada, K., Kato, K., Oyama, R., Ose, T., Mannoji, N., & Taira, R. (2007). The jra-25 reanalysis. *Journal of the Meterological Society of Japan*, *85*(3), 369–432.

Parks Canada (2010). Feasibility assessment for the proposed lancaster sound national marine conservation area. Web.
URL www.pc.gc.ca/progs/amnc-nmca/lancaster/intro.aspx

Petit, B. (1997). Oil-spill modelling in the weddell sea. In Caschetto (Ed.) *Belgian Research Program on the Antarctic, Scientific Results of Phase III (1992-1996):*

*Part A, Hydrodynamic*, (pp. 1–25). Belgian Research Program on the Antarctic.

Pfirman, S. L., Campbell, G. G., Tremblay, B., Newton, R., & Meier, W. (2013). New icetracker tool depicts forward and backward arctic sea ice trajectories. In *AGU San Francisco*, C51A-0490.

Purves, W., Canada Environmental Protection Service, & Canada Environmental Impact Control Directorate (1978). *The interaction of crude oil and natural gas with laboratory-grown saline ice*. Environmental Protection Service.

Reed, M., & Aamo, O. M. (1994). Real time oil spill forecasting during and experimental oil spill in the arctic ice. *Spill Science & Technology Bulletin*, *1*(1), 69–77.

Reed, M., French, D., Rines, H., & Rye, H. (1995). A three-dimensional oil and chemical spill model for environmental impact assessment. In *International Oil Spill Conference*.

Reed, M., Johansen, O., Brandvik, P. J., Daling, P., Lewis, A., Fiocco, R., Mackay, D., & Prentki, R. (1999). Oil spill modelling towards the close of the 20th century: Overview of the state of the art. *Spill Science & Technology Bulletin*, *5*(1), 3–16.

Rheem, C.-K., & Yamaguchi, H. (2004). A numerical simulation model for oil spill in ice covered sea. *SEISA-KENKYU*, *56*(6), 67–70.

Rosneft (2013). Russia's arctic seas. Web.
URL `www.rosneft.com/upstream/exploration/arctic_seas/`

Shell Exploration & Production (2013). Revised outer continental shelf lease exploration plan: Chukchi sea, alaska revision 2. Web.

SL Ross Environmental Research Ltd., & DF Dickins Associates LLC. (1987). Field research spills to investigate the physical and chemical fate of oil in pack ice. Tech. Rep. 62, Environmental Studies Research Fund.

SL Ross Environmental Research Ltd., DF Dickins Associates LLC., & Envision Planning Solutions Inc. (2010). Beaufort sea oil spills state of knowledge review and identification of key issues. Tech. Rep. 177, Environmental Studies Research Fund.

Smith, W. H., & Sandwell, D. T. (1997). Global sea floor topography from satellite altimetry and ship depth soundings. *Science*, *277*, 1956–1962.

Sørstrom, S. E., Brandvik, P. J., Buist, I., Daling, P., Dickins, D., Faksness, L.-G., Potter, S., Rasmussen, J. F., & Singsaas, I. (2010). Joint industry program in oil spill contingency for arctic and ice-covered waters: Summary report. Tech. Rep. A14181, SINTEF.

Sorteberg, A., & Kvingedal, B. (2006). Atmospheric forcing on the barents sea winter ice extent. *Journal of Climate*, *19*, 4772–4784.

Trites, R., Lawrence, D., & Vandermeulen, J. (1986). Modelling oil movements from the kurdistan spill in cabot strait, nova scotia. *Atmosphere-Ocean*, *24*(3), 253–264.

Tsahalis, D. (1979). Theoretical and experimental study of wind- and wave-induced drift. *Journal of Physical Oceanography*, *9*, 1243–1257.

U.S. Bureau of Ocean and Energy Management (2013a). Beaufort sea - outer continental shelf lease ownership. Web.

U.S. Bureau of Ocean and Energy Management (2013b). Chukchi sea - outer continental shelf lease ownership. Web.

U.S. Department of the Interior (2013). Review of shell's 2012 alaska offshore oil and gas exploration program. Press Release.

U.S. Energy Information Administration (2014). Norway. Web. URL `www.eia.gov/countries/analysisbriefs/Norway/norway.pdf`

Vallis, G. (2005). *Atmospheric and Oceanic Fluid Dynamics: Fundamentals and Large-Scale Circulation*. Cambridge University Press.

Venkatesh, S., El-Tahan, H., Comfort, G., & Abdelnour, R. (1990). Modelling the behaviour of oil spills in ice-infested waters. *Atmosphere-Ocean*, *28*(3), 303–329.

Wang, Z., Hollebone, B., Fingas, M., Fieldhouse, B., Sigouin, L., Landriault, M., Smith, P., Noonan, J., & Thouin, G. (2003). Characteristics of spilled oils, fuels, and petroleum products: 1. composition and properties of selected oils. Tech. rep., United States Environmental Protection Agency.

Weber, H. R. (2010). Blown-out bp well finally killed at bottom of gulf. Web. URL `www.boston.com/news/nation/articles/2010/09/19/blown_out_bp_well_finally_killed_at_bottom_of_gulf/`

Weiss, J. (2013). Sea ice drift. In *Drift, Deformation, and Fracture of Sea Ice*. SpringerBriefs in Earth Sciences.

World Energy Council (2010). 2010 survey of energy resources. Tech. rep., World Energy Council.

Wotherspoon, P., Swiss, J., Kowalchuk, R., & Armstrong, J. (1985). Oil in ice computer model. Tech. Rep. 19, Environmental Studies Research Fund.

Yapa, P. D., & Chowdhury, T. (1990). Spreading of oil spilled under ice. *Journal of Hydraulic Engineering*, *116*(12), 1468–1483.

Yapa, P. D., & Dasanayaka, L. K. (2006). State-of-the-art review of modeling oil transport and spreading in ice covered waters. In *Arctic and Marine Oilspill Program Technical Seminar*, vol. 29, (pp. 893–909).

Zhang, J., & Hibler, W. (1997). On an efficient numerical method for modeling sea ice dynamics. *Journal of Geophysical Research*, *102*(C4), 8691–8702.

Zhang, J., Hibler, W., Steele, M., & Rothrock, D. (1998). Arctic ice-ocean modeling with and without climate restoring. *Journal of Physical Oceanography*, *28*, 191–217.